LARGE-SCALE DATA ANALYTICS, MODELING AND RESILIENCE OF ENERGY INFRASTRUCTURE AND SERVICE

A Dissertation
Presented to
The Academic Faculty

By

Yun Wei

In Partial Fulfillment
of the Requirements for the Degree
Doctor of Philosophy
in
Electrical and Computer Engineering

School of Electrical and Computer Engineering
Georgia Institute of Technology
May 2017

Copyright © 2017 by Yun Wei

LARGE-SCALE DATA ANALYTICS, MODELING AND RESILIENCE OF ENERGY INFRASTRUCTURE AND SERVICE

Approved by:

Dr. Chuanyi Ji, Advisor
Professor, School of Electrical and Computer Engineering
Georgia Institute of Technology

Dr. Deepakraj M Divan
Professor, School of Electrical and Computer Engineering
Georgia Institute of Technology

Dr. Biing Hwang Juang
Professor, School of Electrical and Computer Engineering
Georgia Institute of Technology

Dr. Pinar Keskinocak
Professor, School of Industrial and Systems Engineering
Georgia Institute of Technology

Dr. A.P. Sakis Meliopoulos
Professor, School of Electrical and Computer Engineering
Georgia Institute of Technology

Date Approved: 01/12/2017

To Yiqiang Wei and Caixian Wang - my parents.

ACKNOWLEDGEMENTS

I would like to present my gratitude to my advisor, Prof. Chuanyi Ji, who offered me the precious opportunity to pursue my Ph.D. study at Georgia Tech and patiently guided me through the successful fulfillment. I appreciate her care and concern for both my intellectual and personal growth. What I have learnt from her will definitely benefit my future career and life.

I am honored to have Profs. Biing Hwang Juang, A P Sakis Meliopoulos, Deepakraj M Divan, and Pinar Keskinocak to be my dissertation committee members. Their broad perspective and suggestions have helped me a lot in refining this dissertation.

I would like to thank Henry Mei and Amir Afsharinejad for collaboration on large-scale data analytics, especially failure scaling law with Henry Mei, and recovery study with Amir Afsharinejad.

I would like to thank Qi Zhou and Zhenhua Yu, who helped me a lot like brothers ever since I came to USA. I am deeply indebted to my sister Jingjing Duan and my friends Yuxuan Jiang, Cong Xiong, Yipu Zhao, Qingsong Wen, and Zhenjiang Dong. They supported my Ph.D. study wholeheartedly from the beginning till the end. My thanks also go to my wonderful labmates, including Yangfeng Ji, Seungho Lee, Ling Wang. My special thanks and love belong to Yingping Zhao, and meeting her is the best gift from God.

Last but not the least, I would like to express my sincerest gratitude to my parents. They are always proud of me. Their love, encouragement, and support are always the source of my self-motivation. This dissertation is dedicated to them.

TABLE OF CONTENTS

LIST OF TABLES

LIST OF FIGURES

SUMMARY

Severe weather events such as storms, flooding and extreme temperatures have been occurring across the United States and the world in recent years, increasingly threatening places where large populations and economic activities are heavily concentrated [3–6]. Among the most affected are the energy infrastructure and services to customers, where weather-induced failures have affected millions of people for days [4, 7, 8]. In response to these disruptions, nation-wide efforts have been initiated on resilience [4, 6, 8–10]. Here resilience refers to the ability to reduce failures under external disruptions and to recover rapidly once failures occur [4, 6, 10].

However, as pointed out by the taskforce report [10], the current understanding of resilience is limited for the power infrastructure under severe weather. It is largely unknown how resilient our infrastructure really is to severe weather [4]. In fact, the problem is not just about fixing the physical infrastructure. Services (i.e., electricity supplies to customers) are pertinent that involve users, service providers (i.e., distribution system operators, or DSOs) and policy makers [11].

This thesis studies the challenging issues to date on resilience. The focus is on how to quantify resilience of the energy infrastructure and services to customers. Here the infrastructure refers to power distribution grids that deliver electricity directly to users. Power distribution grids are found particularly vulnerable to severe weather disruptions, where 90% of failures have occurred [6]. Furthermore, the current power distribution infrastructure is not yet fully equipped with the state-of-art technologies for efficient monitoring and protection [12–14]. Services at power distribution grids that involve a large number of customers in disjoint service regions managed by disparate distribution system operators and regulators are particularly challenging. A severe weather event can have a wide geographical span. For example, Super Storm Sandy affected eight million customers in 21 DSO service regions in the United States. In the face of these issues, quantifying resilience

remains a challenging problem, involving both infrastructure and services [4, 11, 15–17].

Notably, resilience centers on complex networks involving weather, the power distribution infrastructure, customers and service providers [4, 6]. The failure aspect of resilience relates to the interactions between the physical infrastructure and weather. The recovery aspect relates mainly to services. Services depend on complex factors, not only the infrastructure but also DSOs, customers and policies. Both aspects require advanced modeling to incorporate a large number of dependent variables, and data analysis to gain knowledge about what determines resilience.

In particular, this thesis identifies and studies three technical challenges: stochasticity, data analytics, and resilience metrics (preliminary). The contributions can be summarized as follows.

A first challenge is how to model complex dependences among failures at the infrastructure, recoveries by service providers governed by policies, and impacts on customers, both at a fine granularity and large scale. This work has developed spatiotemporal models and novel formulation for dependent failures and recoveries based on non-stationary random processes [11, 16, 18, 19]. Assume that failures have already been detected. The model is derived from bottom up, relating individual failures with outages (losses of power but without being damaged) and dynamic network topology. Radial topology, commonly-used in power distribution grids, is incorporated explicitly, although the mathematical model is applicable to other types of topologies. The resulting model thus incorporates multiple spatiotemporal scales that span a distribution system locally and service areas regionally, from sub-seconds for outages, minutes or hours for weather-induced failures, and hours or days for recovery [11, 16, 18].

A second challenge is data analytics that can learn how resilient the infrastructure and services really are from measurements. The power industry has been collecting data on failures and restoration. Such data can potentially be turned into knowledge to guide resilience study. A challenge is the availability of detailed data at a large scale across multiple

service territories. As data are owned by DSOs, large-scale analytics calls for active participation of DSOs and policy makers. This work has used granular data from five DSOs, one at Louisiana and four at upstate New York. The data represent the state of art of existing collection methods, where distribution system operators (DSOs) have taken great care to ensure measurement accuracy. However the data are not from emerging technologies such as advanced metering infrastructures nor PMUs. Using such measurements, the thesis shows that data analytics can provide insights and quantification beyond experiences. In particular, the data analytics has found that local power failures have a disproportionally large non-local impact on customers, where top 20% failures affected 80% customers during severe weather events and daily operations. In contrast, an aggregation of small disruptions and commonplace devices result in major cost in customer downtime, where bottom 89% failures that affected 34 customers amount to 56% of the total cost. Importantly, such findings are also obtained from data during daily operations. Therefore, extreme weather does not cause but exacerbates the vulnerabilities in daily operations.

Finally, a third challenge is how to measure resilience in a way that incorporates the infrastructure, services, customers and weather. Such resilience metrics are needed for quantifying threats and system-wide performance. The thesis has identified and analyzed the insufficiency of the existing metrics that are widely applied by industry, and derived as a preliminary study, a dynamic metric that incorporates the intrinsic characteristics of failures, recoveries and impacts on customers. Conditioning on the external disruption impacts and existing utility service, the thesis estimated the system resilience using data in response to the storm events.

CHAPTER 1

INTRODUCTION

1.1 Motivation

Power distribution system lies at the edge of the energy grid, delivering medium and low voltages to residence and industry customers [20]. Distribution system consists of leaf nodes of the energy infrastructure, where populated electric equipments and customers are clustered and exposed in large geographical area. Power distribution is thus susceptible to severe weather events, such as hurricanes, flooding, and extreme temperature [4, 6, 10]. Severe weather events have been occurring more frequently in the U.S. in recent years and resulted in millions of customers without electricity for days [21]. How to improve the resilience of power distribution systems to large-scale external disruptions from severe weather has become a fundamental research issue. Resilience here corresponds to the ability of the system to avoid power failures and to recover rapidly from failures [4, 10]. However, the current understanding on resilience is still limited for the power infrastructure under severe weather.

The focus of the work is to model and learn the resilience of power distribution under severe weather systematically [16, 18, 22]. Multiple factors are involved, such as the physical infrastructure, the exogenous weather, and the services to electric customers. Unique challenges emerge for quantifying how power distributions respond to the large-scale external disruptions.

The first challenge is stochasticity. The exogenous weather impact, such as the evolution of hurricanes, exhibits random behaviors. This results in the dynamic (i.e., random and non-stationary) power failures that occur at power distribution [16]. The restorations also exhibit dynamics as they are highly correlated with power failures [16]. Hence, non-stationarity is an intrinsic characteristic of large-scale failures and recoveries at power distribution. Stochastic models are thus needed to include generic characteristics of failure,

recovery, and network structures [16, 18].

The second challenge is the resilience of power distribution. Resilience is a system measure of power distribution, manifesting itself in two major aspects [22, 23]. One is the ability for the system to avoid failures, which relates to the physical infrastructure and exogenous weather impact [22]. The other is the ability for the system to recover rapidly from failures, which concerns the services to customers [22]. Existing works are not sufficient to characterizing all the pertinent factors, and new models and metrics are required [22].

The third challenge is the computational methods and large-scale real data. Real data is needed for estimating unknown model parameters, so models and real data together can assess the resilience. Recent works have shown the strength of combining algorithmic approaches with real data [24, 25]. However, lack of data is a common problem for the study [26]. One severe weather event, such as a hurricane, generates only one sample, i.e., one snap-shot of failures and recoveries of power distribution [16]. The accuracy and resolution of real data is another problem. Data was aggregated spatially and temporally in previous works [24, 27], so the information is missing at components and the small time scale of minutes. How to use real data to enable the learning of models from individual component up to the entire system is a major issue.

These three aspects are inter-related as illustrated in Fig. 1.1. Modeling lays a foundation to guide data analytics (i.e., on what simple quantities to evaluate from complex failure and recovery processes, and what data to use to gain knowledge on resilience). Meanwhile, modeling provides a basis from which resilience metrics can be derived as system-wide performance. Data analytics provides knowledge and insights on resilience of operational distribution grids and services. Data also underlay measures of resilience metrics and model parameters. Such knowledge should in turn improve modeling and data analytics.

The quantification of resilience depends on characterization of the performance of

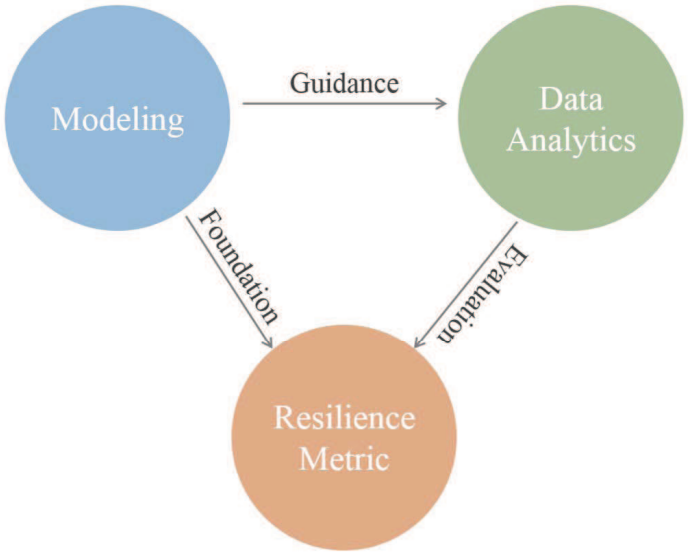

Figure 1.1: Illustration of three inter-related challenges.

power systems. Resilience can be understood as the ability of the power systems to avoid or reduce power failures and to recover quickly after failure occurrences. These two aspects are inter-related through the concepts of resilience across multiple spatiotemporal scales as stated below.

1.1.1 Infrastructure

A first aspect of resilience is that of reducing failures in the energy infrastructure. Here, as noted above, the infrastructure refers to power distribution systems, the last stage of the grid [28]. Severe weather events (e.g., high winds and flooding) damage power components such as down-wires from fallen debris, damaged transformers or non-functional distribution substations. Component failures in a power distribution system are local (i.e., do not cascade for radial topology) but can involve large numbers of customers and span a wide geographical area [29]. Protective devices, activated by failures or fault currents, are also considered as infrastructural failures since they interrupt electricity supplies to customers [28]. Examples of activated protective devices include open switches and blown fuses [30]. Outages are further caused by failures within a distribution system, where devices downstream lose power but are not damaged [11, 18].

1.1.2 Services

The second aspect of resilience relates to services (i.e., maintaining electricity supplies to customers). Recovery from failures thus signifies the service aspect of resilience. DSOs are responsible for restoring electricity supplies to customers when disruptions occur. Thus, services are provided in a decentralized fashion, where individual DSOs are responsible for their own managed territories. Services are also governed by policies in the form of guidelines from state and federal governments [31]. Policy makers also participate actively in recovery processes (i.e., help guide restoration crews as shown in Super Storm Sandy and Hurricane Matthew). Hence customers, DSOs and policy makers form a community relevant to resilient energy services.

1.1.3 Multiple Spatiotemporal Scales

Resilience involves interactions among power distribution grids, services to customers, the community and weather as illustrated in Fig. 1.2. Such interactions occur dynamically across multiple spatiotemporal scales. For example, high winds cause fallen debris that induce failures to overhead power distribution lines in minutes [16]. Outages caused by failures occur in seconds or sub-seconds within a distribution infrastructure [18, 32]. Recovery occurs in seconds for restoring outages and in days for difficult manual repairs [11, 16]. Spatial scales vary from components in a local distribution system to townships, one service region and multiple service territories [33].

1.2 Literature Review

1.2.1 Power Distribution

An electric power grid is an interconnected network that delivers electricity to customers, which typically consists three part: power generation, power transmission, and power distribution [20]. Figure 1.3 shows a simplified diagram of power grid. Power distribution lies at the edge of the electric grid, and provides medium and low voltages (35KV to 120V) from substations to customers as the final stage [20]. Power grid is susceptible to severe

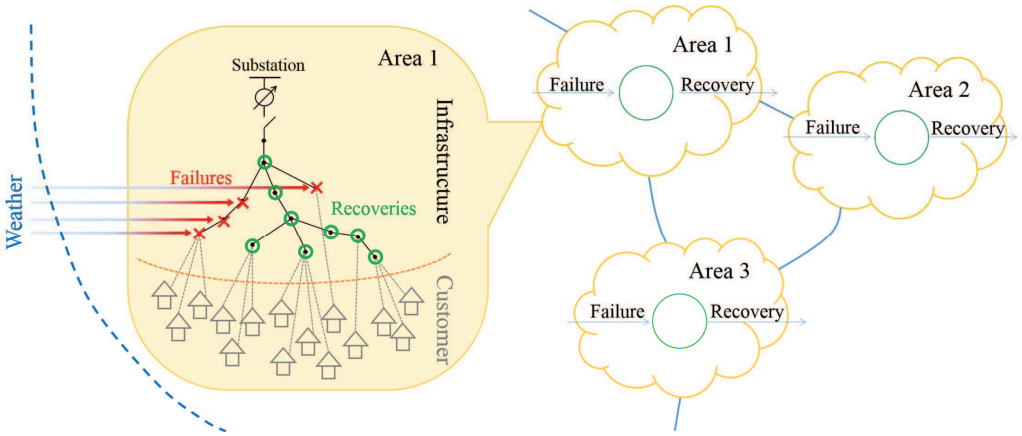

Figure 1.2: Illustration of interactions among weather, infrastructure, and community.

weather events, such as hurricanes, ice storms, and flooding. As reported, 58% of total disruptions of electricity services were due to severe weather, and 87% of each such failure event affected 50,000 customers or more since 2002 [6]. Especially, about 90% of the total failures occurred at power distribution [6]. Hence, power distribution is more vulnerable to severe weather than power generation and transmission.

The vulnerability of power distribution is due to its unique characteristics compared to power transmission. First of all, there are significantly more miles of power distribution that are exposed to severe weather than transmission. For example, Georgia Power has over 154,000 miles of distribution lines, but has only 27,000 miles of transmission lines [34]. Second, power distribution consists of widely-distributed electric devices. The devices are often mounted on poles and are exposed to external threats such as fallen trees under high winds [28, 35]. Third, power distribution is not designed as reliable as generation or transmission [27]. For example, overhead distribution lines are typically strung between poles that are 30 to 40 ft high and 100 to 200 ft apart, and such height and distance are susceptible to fallen trees [35].

Power distribution is classified to overhead distribution and underground distribution. Overhead distribution is used for about 80% of power distribution in U.S., [28]. High wind

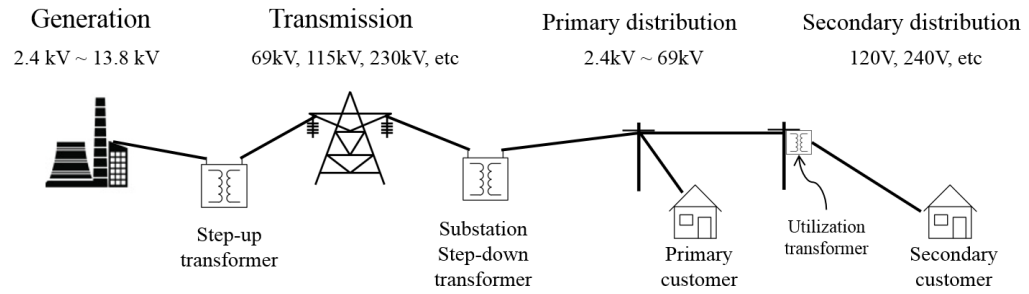

Figure 1.3: Diagram of typical electric power grid: generation, transmission and distribution [1, 2].

is the major threat to the overhead system. A radial topology is typical for overhead distribution for the simplicity and low cost [1], but radial topology can result in correlated outages to electric devices and customers [18]. Underground networks keep power lines and equipment buried and are more resilient to high winds [4]. But underground distribution is susceptible to surge, flooding and salt water damages [3, 6].

1.2.2 Modeling

An objective of modeling is to characterize relationships among a large number of dependent variables. Such variables include weather, failures at the distribution grid level, recoveries, impacts on customers and the community overall. To date, there does not exist such a model that incorporates all these pertinent factors. Different aspects have been studied in prior work, from static models to non-stationary spatiotemporal random processes.

1.2.2.1 Static Models in Machine Learning

A large body of prior work addresses the modeling of how severe weather induces initiating failures [30, 36–38]. These models are static, focusing on finding a mapping between weather variables and failures. Such models pioneered the work in this area, starting with one node (e.g., a power distribution line or a component), and one to multiple weather variables [24,30,37]. For example, the failure rate, which is the average number of new failures occurring per mile per hour of overhead power lines, is modeled as a quadratic function of wind intensity in [28]. Fragility, which is the conditional probability of a component failure

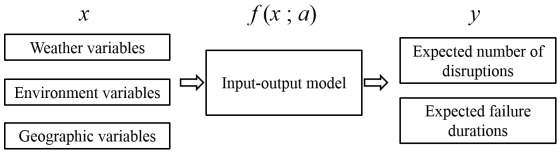

Figure 1.4: Machine Learning View of Static Models.

given weather variables, is modeled as a function of wind intensity or gust, precipitation, and surge elevation respectively in [39] and [40].

These models, although diverse, can be unified through machine learning as illustrated in Fig. 1.4. Consider an n-dimensional vector of exogenous variables $x \in R^n$ at a given location for $1 \leq n$. Modeling can be viewed as finding a static mapping, $f(x; a) : x \rightarrow y$, between exogenous variables x and targets $y \in R^m$ for $1 \leq m$. Here y describes failures (i.e., as the number of failures or failure durations, or the probability of failures/durations), and $a \in R^l$ is a vector of unknown parameters for $1 \leq l$. The data set $D = \{x^{(k)}, y^{(k)}\}$ is obtained on pairs of exogenous and failure variables, where $(x^{(k)}, y^{(k)})$ are the k-th sample of the exogenous input x and desired output y of the learning machine. The goal of learning is to obtain either f or the parameter a for a chosen f using data D so that f approximates an underlying mapping from x to y. This is clearly a context of supervised learning [41]. The models are static, where neither f nor the parameters a nor the inputs and outputs (x, y) vary with time.

The input variables x mainly represent weather, including wind-intensity, speed and gust; as well as precipitation. Several example models on f have been studied:

(a) Poisson generalized linear model (GLM) [27]: The number of power failures in a grid cell is modeled as a Poisson random variable with mean μ, where $\ln(\mu)$ is assumed to be a linear function of weather variables x.

(b) Negative binomial generalized linear model (NBGLM) [30]: An error term ϵ is introduced into the GLM to model the dispersion (i.e., the inconsistency between the mean

and the variance).

(c) Generalized additive model (GAM) [24]: The linear function is replaced by a non-linear mapping f, including cubic splines and non-parametric models.

(d) Spatially dependent Poisson linear models [42]: Spatial correlation is included in GLM as a multivariate normal distribution across different grid cells.

The above models have been used widely in subsequent works [43–46]. Resulting models identify fallen trees as major causes of power failures [30, 47]; and transformers as affected most by severe storms [27, 43].

Other learning methods have been applied, including classification and regression trees, Bayesian additive regression trees, and multivariate adaptive regression splines [37]. Bayesian additive regression trees are found to be most accurate in predicting durations of failures given weather variables [37]. Principal Component Analysis (PCA) is found to be effective in learning from correlated weather variables [43].

The static models assume that failures occur independently of time and locations [30, 42]. This assumption on temporal independence is reasonable if evolution of failures is not considered. The assumption on spatial independence can be invalid since locations at sufficiently close proximities may experience similar weather impacts [42]. In addition, certain geo-locations exhibit a higher likelihood of weather-induced failures than the others [4]. Due to these assumptions, certain static models are obtained by aggregating over time and service regions [30]. However, the aggregation may lose spatiotemporal information needed for failure and recovery studies (see Section IV for further discussions).

1.2.2.2 Spatiotemporal Random Processes

When sufficiently fine spatial and temporal scales are taken into consideration, failures and recoveries need to be modeled as spatiotemporal random processes [11, 16, 48–50]. Such models characterize dynamic interactions of infrastructural failures, services and customers, which are not quantified by static models [11, 16].

The prior works motivate such modeling albeit the problem they consider is on cascading failures that occur at power transmission rather than distribution grids [51, 52]. For example, dynamic models are developed for cascading failures through Branching processes [51, 53], Markov decision processes [54], hybrid system models for random and sporadic failures [55], and other probabilistic temporal models (see [56–58] and references therein).

These models are based on stationary probability distributions while weather-induced failure-recovery processes are non-stationary [11, 16]. Furthermore, severe-weather induced disruptions span a wide geographical area. Therefore, spatiotemporal processes are needed for weather-induced failures and recoveries.

Some recent work has developed a spatiotemporal non-stationary model for dependent failure-recovery processes [16, 18]. This model is motivated by non-stationary queues [59]. Such models have been applied to failure-recovery processes from severe weather events [16, 19]. However, the queuing model is inapplicable when a finer spatiotemporal scale is considered for impacts on customers by each failure and recovery; and restoration is conducted with priorities for critical customers [60].

A formulation is then developed from bottom-up, starting with failures at the power distribution infrastructure, incorporating service recovery through failure durations, and impacts on customers [11]. Such models integrate a large number of interdependent variables at the finest spatiotemporal scale.

To consider this model, assume failures are already detected. $I_i^{(d)}(t)$ $(d = f, o)$ is an indicator function, representing a failure (f) or an outage (o) for $I_i^{(d)}(t) = 1$; otherwise, $I_i^{(d)}(t) = 0$. i includes the type, geo-location and system-location of device i. Service is characterized by how rapidly power supply is restored to customers [4]; thus represented by downtime duration $D_i(v)$ for failure or outage i that occurs at time v. An indicator function $I[D_i(v) > t - v]$ represents the recovery event, where failure or outage i is not yet recovered at t, $0 < v < t$. Finally, the impact to customers evaluated at time t is modeled via

a function $G_i(v,t)$ for disruption i, which occurs at time v for $v < t$. As a simple example, $G_i(v,t)$ is the customer downtime resulting from failure or outage i.

Failures, outages, recoveries and costs are dependent for a given weather event, evolving in time and locations. Incorporating randomness from weather disruptions, the spatiotemporal non-stationary random processes model a collection of dependent infrastructural failures, recoveries and costs as coupled processes:

(a) Failure (and outage): $\{I_i^{(d)}(v), i \in S(v), v > 0\}$,

(b) Recovery: $\{I[D_k(v) > t - v], k \in \overline{S(t)}, 0 < v < t\}$,

(c) Cost: $\{G_j(v,t), j \in S(v), 0 < v < t\}$.

Here, $S(v)$ and $\overline{S}(t)$ consist of nodes in normal operation at time v and disruptions at time t, respectively. While such a model starts from the finest spatial scale of individual components and customers, aggregation can be done to an area, a township, one service region and multiple DSO territories as illustrated in Fig. 1.2.

Quantifying completely the spatiotemporal non-stationary random processes is prohibitive since that requires joint probability distributions at all time epochs. The first moments are used in an initial effort, including the time-varying failure rates and marginal conditional probability of downtime duration given failure occurrence time [11].

1.2.3 Resilience of Power Distribution

1.2.3.1 Resilience Concepts

Resilience is a system measure in response to exogenous disruptions. Here a system corresponds to large-scale power distribution, and exogenous disruptions are severe weather events. Definitions and approaches on resilience are extensible beyond power distribution under severe weather [23]. Various definitions have been provided previously (for example, [4, 6, 29, 61], just to name a few). Despite the differences in terminologies, the definitions share a common concept that resilience is the capacity of a system to adapt to changes from environments and the climate [6]. In relating to severe weather disruptions of the infrastructure, resilience is defined through the two aspects:

- The ability to avoid failures under exogenous disruptions,
- The ability to restore services rapidly if failures occur.

Industry adopts similar definitions of resilience, with an emphasis on providing seamless services to customers. Rapid recovery from damages is the focus of power utilities in the U.S. [31, 62]. This corresponds to the second aspect of resilience. The first aspect is often related to as hardening the power grid [31]. Hence, resilience adopted by power utilities also involves two aspects.

Resilience is a dynamic measure for the system performance in major disruptions. Distributed backup resources and highly flexible new loads are designed and installed, which makes today's power distribution system more dynamic [63]. The dynamic infrastructure further results in the dynamic system performance that evolves with environment changes, and finally the dynamic system resilience [6].

1.2.3.2 Resilience Metrics

Most of existing resilience metrics are static metrics, which characterize the average measures of system performance. Power utilities use widely the IEEE defined standard sustained-interruption indices, such as System Average Interruption Frequency Index (SAIFI) and System Average Interruption Duration Index (SAIDI) [64]. SAIFI/SAIDI characterize the system reliability in daily operations excluding major storm events [64]. To evaluate the severe weather events, SAIFI was revised to Storm Average Interruption Frequency Index (STAIFI) [65], and SAIDI was revised to Storm Average Interruption Duration Index (STAIDI) [66]. They both aggregate the number of interrupted customers and customer interruption durations over an entire major storm. As the result, STAIFI/STAIDI have large errors for major storms [22].

Estimated Time of Restoration (ETR) is also widely used by power utilities, which is provided to the customers informing the expected time needed for restoring electricity services after failure occurrences [62]. Fragility is another static metric, which characterizes

the first ability of reducing failures. Variations of fragility can be found in [45, 65, 67–69]. Conceptually, fragility is the conditional probability or frequency of interruptions given exogenous variables. As the static metrics reflect only the global system resilience in aggregation over time and locations, they are insufficient to capture the dynamics and non-stationarity of the resilience.

Dynamic metrics have been studied less previously. A metric called "quality", or "loss function", is a dynamic metric that characterizes over time the percentage of either an operational system [70] or the number of customers with normal service [23]. Several variations were defined based on the metric, such as "robustness" and "rapidity" [39, 71]. Although the time variable t is involved, these metrics fails to characterize the dynamic resilience either. First, the dynamic topology of power distributions is opaque. Second, mapping from weather variables is missing. Expressing by pre-assumed stationary parametric functions, they cannot reflect the actual evolution of failures and recoveries. Involving time variable t only is far from sufficient.

1.2.4 Non-Stationary Learning

Smart power grid is an emerging area for new applications of machine learning in a non-stationary environment. Such a non-stationary environment emerges when large-scale failures occur at power distribution networks due to external disruptions such as hurricanes and severe storms. Non-stationary random processes have been studied in the context of drifting concepts (see [72–74] and references therein). Samples for learning thus need to be dynamically drawn from a non-stationary environment. An issue of sample size arises whether data is sufficient for characterizing underlying drifts of distributions. On-line learning algorithms have been developed to identify a drift, to collect and learn from samples accordingly [75].

The problem of learning non-stationary processes exhibits unique challenges in terms of sample size. For simplicity, batch data is assumed to be collected for learning an entire non-stationary life cycle of failure and recovery processes. This setting allows off-line

learning of a non-stationary random process, which is usually easier than on-line learning. However, a challenge here is that data is insufficient for even off-line learning. There is only one snapshot of a distribution network in space and time from one external disturbance. Therefore, combining model-based and data-driven approaches becomes important, where data can be used to learn a small number of model-parameters [76].

Combining model-based and data-driven approaches for learning is also required by the problem here. There has been tremendous work on learning spatial-temporal data over the years (see [77] and [78] as examples). Most of these learning approaches are data-centric, i.e., aiming at modeling and extracting information directly from data. The problem studied in this work is on power distribution networks. Thus, learning approaches need to explain, i.e., to model network behaviors upon external disturbances. Identifying models of network behaviors then becomes a pre-requisite for learning. Learned models or model-parameters can provide insights on network behaviors under external disruptions.

1.2.5 Data Analytics

Data analytics learn knowledge from measurements on failures, recoveries and weather variables. Knowledge learned helps to answer such questions as how resilient the infrastructure and services really are; and what governs resilience or the lack thereof. Here modeling provides a pertinent role of guiding data analytics (i.e., on what measurements to use and what quantities to estimate). Data determines significantly what knowledge can be learned about resilience.

1.2.5.1 Data on Failure and Recovery

The power industry has been collecting data on failures, restoration and impacts to customers [28]. The objectives of this collection have been for outage management, customer communication and reporting [31]. Data analysis is yet to become a focus.

As a typical example of granular data, an item on a failure includes “occurrence- and restoration-time, geo-location, system-location, the type of activated protective device, the

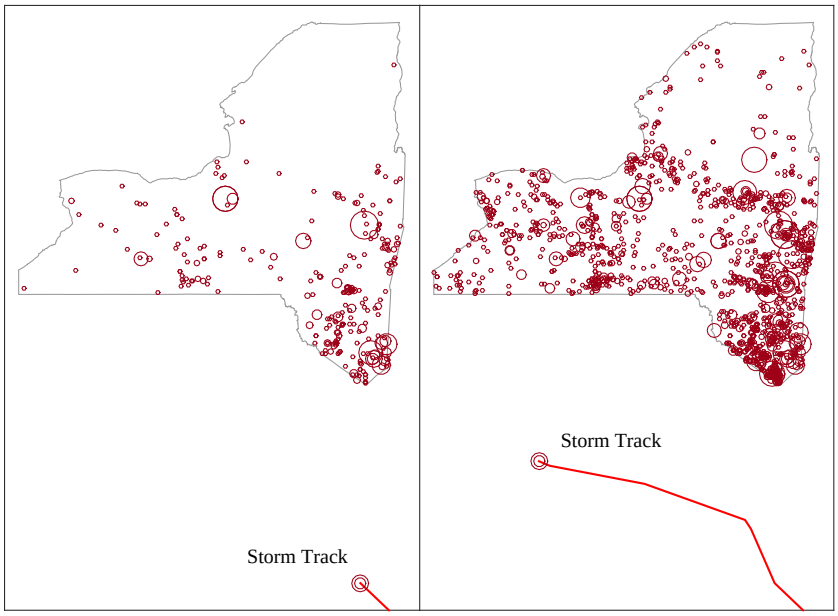

Figure 1.5: Geo-locations and occurrences of failures, and the storm track during Super Storm Sandy.

number of customers affected" [11, 16, 24]. Here activated protective devices signify the actual failed components, and themselves interrupt electricity service to customers [27,43].

One minute is the finest temporal resolution of the available data for failure occurrence and restoration time. Resulting from customer reports on service interruptions, such a time scale is consistent with that of weather-induced failures from dynamic evolution of severe storms [11, 16, 27, 30]. Failures can further cause outages in a distribution system, where certain components lose power but are not damaged [18]. Outages occur in seconds or less [18, 32]. Therefore, the temporal scale of failure data should ideally be less than a second. Such a fine temporal scale is not yet achieved in current data collection. Advanced technologies are required to attain such granularity beyond customer reports. The current resolution on restoration time is also a minute, where failure durations vary from minutes to hours and days.

Geo-locations of failures and outages are provided in exact coordinates of (latitude,

longitude) [11]. The location information is usually available on activated protective devices rather than actual failed components [11, 18, 42]. Data on locations of failed power components are more informative for studying relationships between failures and weather variables [42, 45]. Although not usually available for research, the information on failed devices is known in principle after restoration. Detecting power failures and identifying their locations in real-time have been of research interest, especially with deployment of smart meters, (micro) phasor measurement units (PMUs) for distribution systems, field sensors, and control units [13, 79–82]. Overall, accurate geo-locations together with down-time of both failed components and activated protective devices are desirable for studying spatiotemporal variability of severe weather impacts (Fig. 1.5).

Accuracy of the data is another pertinent issue. Existing collection methods can fail to generate high resolution data, especially in severely impacted service regions [83]. For example, a large number customer calls in a short time duration hinders failure isolation [83]. Repair crews are typically busy fire-fighting to restore services to customers; data collection on recovery time is thus not a priority [83]. Therefore, automated approaches are pertinent for accurate data collection.

Impacts on customers provide another important source of information on resilience. Available data on the impact is currently measured as the number of customers affected by each failure [11, 24, 27]. Total customer down-time can then be obtained, reflecting impacts from both failures and recoveries [11].

1.2.5.2 Data on Weather Variables

Data on weather variables offer pertinent information on external causes of failures and delays on recovery. Commonly-used data on severe storms have been collected on wind intensity and gust, precipitation, moisture, and temperature [24, 27]. Such data are usually provided by additional sources outside DSO service regions. While an extensive survey of weather data is beyond the scope of this work, well-known example data on wind and precipitation are from the National Oceanic and Atmospheric Administration (NOAA) [11,

27, 43, 84]. The spatiotemporal granularity of the data varies. For example, the wind speed is measured in minutes and at the centroid of each zip code [47]. The resolution for gust wind-speed is estimated at three-second intervals and each 3.66 km $\times$ 2.44km grid cell [43]. Weather data with a coarse spatiotemporal resolution can be insufficient for terrains with dynamically varying weather conditions. Recent data collection and forecasting techniques improve spatial resolution by incorporating community weather-stations [84, 85].

Several DSOs have installed densely distributed weather stations in their service regions, where existing regional weather service is insufficient for dynamic local-conditions. This allows data to be collected on both weather and power failures at comparable spatiotemporal scales [36]. For instance, National Grid has deployed weather stations, each of which covers five square miles in a service area [36]. Central Hudson Electric and Gas has weather stations needed for the varying terrain conditions in the service region [86]. San Diego Gas and Electric has sensors and mini weather stations for predicting wildfires and the resulting power failures [87]. Furthermore, a commercial product (Deep Thunder) by IBM offers localized weather prediction at a spatial scale of city blocks [85].

Storm surge and flooding result in damages on power components [83]. However, data on surge and flooding are available at a fewer sources [88]. Synthetic data have been generated from simulation on storm surge and flooding as well as high winds when detailed data are difficult to obtain [89, 90]. A challenge is for simulated data to be sufficiently accurate relating to failures in the infrastructure.

Other exogenous variables include land cover, where residential, forest, commercial, industrial, and transportation land use seem to be related to impacts of service interruptions on customers [27, 30, 42]. For example, tree density is an exogenous variable used in prior work that results in down-wire and other initiating failures from high winds [27, 30, 42].

1.2.5.3 Analytics

As modeling and available measurements lay foundations for data analytics, a pertinent question is what knowledge can be learned from data.

DSOs have long been collecting data on failures and recoveries [28]. A major use of data is on outage management [28, 83]. For example, customer reports on service interruption are combined with outage management systems to localize failures. Such information is then used for guiding repair crews. Outage maps are generated for customers on evolution of failures and restoration [91]. Aggregated information on failure and recovery is used for reporting impacts and performance on service restoration [92]. Data analytics have not been a significant part of standard outage management in practice.

Failure prediction has been studied by the prior works [27, 36, 37] and [38]. One of the first works, although mainly focused on reliability rather than resilience, applies machine learning to predict equipment failures in the New York City power grid [38]. An objective is to enable proactive maintenance for reducing severe impacts of power failures resulting in events such as explosions or fires. Data on failures and assets are collected from manholes in multiple years. Reactive point processes are used to learn model parameters from the data [93]. Although the power grid in New York City is complex, the data analytics showed promise for failure prediction [38, 93].

Several other prior works pioneered failure prediction using weather data and regression models (see Section 1.2.2). The premise is that if the likelihood of failures can be obtained given weather variables, failures can be predicted through weather forecasts [27, 36, 37]. Data on failures and weather from one service region are used for parameter estimation and model validation [24, 30, 36, 37, 39, 40, 43, 45, 47].

A challenge is that detailed data is often unavailable on failures due to security issues [45]. As such, the early works have had to use aggregated failure data [24, 30, 39, 40, 43]. Temporal aggregation results in the number of failures, ranging from one day to an entire period of a hurricane [30, 39, 94]. Spatial aggregation of failure locations ranges from a small grid cell of 0.42 km^2 to an area specified by a geocode or zip-code [30, 39, 45, 67].

On other occasions failure and weather data have different granularity [30]. Failure data are then aggregated to match the coarser geographic resolution of measurements on

weather and other exogenous variables [30]. Overall, aggregated information over time and locations cannot specify exactly when and where individual failures occur and recover. Thus data on weather and failures, when either are aggregated, can affect the accuracy of a learned model and consequently prediction.

With densely-installed weather stations in a service territory, several recent works have been able to use detailed data on both weather and power failures, resulting in a few failure prediction systems for DSOs [36, 85, 87].

In this thesis, as data plays an important role, we took extremely care of the data that used in the analytics. The temporal accuracy and spatial resolution of the data was the most refined up to date and we kept high granularity of the data.

1.2.5.4 Regression Study at National Scale

As a severe weather event often spans multiple service regions, a question is how to extend data analysis from one service territory to a regional or national scale. Granular data on power failure and recovery are owned privately by individual DSOs. A recent work explores a novel option of publicly available data [95]. Such data result from DSO annual report on the IEEE standard reliability indices: System Average Interruption Frequency Index (SAIFI) and System Average Interruption Duration Index (SAIDI) [64]. SAIFI and SAIDI are the average number of power failures and downtime durations per customer per year. Thus such data are aggregated with a spatial resolution of a service region and temporal scale of a year [92].

The data are collected at the national scale across the US over the past 13 years [95]. Data on exogenous variables are also obtained on weather, DSO expenses on reliability, and the density of power lines. The data from all sources are used to learn parameters of regression models [95]. The failure and duration indices are found to correlate with weather variables, especially when major weather events occurred.

While this approach explores new large-scale data sources, stationarity of the variables may be required so that regression using aggregated data can equivalent to using detailed

measurements. Intuitively, the approach is expected to perform well for daily operations when the stationarity is natural for failures and restorations. When including a severe weather event, detailed data are needed at sufficiently fine spatiotemporal scales.

1.3 Our Approaches and Thesis Outline

The major goal of this research is to investigate what is the nature of large-scale power failures and recoveries at distribution systems impacted by severe weather events. The proposed dynamic models of non-stationary spatiotemporal random process provides a fundamental characterization from bottom-up. Modeling provides basis for the analytics of the large-scale real data, which further reveals the vulnerability of the power infrastructure and cost to services and customers. Modeling and data analytics together enable the quantification of the resilience of the power distribution systems.

As the first step, we propose a spatiotemporal models of random processes. In Chapter 2, we analyze the non-stationarity and dynamics of the large-scale power failures occur at power distribution systems that are due to external disruptions. We address the issues of how to model such non-stationary behaviors in three aspects. First, a novel formulation is derived for an entire life cycle of large-scale failure and recovery of power distribution. Second, spatiotemporal models of failure and recovery of power distribution are developed as geo-location based multivariate non-stationary $GI(t)/G(t)/\infty$ queues. Third, the non-stationary spatial-temporal models identify a small number of parameters to be learned. Learning is applied to two real-life examples of large-scale disruptions. One is from Hurricane Ike, where data from an operational network is exact on failures and recoveries. The other is from Hurricane Sandy, where aggregated data is used for inferring failure and recovery processes at one of the impacted areas. Model parameters are learned using real data. Data analytics reveals, that failure rates behave similarly at the two different provider networks for two different hurricanes but differently at the geographical regions, and that both rapid- and slow-recovery are present for Hurricane Ike but only slow recovery is shown

for a regional distribution network from Hurricane Sandy.

In addition to aggregating failures to a spatial region, we include a new term of dynamic topology of the distribution systems in the modeling. In Chapter 3, we address the issues of topological impact of distribution system structures on power failures and recoveries. A focus is on incorporating pertinent characteristics of topological network structures into spatial temporal modeling. Such characteristics are new notations as dynamic failure- and recovery-neighborhoods. The neighborhoods quantify correlated failures and recoveries due to topology and types of components in power distribution. The resulting model is a multi-scale non-stationary spatial temporal random process. Using the model and large-scale real data from Hurricane Ike, unique characteristics are identified: The failures follow the 80/20 rule where 74.3% of the total failures result from 20.7% of failure neighborhoods with up to 72 components "failed" together. Thus the hurricane caused a large number of correlated failures. Unlike the failures, the recoveries follow 60/90 rule: 59.3% of recoveries resulted from 92.7% of all neighborhoods where either one component alone or two together recovered. Thus about 60% recoveries were uncorrelated and required individual restorations.

Next, we extend the dependent spatiotemporal random processes to further include the utility services and customers in Chapter 4. We also apply the models to study the impact of power infrastructure and the cost on customers. We analyse data from four major service regions representing Upstate New York during Super Storm Sandy and daily operations. Using non-stationary spatiotemporal random processes that relate infrastructural failures to recoveries and cost, our data analysis shows that local power failures have a disproportionally large non-local impact on people (i.e., the top 20% of failures interrupted 84% of services to customers). A large number (89%) of small failures, represented by the bottom 34% of customers and commonplace devices, resulted in 56% of the total cost of 28 million customer interruption hours. Our study shows that extreme weather does not cause but rather exacerbates existing vulnerabilities, which are obscured in daily operations.

Finally, we define and formulate a new dynamic resilience metric and use real data to quantify the vulnerability (non-resilience) of real distribution systems under super storms such as hurricanes. In Chapter 5, we develop a resilience metric from bottom-up that incorporates such pertinent characteristics as non-stationary failure-recovery processes and impacts to customers. The metric builds from our prior work that derives a problem formulation and a spatiotemporal model. The modeling starts from failures and recoveries at individual components. Topological dependence of disruptions and recoveries in power distribution is characterized through the dynamic topology. Dependent failures and recoveries are thus characterized by non-stationary spatiotemporal random processes. We further include the impacts on customers in the model. The resulting model is a coupled non-stationary random process on costs, allowing us to measure not only the resilience of the infrastructure but also combined the impacts with services on customers.

CHAPTER 2

NONSTATIONARY SPATIOTEMPORAL FAILURE-RECOVERY PROCESSES OF POWER DISTRIBUTION SYSTEMS

Large-scale power failures occur at power distribution systems that are due to external disruptions such as hurricanes and severe storms exhibit spatiotemporal non-stationarity and dynamics. In this chapter, we address the issues of how to model such non-stationary behaviors in three aspects. First, a novel formulation is derived for an entire life cycle of large-scale failure and recovery of power distribution. Second, spatiotemporal models of failure and recovery of power distribution are developed as geo-location based multivariate non-stationary $GI(t)/G(t)/\infty$ queues. Third, the non-stationary spatial-temporal models identify a small number of parameters to be learned. Learning is applied to two real-life examples of large-scale disruptions. One is from Hurricane Ike, where data from an operational network is exact on failures and recoveries. The other is from Hurricane Sandy, where aggregated data is used for inferring failure and recovery processes at one of the impacted areas. Model parameters are learned using real data. Data analytics reveals two findings. First, failure rates behave similarly at the two different provider networks for two different hurricanes but differently at the geographical regions. Second, both rapid- and slow-recovery are present for Hurricane Ike but only slow recovery is shown for a regional distribution network from Hurricane Sandy.

The rest of the chapter is organized as follows. Section 2.1 provides background knowledge and an example of large-scale failures at a power distribution network. Section 2.2 and 2.3 develops a problem formulation of spatial-temporal non-stationary random processes. Section 2.4 describes the real data from Hurricane Ike and learns a geo-temporal model. Section 2.5 studies non-stationary failure and recovery using parts of real data from Hurricane Sandy. Section 2.6 discusses our findings. Section 2.7 concludes the chapter.

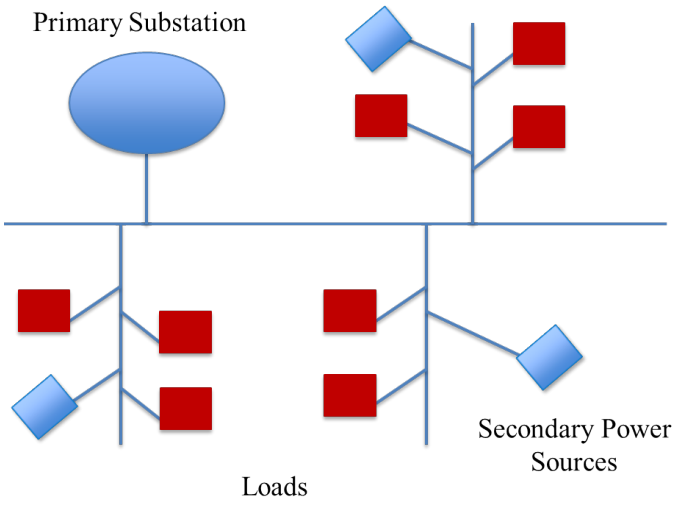

Figure 2.1: A Section in A Distribution Network.

2.1 Background and Example

In this section, we provide examples on the temporal scale, and non-stationarity of failure and recovery.

2.1.1 Time Scale of Failure and Recovery

We first discuss the time scale for modeling weather induced failures and recoveries. A power distribution network consists of components such as substations, feeders, transformers, power circuits, transmission lines, and meters. An example power distribution system is illustrated in Figure 2.1, with a commonly used radial topology. Three types of components are shown for illustration: A primary substation, three secondary power sources, and loads. Links correspond to power lines. Assume that either a component or a link can fail during a hurricane. Assume that the substation is used as a primary source during normal operation. The secondary sources, that can be distributed renewable sources, are used for back-up when the primary source fails [96]. Then the following scenarios can occur for failure and recovery:

(a) If all the sources fail due to an external disruption, there is no electricity supply to any loads. Hence, the loads experience dependent failures that can occur instantaneously.

The scenario of dependent failures also applies to other components upstream in a radial topology that cause loss of electricity at nodes downstream. Dependent failures are often experienced by loads in sub-seconds.

(b) If a link that connects a load to the network fails due to an external disruption, there is no electricity supply to the load. Such link failures can occur independently due to fallen trees or power lines. Thus loads experience independent loss of electricity. As such independent failures are caused by exogenous weather, they are assumed to occur at a time scale of a minute or beyond. Such a time scale can be estimated through how rapidly a hurricane force wind passes a city. Consider a small city of $1,600$ acres as an example. Based on the IEEE standard (IEEE/ASTM SI 10-1997) [97], an approximated "diameter" of the city is about 1.6 miles. Consider the speed of the force wind at 60 miles per hour. It takes about 1.6 minutes for the wind to pass the city. This provides a basis of using a minute as a time scale of weather-induced failures.

(c) Recovery depends on the types of failures and recovery schemes. Certain failures can be repaired through self-recovery [32]. For example, if the primary substation fails, the electricity supply to all loads can be recovered when the three secondary sources are in operation. In general, self-recovery and automated reconfiguration built in power distribution usually operate at a time scale of sub-seconds or seconds [32]. However, failures due to external disruptions, e.g., falling trees and power lines, often require manual repair by field crews. Recovery time depends on not only restoration schemes but also environmental constraints, and is thus considered as random in this work. Such manual recovery time is in either minutes or hours or days from failures.

In summary, failures and self-recoveries at a small time-scale of seconds or sub-seconds depend on detailed network structure and self-recovery schemes. Failure and recovery at a larger time scale of a minute and beyond are often due to external disruptions that evolve dynamically and randomly.

2.1.2 Example of Non-Stationary Failure and Recovery

To gain intuition on an entire life cycle of failure and recovery of a distribution network, we consider a real-life example of large-scale power failures occurred during Hurricane Ike in 2008. Figure 2.2 shows a histogram on failure occurrence time and duration at an operational distribution network before, during and after the hurricane. Each bin has length (failure occurrence time) of 1 hour and width (duration) of 4 hours. The height of each bin represents the number of failures that occur at time t and last for duration d. Figure 2.3 shows geographical distributions of failure occurrences at two different time epochs, where failure occurrence is evidently non-stationary across geographical regions. Hence,

(a) Failure occurrence is non-stationary, i.e., random and time-varying;

(b) Recovery time is non-stationary, i.e., obeys different probability distributions for failures occurred at different time;

(c) Failure occurrence and recovery time are also non-stationary spatially, i.e., exhibit different distributions for different geo-locations.

Hence, samples on failure occurrence time and duration are not identically distributed but exhibit geo-temporal non-stationarity.

2.1.3 Non-Stationary Learning

Non-stationary random processes have been studied in the context of drifting concepts (see [72–74] and references therein). Samples for learning are dynamically drawn from a non-stationary environment. An issue arises on the sample size, i.e., whether data is sufficient for characterizing underlying drifts of distributions.

The problem of learning non-stationary processes in this work exhibits unique challenges in terms of sample size. For simplicity, batch data is assumed to be collected for learning an entire non-stationary life cycle of failure and recovery processes off-line. A challenge here is that there is only one snapshot of a distribution network in space and time from one external disruption. The number of data sets is often small, i.e., from a few severe storms. Therefore, combining model-based and data-driven approaches becomes

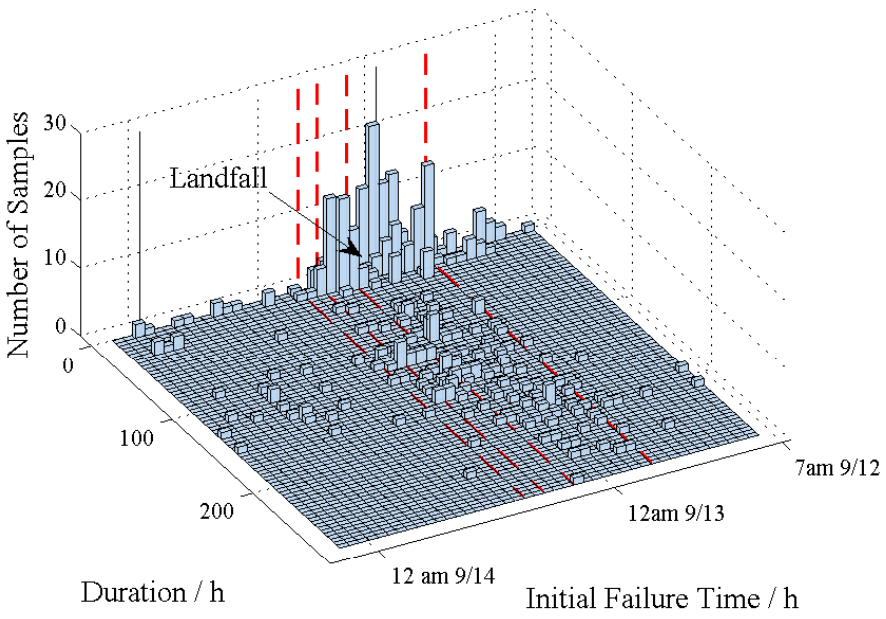

Figure 2.2: Empirical temporal distribution of failure durations in 3D.

important, where data can be used to learn a small number of model-parameters from one external disruption at a time [76]. In addition, combining model-based and data-driven approaches for learning is required by the problem: Learned model parameters need to exhibit physical meaning for generic network behaviors upon external disruptions.

2.2 Stochastic Model

We now formulate large-scale failure and recovery based on non-stationary random processes. We begin with the detailed information on nodal statuses in a distribution system. We then aggregate the spatial variables of nodes to obtain temporal evolution of failure and recovery across geo-graphical areas.

2.2.1 Failure and Recovery Probability

A geo-temporal random process provides a theoretical basis for modeling large-scale failures. The temporal variable is time t that is assumed to be continuous at the scale of a

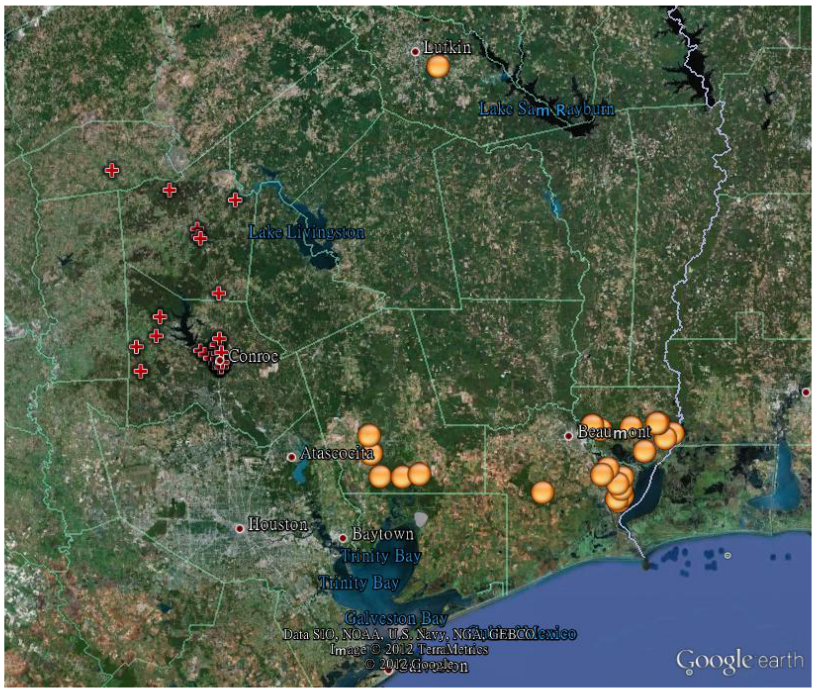

Figure 2.3: Geo-locations of failures occurred in different time durations. Red marker: Failures occurred from 7 p.m to 8 p.m. Sep. 12. Yellow marker: Failures occurred from 5 a.m. to 6 a.m. Sep. 13. Graphical tool: Google Earth.

minute. The spatial variable can be either geo- or network-location of a node. For simplicity, this work considers geo-location as a spatial variable to focus on location-based failures induced by severe weather. Nodes can be components in a distribution system such as substations, feeders, hubs, transformers, transmission lines, and distributed energy sources. A shorthand notation i is used to specify the index of node i located at z_i. $i \in S = \{1, 2, ..., n\}$ for a power distribution network with n nodes. An underlying network topology is assumed to be radial so that cascading failures occurred in mesh networks are not considered.

Let $X_i(z_i, t)$ be the status of the i-th node at time $t > 0$ for $1 \leq i \leq n$. We assume for simplicity that nodes only exhibit two states: $X_i(z_i, t) = 1$ if the i-th node is in a failure mode, i.e., without power supply. $X_i(z_i, t) = 0$ if the node is in normal operation. Failures caused by external disruptions exhibit randomness. Whether and when a node fails is random. Whether and when a failed node recovers is also random. Hence, random processes can be used to characterize failure and recovery for all nodes in a network.

Given time $t > 0$, $P\{X_i(z_i, t+\tau) = 1\}$ characterizes the probability that node i is failed in the near future $t + \tau$, where $\tau > 0$ is a small time increment. Assume a node changes state, i.e., from failure to normal and vice versa. Then for the ith node, $1 \leq i \leq n$, the probability that node i stays in failure mode in $[t, t + \tau]$ is,

$$\begin{aligned} &P\{X_i(z_i, t+\tau) = 1\} - P\{X_i(z_i, t) = 1\} \\ =&P\{X_i(z_i, t+\tau) = 1, X_i(z_i, t) = 0\} \\ &- P\{X_i(z_i, t+\tau) = 0, X_i(z_i, t) = 1\}. \end{aligned} \tag{2.1}$$

Equation 2.1 assumes Markov temporal dependence, and can be applied to n nodes in a distribution network. The n equations together form a geo-temporal model of a network. Note that statistically dependent failures at the small time scale less than a minute are not considered here, as such failures are often caused by an internal network structure rather than exogenous weather. Spatial dependence is embedded in the model but will be studied explicitly in subsequent work.

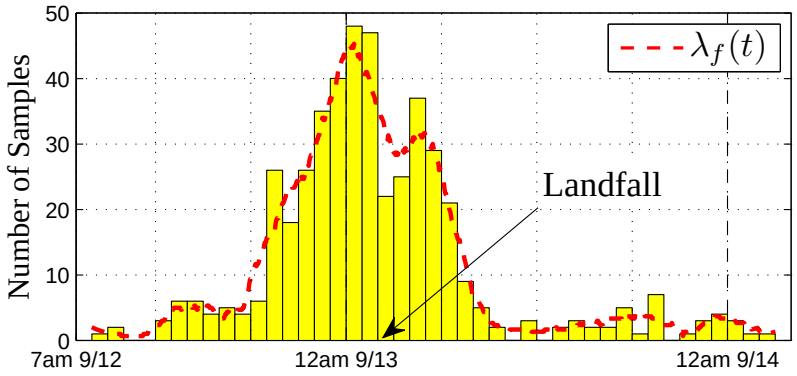

Figure 2.4: Histogram of failure occurrence time and the failure rate $\lambda_f(t)$ during Hurricane Ike.

2.2.2 Aggregated Geo-Temporal Process

When large-scale failures are caused by one external disruption, information available is from one "snapshot" of temporal spatial network statuses, and thus insufficient for specifying a complete temporal-spatial model at the node level. Hence, nodes are aggregated over a geographical region (Z), resulting in

$$\begin{aligned} &\sum_{i;z_i\in\mathbb{Z}} P\{X_i(z_i,t+\tau)=1\} - \sum_{i;z_i\in\mathbb{Z}} P\{X_i(z_i,t)=1\} \\ &= \sum_{i;z_i\in\mathbb{Z}} P\{X_i(z_i,t+\tau)=1, X_i(z_i,t)=0\} \\ &\quad - \sum_{i;z_i\in\mathbb{Z}} P\{X_i(z_i,t+\tau)=0, X_i(z_i,t)=1\}. \end{aligned} \tag{2.2}$$

Here $P\{X_i(z_i,t)=1\} = E\{I[X_i(z_i,t)=1]\}$, where $I()$ is an indicator function. $I(A)=1$ if event A occurs, and $I(A)=0$ otherwise. We can define a geo-temporal process as follows.

Definition: $\{N(t,\mathbb{Z}) \in \mathbb{N}, t>0\}$ is a geo-temporal process where the spatial variables (i's) are aggregated for all nodes z_i in a predefined region $\mathbb{Z}$. $N(t,\mathbb{Z})$ is the number of nodes in failure state at time t located in $\mathbb{Z}$,

$$N(t,\mathbb{Z}) = \sum_{i;z_i\in\mathbb{Z}} I[X_i(z_i,t)=1]. \tag{2.3}$$

Combining Equations 2.2 and 2.3, we have,

$$E\{\Delta N(t,\mathbb{Z})\} = \sum_{i;z_i\in\mathbb{Z}} P\{X_i(z_i,t+\tau)=1\} - \sum_{i;z_i\in\mathbb{Z}} P\{X_i(z_i,t)=1\}, \tag{2.4}$$

where $\Delta N(t,\mathbb{Z}) = N(t+\tau,\mathbb{Z}) - N(t,\mathbb{Z})$ is an increment of the number of failed nodes in a certain region. $\Delta N(t,\mathbb{Z})$ is the result of either newly-failed or newly-recovered nodes. Hence, we define a failure process and a recovery process respectively.

Definition: Failure process $\{N_f(t,\mathbb{Z}) \in \mathbb{N}, t \geq 0\}$ is the number of failures occurred up to time t. Recovery process $\{N_r(t,\mathbb{Z}) \in \mathbb{N}, t \geq 0\}$ is the number of recoveries occurred up to time t.

Assume $\tau > 0$ is sufficiently small so that failure or recovery occurs at most once to a node during $(t, t+\tau)$. The increments on a failure process and a recovery process satisfy respectively,

$$\begin{aligned} E\{\Delta N_f(t,\mathbb{Z})\} &= \sum_{i;z_i\in\mathbb{Z}} P\{X_i(z_i,t+\tau)=1, X_i(z_i,t)=0\}, \\ E\{\Delta N_r(t,\mathbb{Z})\} &= \sum_{i;z_i\in\mathbb{Z}} P\{X_i(z_i,t+\tau)=0, X_i(z_i,t)=1\}, \end{aligned} \tag{2.5}$$

where $\Delta N_f(t,\mathbb{Z}) = N_f(t+\tau,\mathbb{Z})\} - N_f(t,\mathbb{Z})$. Similarly, for a sufficiently small $\tau > 0$, it can be assumed that at most one recovery occurs during $(t, t+\tau)$. Hence, Equation 2.2 is simplified as,

$$E\{\Delta N(t,\mathbb{Z})\} = E\{\Delta N_f(t,\mathbb{Z})\} - E\{\Delta N_r(t,\mathbb{Z})\}. \tag{2.6}$$

Furthermore, we assume at time $t_0 = 0$, $N(t,\mathbb{Z}) = 0$, $N_f(t,\mathbb{Z}) = 0$, and $N_r(t,\mathbb{Z}) = 0$. Aggregating increments in Equation 2.6 from 0 to t, we have,

$$E\{N(t,\mathbb{Z})\} = E\{N_f(t,\mathbb{Z})\} - E\{N_r(t,\mathbb{Z})\}. \tag{2.7}$$

Hence, the expected number of nodes in the failure state equals to the difference between the expected failures and the expected recoveries. We now group a distribution network of n nodes into m geographical regions $\mathbb{Z}_j$, $1 \leq j \leq m$, based on their geo-locations.

A city, e.g., a subdivision, is an example of a geo-graphical region widely-used by utilities. Then the failure-recovery process for the entire distribution network $N(t)$ is defined as,

$$N(t) = [N(t, \mathbb{Z}_1), N(t, \mathbb{Z}_2), ..., N(t, \mathbb{Z}_m)]^{\mathrm{T}}, \tag{2.8}$$

where $N(t, \mathbb{Z}_j)$ characterizes how local power distribution in region $\mathbb{Z}_j$ responds to an external disruption.

2.3 Non-Stationary Failure and Recovery

In this section, we derive non-stationary characteristics on failure and recovery. Our derivation reveals pertinent quantities that completely model the behaviors of large-scale power failures and recoveries in expected values. This is pertinent to learning a small number of parameters in Section 2.4.

2.3.1 Failure Process

A failure process can be characterized to the first moment by failure rate functions. Let $\lambda_f(t) = [\lambda_f(t, \mathbb{Z}_1), \lambda_f(t, \mathbb{Z}_2), ..., \lambda_f(t, \mathbb{Z}_m)]^{\mathrm{T}}$ be a vector that consists of the rate function of a failure process, where $\lambda_f(t, \mathbb{Z}_j)$ is the expected number of new failures per unit time at epoch t and region $\mathbb{Z}_j$, $j = 1, 2, ..., m$,

$$\lambda_f(t, \mathbb{Z}_j) = \lim_{\tau \to 0} \frac{1}{\tau} E\{N_f(t + \tau, \mathbb{Z}_j) - N_f(t, \mathbb{Z}_j)\}. \tag{2.9}$$

The larger $\lambda_f(t, \mathbb{Z}_j)$ is, the faster failures occur in $\mathbb{Z}_j$ at time t. $\lambda_f(t, \mathbb{Z}_j)$ is referred to as the rate function of the failure process $N_f(t, \mathbb{Z}_j)$. Hence, failure rate quantifies the intensity of failure occurrence. An non-stationary failure process has a time-varying intensity function $\lambda_f(t, \mathbb{Z}_j)$ across geo-locations. Assuming a failure process begins at $t = 0$, we have $E\{N_f(t)\} = [E\{N_f(t, \mathbb{Z}_1)\}, ..., E\{N_f(t, \mathbb{Z}_m)\}]^{\mathrm{T}}$, where

$$E\{N_f(t, \mathbb{Z}_j)\} = \int_0^t \lambda_f(v, \mathbb{Z}_j) dv, \tag{2.10}$$

for $1 \leq j \leq m$.

2.3.2 Recovery Process

A recovery process can be characterized by recovery rate function $\lambda_r(t)$, where $\lambda_r(t) = [\lambda_r(t, \mathbb{Z}_1), \lambda_r(t, \mathbb{Z}_2), ..., \lambda_r(t, \mathbb{Z}_m)]^{\mathrm{T}}$. $\lambda_r(t, \mathbb{Z}_j)$ is the expected number of new recoveries per unit time at epoch t and region $\mathbb{Z}_j$,

$$\lambda_r(t, \mathbb{Z}_j) = \lim_{\tau \to 0} \frac{1}{\tau} E\{N_r(t + \tau, \mathbb{Z}_j) - N_r(t, \mathbb{Z}_j)\}. \tag{2.11}$$

An non-stationary recovery process $N_f(t, \mathbb{Z}_j)$ has a time-varying rate function. Assuming the temporal failure process begins at $t = 0$, we have for $1 \leq j \leq m$,

$$E\{N_r(t, \mathbb{Z}_j)\} = \int_0^t \lambda_r(v, \mathbb{Z}_j) dv. \tag{2.12}$$

The recovery rate characterizes how rapidly recovery occurs, which is measured by failure duration D. For an non-stationary recovery process, a failure duration depends on when and where a failure occurs as illustrated in Figure 2.2. Such non-stationarity of recovery is characterized by $g(d|t, \mathbb{Z}_j)$ which is a conditional probability density function of failure duration $D = d$ given failure time $T = t$ at region $\mathbb{Z}_j$. For a given threshold $d_0 > 0$, the conditional probability that a duration is bounded by d_0 for failures occurred at time t is

$$P\{D < d_0|t, \mathbb{Z}_j\} = \int_0^{d_0} g(v|t, \mathbb{Z}_j) dv. \tag{2.13}$$

When d_0 is sufficiently small, this probability characterizes rapid recovery that occurs shortly after failures. For a given d_0, the larger $P\{D < d_0|t, \mathbb{Z}_j\}$ is, the more rapid recovery dominates a recovery process. Given desired value of probability $P\{D < d_0|t, \mathbb{Z}_j\}$, the smaller d_0 is, the more dominating the rapid recovery is.

Rapid recovery is referred to as infant recovery. This terminology is borrowed from infant mortality in survivability analysis [98]. Infant recovery is a desirable characteristic of the smart grid. In contrast, slow recovery is referred to as aging recovery in analogous to aging mortality [99]. Infant and aging recovery can be formally defined as follows.

Definition: Let $d_0 > 0$ be a threshold value. If a node remains in failure for a duration less than d_0; a recovery is an infant recovery. Otherwise, the recovery is aging recovery.

Infant recovery is characterized by $P\{D < d_0|t, \mathbb{Z}_j\}$. Aging recovery is characterized by $P\{D > d_0|t, \mathbb{Z}_j\}$.

2.3.3 Joint Failure-Recovery Process

A joint failure-recovery process characterizes an entire life cycle of a failure-recovery process (FRP), and represents the total number of nodes $N(t, \mathbb{Z})$ in failure state at time t in region $\mathbb{Z}$(Equation 2.3). The expected number of nodes in failure can be expressed in rate functions,

$$E\{N(t, \mathbb{Z}_j)\} = \int_0^t [\lambda_f(v, \mathbb{Z}_j) - \lambda_r(v, \mathbb{Z}_j)]dv. \tag{2.14}$$

Failure-and-recovery process can be viewed as a birth-death process. However, commonly used birth-death processes have a stationary distribution of failure duration and assume independence between failure occurrence t and failure duration d [100]. Here, these two assumptions do not hold. This implies that failures occurred at different time can last different duration. For example, under strong and sustained hurricane wind, failures that do not happen in day-to-day operation can occur due to falling debris and power lines. We shall further elaborate this through the real-life examples in Sections 2.4 and 2.5.

A recovery process is related to a failure process through a probability density function of failure durations.

Theorem *Let $\{N_f(t, \mathbb{Z}_j)\}$ be an independent increment (failure) process with a rate function $\lambda_f(t, \mathbb{Z}_j)$, $1 \le j \le m$. Let $D(t)$ be the duration of a failur occurred at time t and region $\mathbb{Z}_j$. $D(t)$ has a conditional probability density function $g(d|t, \mathbb{Z}_j)$, where $d \ge 0$, $t \ge 0$. Then recovery rate $\lambda_r(t, \mathbb{Z}_j)$ satisfies*

$$\lambda_r(t, \mathbb{Z}_j) = \int_0^t g(t - s|s, \mathbb{Z}_j)\lambda_f(s, \mathbb{Z}_j)ds, \tag{2.15}$$

where $1 \le j \le m$, $d = t - s$ with s and t being the failure time and recovery time respectively.

The theorem is a corollary of the Transient Little's Theorem [59]. Intuitively, $g(t - s|s, \mathbb{Z}_j)ds$ can be viewed as the probability that a failure occurred at time s and region $\mathbb{Z}_j$ lasts $t - s$ duration. $g(t - s|s, \mathbb{Z}_j)ds\lambda_f(s, \mathbb{Z}_j)$ is the average number of failures per unit time

recover after $t-s$ duration, i.e., the recovery rate by definition. Aggregating over all failures occurred prior to time t results in Equation 2.15.

2.3.4 What to Learn

What to learn now becomes apparent. Failure rate functions and probability density functions of recovery time completely specify our model to the first moment, i.e.,

- $\lambda_f(t, |\mathbb{Z}_j)$, for $1 \leq j \leq m$,
- $g(t-s|s, \mathbb{Z}_j)$, for $1 \leq j \leq m$.

In general, the forms and the parameters of these two functions are unknown, and need to be learned from real data. The learned functions and the parameters can then be used to estimate the empirical processes. The empirical processes are the sample means $\hat{N}(t, \mathbb{Z}_j)$, $\hat{N}_f(t, \mathbb{Z}_j)$, and $\hat{N}_r(t, \mathbb{Z}_j)$ that estimate the true expectations $E\{N(t, \mathbb{Z}_j)\}$, $E\{N_f(t, \mathbb{Z}_j)\}$, and $E\{N_r(t, \mathbb{Z}_j)\}$, respectively.

2.4 Hurricane Ike

In this section, we apply learning to a real-life example of large-scale utility-service disruptions caused by a hurricane.

2.4.1 Data From Hurricane Ike

Hurricane Ike was one of the strongest hurricanes occurred in 2008. Ike caused large scale power failures, resulting in more than 2 million customers without electricity, and marked as the second costliest Atlantic hurricane of all time [101] [102].

Reported by National Hurricane Center [103], the storm started to cause power failures across the onshore areas in Louisiana and Texas on September 12, 2008 prior to the landfall. Ike then made a landfall at Galveston, Texas on 2:10 a.m. (CDT), September 13, 2008, causing strong winds, flooding, and heavy rains across Texas. The hurricane weakened to a tropical storm at 1:00 p.m. September 13 and passed Texas by 2:00 a.m. September 14.

A major utility provider collected data on power failures from more than ten cities. The failures include failed circuits, fallen poles and power lines, and non-operational substations. The raw data set has of 5152 samples. Each sample consists of the failure occurrence time (t_i) and duration (d_i) of a component (i) in a distribution network from September 12 through 14, 2008. The accuracy for time t is a minute.

2.4.2 Data Processing

The data set contains bursts of failures that occurred within a minute. As a minute is the smallest time scale for each sample, the bursts are considered as dependent failures. Dependent failures are grouped as one failed entity (i), with a unique failure occurrence time t_i and duration d_i. After such preprocessing, the resulting data set has 465 failed entities. Two outliers with negative failure duration are further removed. The remaining 463 failed entities from 7 am September 12 to 4 am September 14 are referred to as nodes. $D = \{t_i, d_i\}_{i=1}^{463}$ is the data set we use for learning.

Spatial variables $\{\mathbb{Z}_i\}$'s can be either chosen a priori or through learning from data. In this work, we choose $\{\mathbb{Z}_i\}$'s to be small cities to include a natural living environment of customers and this method is widely-used by utility providers. There are 13 cities in the data set as illustrated in Figure 2.7.

2.4.3 Temporal Failure Process

We first study the temporal non-stationarity of the failure-and-recovery process. Spatial variables are aggregated across the entire network. This is equivalent to reducing multiple geo-graphical areas to one entire impact-region from the hurricane. Then the geo-temporal failure-recovery process reduces to a temporal process. For notational simplicity, spatial variables are omitted for temporal processes.

The empirical rate function is estimated using a simple algorithm based on moving average [104]: $\hat{\lambda}_f(t) = \frac{\hat{N}_f(t+\tau)-\hat{N}_f(t-\tau)}{2\tau}$, where τ is chosen to be 5 hours. The resulting rate function is overlaid with the samples on the number of failures $\hat{N}_f(t)$ in Figure 2.4, where

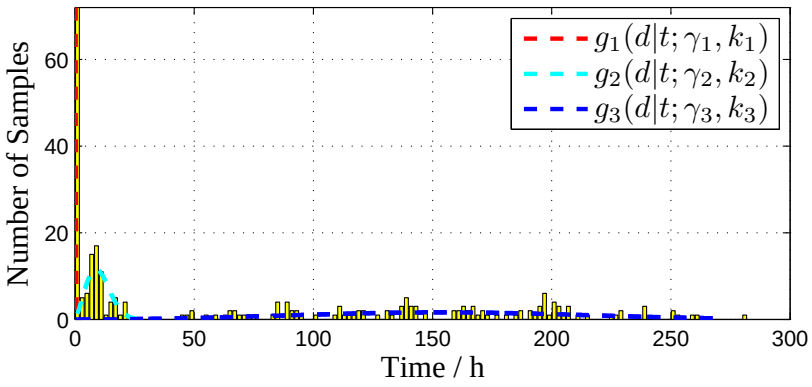

Figure 2.5: Empirical distribution of failure duration for failures occurred during the landfall.

each bin is of duration 1 hour.

The learned failure rate function shows a time-varying rate of new failure occurrence:

(a) Prior to 7 p.m. September 12, the rate was low, i.e., fewer than 5 new failures occurred per hour. Hence 5 per hour is considered as the failure rate in day-to-day operation.

(b) At 7 p.m. September 12, the rate increased sharply first to 25 new failures per hour. In the next 6 hours, the rate reached the peak value of nearly 50 new occurrences per hour. This is consistent to the weather report [103] that the strong wind about 145 mph and flooding impacted the onshore areas prior to the landfall. The time of the peak coincides with the landfall at 2:10 a.m 9/13 CDT.

(c) After staying at the high level for about 12 hours (from 7 p.m. September 12 to 7 a.m. September 13), the rate decreased rapidly back to a low level of less than 5 new failures per hours.

2.4.4 Temporal Recovery Process

We now learn the empirical recovery process characterized by $g(d|t)$, the conditional probability density function of failure duration given failure occurrence time t. As the spatial aggregation removes the geo-location variables, $g(d|t)$ is the conditional density function of failure duration of an entire network.

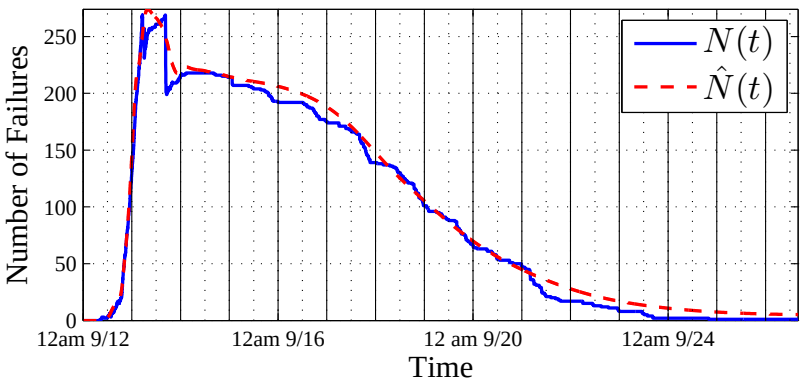

Figure 2.6: Comparison between the joint failure-recovery process $N(t)$ from the data set and the reconstructed process $\hat{N}(t)$ using learned parameters.

We use the 463 samples on the failure durations and occurrences in our data set. These samples result in a joint empirical distribution $\hat{g}(d,t)$ in Figure 2.2. The height of each bin located at (t,d) represents the number of failures that occur at time t and last for duration d. Figure 2.2 shows non-stationarity of failure durations. For example, a large number (217) of failures occurred between 7 p.m. September 12 and 8 a.m. September 13 lasted for more than a day. This indicates that many failures occurred during the surge of the hurricane were difficult to recover. Hence, a non-stationary distribution for $g(d|t)$ is an appropriate assumption.

Given failure occurrence time t, we observe that the distribution of duration is a combination of two components: Infant and aging recoveries. We thus select a mixture model for the probability density function $g(d|t)$ where $d > 0$,

$$g(d|t) = \sum_{j=1}^{l(t)} \rho_j(t) g_j(d|t), \tag{2.16}$$

where $l(t)$ is the number of mixtures at time t, $\rho_j(t)$ $(1 \leq j \leq l)$ is a weighting factor for the jth mixture function $g_j(d|t)$, and $\sum \rho_j(t) = 1$. Weighting factor $\rho_j(t)$ signifies the importance of the jth component $g_j(d|t)$. For a non-stationary recovery process, these parameters vary with failure time t.

A mixture model is chosen since its parameters exhibit interpretable physical meaning [41, 105, 106]. A parametric family of Weibull mixtures is particularly appealing as the parameters correspond to infant and aging recovery directly. Weibull distributions have been widely used in survival analysis [98,99] and reliability theory [100], but not in characterizing recovery from large-scale external disruptions. Specifically, a Weibull distribution is

$$w(d|t;\gamma(t),k(t)) = \frac{k(t)}{\gamma(t)}(\frac{d}{\gamma(t)})^{k(t)-1}e^{-(\frac{d}{\gamma(t)})^{k(t)}}, \tag{2.17}$$

where $d > 0$, $k(t)$ and $\gamma(t)$ are the shape and scale parameters respectively. Hence, jth component in Equation 2.16 is $g_j(d|t) = w(d|t;\gamma_j(t),k_j(t))$.

Shape and scale parameters, $k(t)$ and $\gamma(t)$, are pertinent for characterizing the type of recovery. The smaller $k(t)$ and $\gamma(t)$ are, the faster the decay of $g(d|t)$, the shorter the failure duration and thus the faster the recovery. Hence, $k(t) < 1$ and moderate $\gamma(t)$ (e.g., $\gamma(t) \sim 10h$ or smaller) correspond to infant recovery. $k(t) > 1$ and large $\gamma(t)$ (e.g., $\gamma(t) \sim 100h$) correspond to aging recovery.

For simplicity, we use a piecewise homogeneous function to approximate $g(d|t)$. The failure time t is divided into 5 intervals shown in Figure 2.2. Within interval ψ_i for $1 \le i \le 5$, $g(d|t \in \psi_i) = g_i(d)$ is assumed to be stationary that does not vary with failure time t. For different intervals, $g(d|t \in \psi_i)$'s have different parameters for non-stationarity,

$$g(d|t \in \psi_i) = \sum_{j=1}^{l_i} \rho_{i,j} g_{i,j}(d;\gamma_{i,j},k_{i,j}). \tag{2.18}$$

The parameters of the Weibull mixtures within each interval are learned through maximum likelihood estimation [41] from the data. Failure durations obey different distributions for failures occurred at different intervals, showing the non-stationarity. For example, the first duration ψ_1 (7 a.m. September 12 to 7 p.m. September 12) is when the network was not yet impacted widely by Hurricane Ike. Three Weibull mixtures are learned from the data, with the shape, the scale and weighting parameters as $(1, 0.71, 0.486)$, $(10.5, 14.4, 0.257)$ and $(10.7, 211.8, 0.257)$. The first two components result in dominating infant recovery,

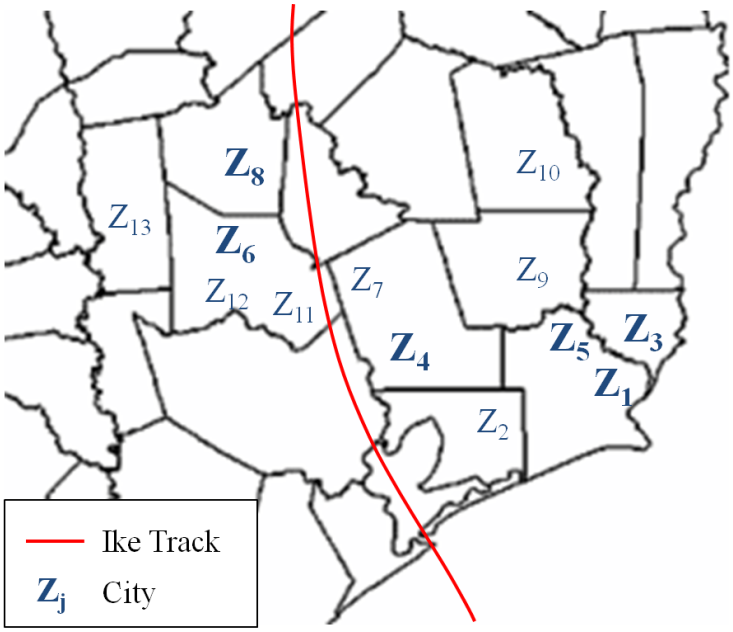

Figure 2.7: Geographical location of the 13 regions (cities).

where 74.3% of failures recovered within a day. In contrast, the third duration ψ_3 (3 a.m. September 13 to 3 p.m. September 13) is when the large-scale failures continued to occur after the landfall. Two Weibull mixtures are learned from the data. The shape, the scale and weighting parameters are $(5.3, 11.0, 0.323)$ and $(12.4, 112.2, 0.677)$, showing dominating aging recovery. As the result, only 32.2% of failures recovered within a day. The second duration ψ_2 (7 p.m. September 12 and 8 a.m. September 13) is around the hurricane landfall, where about a half of the failures occurred experienced infant recovery within a day (see Figure 2.5 for the three Weibull mixtures). For 5 durations overall, the probability of infant recovery within a day changes over time, showing the non-stationary of failure-recovery processes.

We then reconstruct the empirical temporal failure-recovery process $\hat{N}(t)$ with learned $\hat{\lambda}_f(t)$ and $\hat{\lambda}_r(t)$ through Equation 2.14. Figure 2.6 shows the comparisons between $\hat{N}(t)$ and

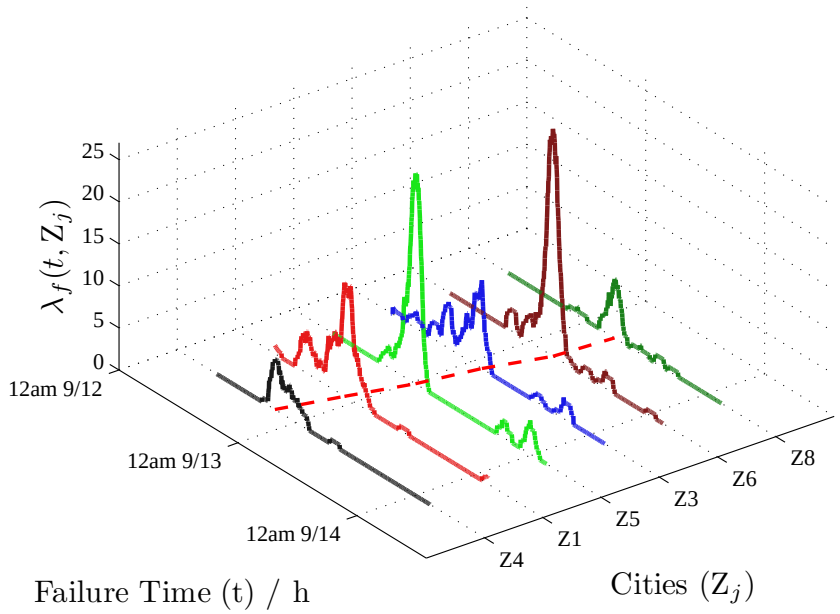

Figure 2.8: Empirical geo-temporal failure rate λ_f during Hurricane Ike. Cities are sequenced with respect to the time when the failure rate reached the peak value in each region.

$N(t)$, the reconstructed and the actual sample paths of the failure-recovery process repectively. The closeness between the two sample pathes shows that the piecewise stationary $g(d|t)$ approximates well the actual failure-and-recovery process.

2.4.5 Geo-Temporal Failure Process

We now incorporate geo-location variables to learn the geo-temporal non-stationarity. Failure process $N_f(t)$ is a geo-temporal process with multiple attributes $N_f(t, \mathbb{Z}_j)$ from m geographical regions, $1 \leq j \leq m$. The empirical failure rate functions $\lambda_f(t, \mathbb{Z}_j)$ for $1 \leq j \leq m$ are estimated using the same algorithm of moving average. The resulting rate vector $\lambda_f(t)$ is multi-variate, consisting of m time-varying functions. Due to the small sample size, there are 6 out of 13 cities shown in Figure 2.7, each of which has sufficient samples ranging from 27 to 101. The hurricane track is plotted as a reference using data from NOAA [103]. Figure 2.8 shows the failure rates of the 6 cities. The multi-variate failure rates exhibit the

following characteristics:

(a) Temporal non-stationarity: At a given geographical region $\mathbb{Z}_j$, $\lambda_f(t, \mathbb{Z}_j)$ is a time-varying function similar to the bell-shaped curve obtained for the entire network. Consider $\mathbb{Z}_5$ as an example. The failure rate was low (few than 5 failures) prior to 7 p.m. September 12. Then, the rate increased sharply and reached the maximum value of 25 new failures per hour, at about 1 a.m. September 13. After that, the rate decreased rapidly to few than 5 failures.

(b) Spatial non-stationarity: At a given time t, $\lambda_f(t, \mathbb{Z}_j)$ is a spatially-varying function. The peak values of failure rates vary from 1.5 to 27 per hour across the 9 cities. The time when the rate reached the peak value varies between 8 p.m. September 12 to 7 a.m. September 13, and is depicted as a dashed line at the bottom in Figure 2.8.

(c) Spatial temporal non-stationarity: The regions are then labeled with respect to the order of failure rates that reached the maximum value in Figure 2.8. For example, the failure rate at City $\mathbb{Z}_4$ reached the peak value first, followed by the failure rates at City $\mathbb{Z}_1$ through City $\mathbb{Z}_8$. The figure shows the geo-temporal characteristic that failure rates at different city reached their peak values approximately from the coast to inland. This appears to be consistent to the movement of the hurricane track (Figure 2.7).

2.4.6 Geo-Temporal Recovery Process

To learn the geo-temporal non-stationary recovery, we extend the mixture model (Equation 2.16) to a geo-temporal bivariate mixture, where for $1 \leq j \leq m$,

$$g(d|t, \mathbb{Z}_j) = \sum_{i=1}^{l(t,\mathbb{Z}_j)} \rho_i(t, \mathbb{Z}_j) g_i(d|t, \mathbb{Z}_j). \tag{2.19}$$

Again our learning focuses on the 6 cities with sufficient samples. Dependencies of failure durations among cities are not studied in this work because of the small sample size.

We apply the piecewise homogeneous distribution function in Equation 2.18 to each region $\mathbb{Z}_j$,

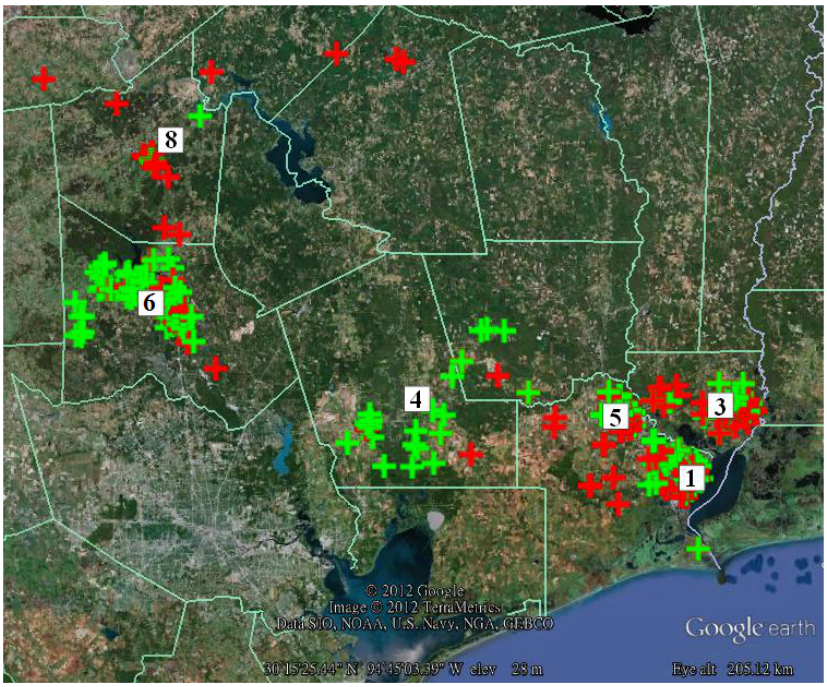

Figure 2.9: Geographical distribution of infant (green) and aging (red) recoveries in the 6 cities: $d_0 = 24$ hours. Graphical tool: Google Earth.

$$g(d|t \in \psi_i, z \in \mathbb{Z}_j) = \sum_{\zeta=1}^{l_{i,j}} \rho_{\zeta,i,j} g_{\zeta,i,j}(d). \tag{2.20}$$

Here, each component $g_{\zeta,i,j}(d)$ is a Weibull distribution $w(d; \gamma_{\zeta,i,j}, k_{\zeta,i,j})$. Mixture $g(d|t \in \psi_i, z \in \mathbb{Z}_j)$'s and their coefficients vary with respect to not only failure occurrence time ψ_i (temporal non-stationarity) but also geo-locations $\mathbb{Z}_j$'s (spatial non-stationarity).

Applying the maximum likelihood estimation [41], we obtain the estimated parameters of Weibull distributions in the 6 cities. Note that due to the small sample size in some of the regions, the parameters of distributions of failure duration have to be assumed, in our implementation, not varying with failure occurrence time within a region. The probability of infant recoveries is also computed accordingly. Three cities (1, 4, 6) show a similar percentage of infant recovery from 66% to 68% whereas the remaining cities (3, 5, 8) have infant recovery from 40% to 45%. Table 2.1 shows the learned model parameters for two example cities. Figure 2.9 shows the geographical distribution of infant and aging recoveries for the 6 cities.

The probability of infant recovery as well as model parameters vary across different geographical regions, showing the spatial non-stationarity of the recovery process. Examining more details, adjacent cities (e.g., 1 and 3) that are close to the coast can exhibit different percentages of infant recovery. Faraway cities (e.g., city 8 which is far in land and city 5 which is close to the coast) can also exhibit a similar percentage of infant recovery. Hence, recovery processes seem to be complex and require further study.

2.5 Hurricane Sandy

We now learn using real data from another real-life example of large-scale disruptions caused by Hurricane Sandy. This provides an understanding how our model and learning approach can be generalized to other hurricanes.

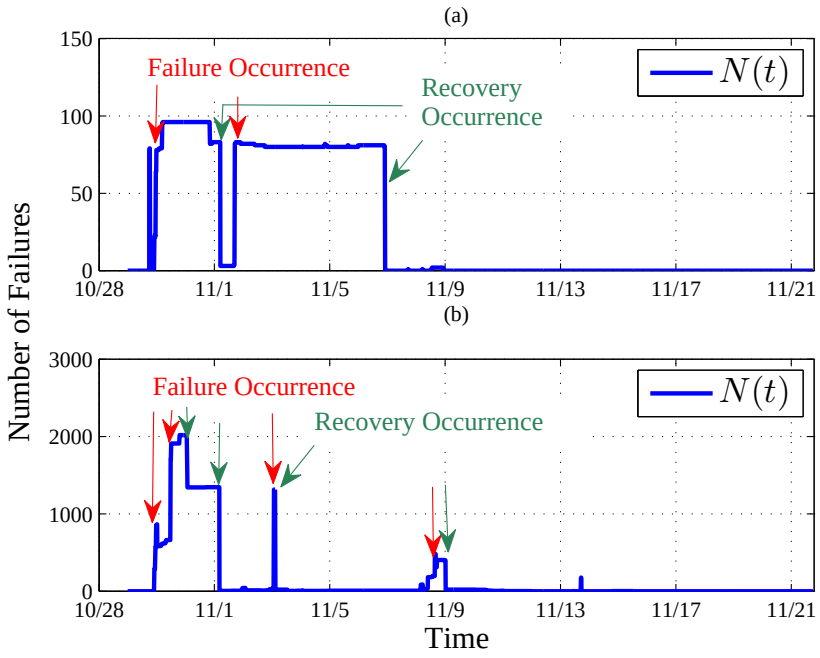

Figure 2.10: Number of customers without power in two counties in New Jersey during Hurricane Sandy: (a) County One; (b) County Two.

2.5.1 Data

Hurricane Sandy had a landfall at Northeastern United States on October 28, 2012. Hurricane Sandy resulted more than 6 million customers without electricity for days. The state with the most customers without power was New Jersey, where about 1.98 million customers lost power supplies [21].

A utility company, reported the number of failures (outages) in more than 10 counties in New Jersey from October 28, 2012 to November 22, 2012. The aggregated number of reported outages is a sample in our data set. Each sample consists of a given geo-location and time t at the scale of 15 minutes (the reporting interval). The geo-location variable $\mathbb{Z}_j$ corresponds to a county in New Jersey for $1 \leq j \leq 14$. The data set consists of 2275 such samples, i.e., $\{N(t, Z_j)\}_{j=1}^{14}$ for time t from October 28 to November 22, 2012. Figure 2.11(a) plots the data. Note that such aggregated data does not provide accurate occurrence time nor duration of each power failure.

Table 2.1: Estimated parameters of distributions of failure durations in 2 cities.

$g(d\|z \in \mathbb{Z}_1)$	1	2	3	$P\{d < 24\}$
$\rho_{1,\zeta}$	0.3478	0.3188	0.3333	
$\gamma_{1,\zeta}$	0.0045	12.1893	197.0316	66.63%
$k_{1,\zeta}$	0.2490	2.7891	3.7629	
$g(d\|z \in \mathbb{Z}_3)$	1	2	3	$P\{d < 24\}$
$\rho_{3,\zeta}$	0.3000	0.1500	0.5500	
$\gamma_{3,\zeta}$	0.0650	12.2138	129.7408	45.37%
$k_{3,\zeta}$	0.2897	3.9992	2.8037	

2.5.2 Empirical Failure Process

Learning now begins with the aggregated number of failures $N(t, Z_j)$ for $1 \leq j \leq 14$, from which failure- and recovery- rates are estimated accordingly. This is a reverse process to learning from detailed failure data in Hurricane Ike.

To learn the failure rate, we recall that $\lambda_f(t) = \frac{d}{dt}E[N_f(t)]$ from Equation 2.10, and $\lambda_f(t) - \lambda_r(t) = \frac{d}{dt}E[N(t)]$ from Equation 2.14. This suggests that a lower bound $\hat{\lambda}_{fl}(t)$ on the failure rate can be estimated from the aggregate number of failures at time t as

$$\hat{\lambda}_{fl}(t, \mathbb{Z}_j) = \frac{d}{dt}N(t, \mathbb{Z}_j), \qquad \text{if} \quad t = t^*, \tag{2.21}$$

where t^* is a time epoch when $N(t^*, \mathbb{Z}_j)$ increases.

To determine how to obtain such an estimate, we examine characteristics of raw (time series) data $N(t, Z_j)$ at the county level. Figure 2.10 shows two examples of the number of aggregated failures $N(t, \mathbb{Z}_j)$ at two different counties in New Jersey. $N(t, \mathbb{Z}_j)$ shows sharp increases and sharp decreases. A sharp increase occurs when the failure rate exceeds the recovery rate whereas a sharp decrease happens when recovery rate exceeds the failure rate. Hence, a change point in $N(t, \mathbb{Z}_j)$ can be used to identify a lower bound for either a failure rate or a recovery rate. In addition, a sharp increase/decrease indicates a salient rather than noisy change point, where a lower bound can be obtained accurately.

We first obtain the positive increments from $N(t, Z_j)$ for each region Z_j using Equation 2.21. We then aggregate the increments over the 14 regions to obtain a lower bound $\hat{\lambda}_{fl}(t)$ for the failure rate of the utility network. $\hat{N}_f(t)$, the estimated lower bound on the number

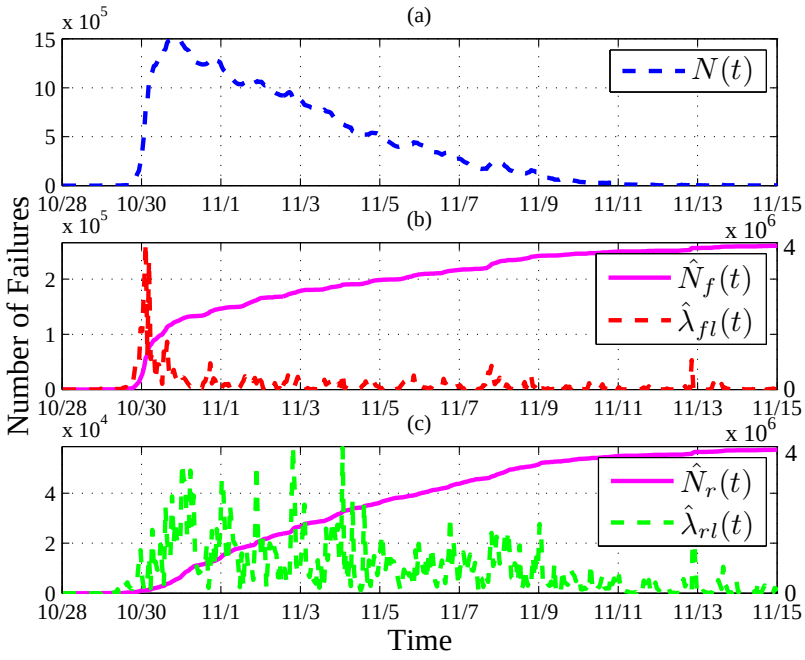

Figure 2.11: Failure process and recovery process from Hurricane Sandy: (a) $N(t)$, (b) $\hat{\lambda}_{fl}(t)$, (c) $\hat{\lambda}_{rl}(t)$.

of failures up to time t, can then be obtained by integrating $\hat{\lambda}_{fl}(t)$, which is shown in Figure 2.11(b).

2.5.3 Empirical Recovery Process

To learn the empirical recovery rate, we apply Equation 2.21 except that t^* corresponds to the time epoch of a decrease in the number of failures. Figure 2.11(c) shows an estimated lower bound $\hat{\lambda}_{rl}(t)$ for recovery rate and the cumulative number of recoveries $\hat{N}_r(t)$ respectively.

Since the aggregated data from Hurricane Sandy does not contain detailed recovery time for each failure, it is impossible to learn the time-varying distribution of failure duration $g(d|t)$. Nevertheless, the aggregated data can be used to estimate a stationary distribution of recovery time, i.e., $g(d)$. As the detailed information on failure duration is not available from the data, we consider a simple distribution with one Weibull mixture $g(d;\gamma,k)$. Applying discrete samples to Theorem 2.3.3, reconstructed recovery rate $\tilde{\lambda}_{rl}(t)$ can be related

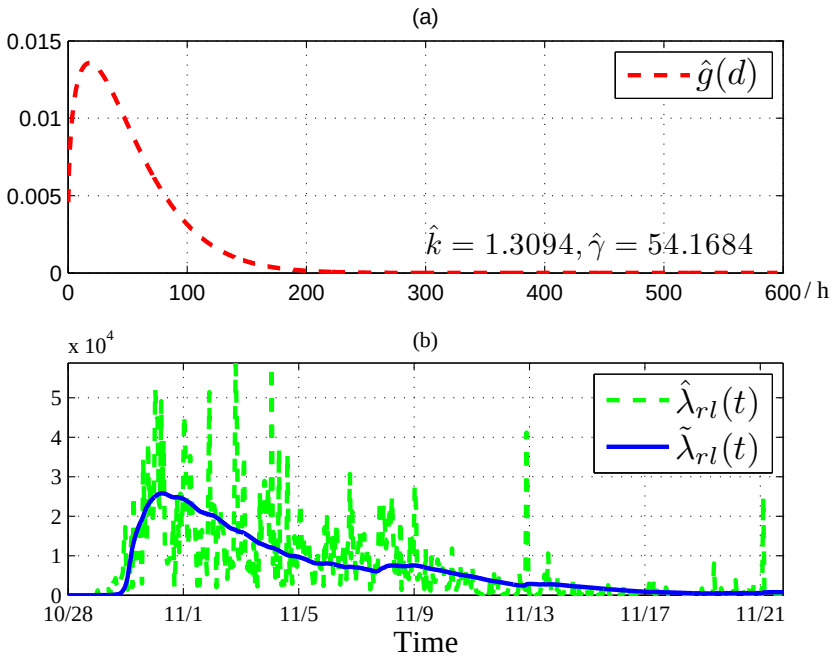

Figure 2.12: Weibull distribution for failure duration $\hat{g}(d)$: (a) Estimated probability density function; (b) Estimated and reconstructed recovery rates.

with $g(d;\gamma,k)$ and $\hat{\lambda}_{fl}(t)$ as

$$\tilde{\lambda}_{rl}(i\cdot\delta) \approx \sum_{j=0}^{i} g(i\cdot\delta - j\cdot\delta)\hat{\lambda}_{fl}(j\cdot\delta)\delta, \tag{2.22}$$

where $\delta = 15$ minuets is the step size, and $i\delta$ is the discrete time. Weibull parameters γ and k are then estimated to minimize the estimation error $\|\tilde{\lambda}_{rl}(t) - \hat{\lambda}_{rl}(t)\|^2$. Figure 2.12 shows the estimated Weibull distribution, where the shape parameter $\hat{k} = 1.3094$ and the scale parameter $\hat{\gamma} = 54.1684$. The resulting stationary distribution of failure durations is then used to reconstruct a lower bound for the recovery rate. Figure 2.12 shows the estimated $\hat{\lambda}_{rl}(t)$ from the data set and the reconstructed $\tilde{\lambda}_{rl}(t)$. Reconstructed $\tilde{\lambda}_{rl}(t)$ thus provides a profile on how the recovery varies with time.

2.6 Findings and Discussions

2.6.1 Findings

Learning from Hurricane Ike and Hurricane Sandy results in the following findings.

2.6.1.1 *Failure process*

Failure rates are time-varying for both Hurricane Ike and Hurricane Sandy. The corresponding failure processes are non-stationary in time and geo-graphical regions. However, the failure rates exhibit different characteristics at the county level for Hurricane Ike and Hurricane Sandy: The failure rates for Hurricane Ike appear to vary gradually. However, the failure rates for Hurricane Sandy exhibit sharp changes, showing that failures occurred in groups. When aggregated over geographical regions, failure rates for both hurricanes exhibit similar characteristics, i.e., first rapidly increasing and then decreasing. More quantitative study is needed to further compare the failure processes for different hurricanes at different spatial scales.

2.6.1.2 *Recovery process*

Learned recovery rates from Hurricane Ike and Hurricane Sandy are both time-varying. For Hurricane Ike, the learned probability distributions of failure durations exhibit non-stationarity in time and geo-locations, i.e., depend on when failures occur. Such distributions constitute both infant and aging recovery, as shown in Table 2.1 and Figure 2.9. The degree of infant recovery, however, is different at different cities. Three out of the six chosen cities recovered more rapidly then the rest. Failures with infant and aging recoveries are also inter-leaving in geo-locations.

The recovery for the provider network from Hurricane Sandy shows a nearly steady rate of 7000 recoveries per hour. In addition, the estimated Weibull distribution of the failure duration exhibits stronger aging recovery than infant recovery. A lack of infant recovery for this utility provider may indicate that power distribution networks suffered virulent disruptions during Hurricane Sandy. The recovery can thus be difficult. Yet, detailed rather than aggregated failure data is needed for accurately estimating distributions of failure durations.

Note that failures and recoveries can occur simultaneously within a 15 minute interval. That is why the amount of increase in $N(t, Z_j)$ is a lower bound of the actual failure rate $\lambda_f(t, Z_j)$. When the number of failures increased rapidly, e.g., from October 28 to October

31, recovery appeared to be minor. When the hurricane passed the area after October 31, recovery dominated. This is shown by the lower bounds of the failure- and the recovery-rate in Figure 2.11 and 2.12.

2.7 Conclusion

This work shows that non-stationary geo-temporal random processes naturally model large-scale failure and recovery of power distribution induced by hurricanes. In particular, multivariate geo-location based $GI(t)/G(t)/\infty$ queues provide such non-stationary failure- and recovery processes. The non-stationary failure and recovery can be completely characterized to the expected values by time-varying failure rate and probability distribution of recovery time across geo-graphical regions.

Real data from two hurricanes have been used to learn failure and recovery processes. Learning detailed failure data from Hurricane Ike reveals that the failure process across different geographical regions follows a similar trend to that of the hurricane. However, the failure- and recovery-processes exhibit different infant and aging recovery across geographical regions. Learning aggregated data from an impact area by Hurricane Sandy shows that our model can infer failure- and recovery rates using aggregated data. The failure rates have more significant discrete components for Hurricane Sandy than for Hurricane Ike at geographical regions. The recovery process is dominated by aging recovery for one utility network from Hurricane Sandy but consists of a significant component of infant recovery for another utility from Hurricane Ike. This shows that $GI(t)/G(t)/\infty$ model is indeed needed for general failure- and recovery-processes in dynamic queues. Note that these findings are for power distribution through open rather than underground networks.

These findings call for subsequent research on how distributed power distribution are impacted by external disruptions. For example, power failures and recoveries are yet to be studied at all impact areas for Hurricane Sandy. Spatial temporal dependencies among power distribution networks at different geographical regions need to be studied explicitly.

This requires combining detailed configurations of power distribution with the dynamic model. These studies shall provide further understanding on how to enhance the distributed power infrastructure.

CHAPTER 3

DYNAMIC MODELING OF TOPOLOGICAL FAILURES AND RECOVERIES OF POWER DISTRIBUTION SYSTEMS

In this chapter, we address the issues of topological impact of distribution system structures on power failures and recoveries. A focus is on incorporating pertinent characteristics of topological network structures into spatial temporal modeling. Such characteristics are new notations as dynamic failure- and recovery-neighborhoods. The neighborhoods quantify correlated failures and recoveries due to topology and types of components in power distribution. The resulting model is a multi-scale non-stationary spatial temporal random process. Using the model and large-scale real data from Hurricane Ike, unique characteristics are identified: The failures follow the 80/20 rule where 74.3% of the total failures result from 20.7% of failure neighborhoods with up to 72 components "failed" together. Thus the hurricane caused a large number of correlated failures. Unlike the failures, the recoveries follow 60/90 rule: 59.3% of recoveries resulted from 92.7% of all neighborhoods where either one component alone or two together recovered. Thus about 60% recoveries were uncorrelated and required individual restorations.

The rest of the chapter is organized as follows. Section 3.1 provides background knowledge and an example of large-scale failures at a power distribution network. Section 3.2 formulate the problem and define dynamic power distribution topology, failure neighborhood and recovery neighborhood. Section 3.3 develops a problem formulation of spatial-temporal non-stationary random processes. Section 3.4 describes the real data from Hurricane Ike and provide data analytics. Section 3.5 concludes the chapter.

3.1 Problem Description

Consider a node that represents a network component such as a substation, a transformer, or a link as a feeder/power line. Severe weather can induce a failure directly to a node.

For example, flooding can cause a non-functional substation and other equipment failures. High winds can cause fallen poles or trees on power lines. Such weather-induced failures often occur in minutes resulting from evolving severe-weather conditions [16].

A weather-induced failure, referred to as a failure in short, can result in secondary failures through a network structure. A network structure consists of a topology and different types of components. For example, unbalanced currents from a failure can cause burned line fuses as secondary failures. A failure upstream can also result in losses of electricity, but no damage, at nodes downstream in a distribution tree. For example, either a non-functional substation or a broken link cause a loss of power to downstream nodes. Those nodes without electricity service are referred to as outages. Secondary failures and outages occur at a smaller time scale of subminutes, as impacted by a network structure. Disruptions include failures, secondary failures and outages.

Recovery occurs at two time-scales also. Self-recovery occurs in subminutes. Manual repairs to damaged nodes occur at the time scale of minutes or longer [16]. When a failure- or an outage-node regains electricity supply, downstream outage nodes regain the service together. Hence, the multi-scale characteristics need to be quantified for disruption and recovery respectively.

3.2 Models of Dynamic Topology

3.2.1 Failure and Neighborhoods

Let $X_i^{(w)}(t)$ be the state of node i at time t, where i specifies both a network location and a geo-location of the node, $1 \leq i \leq n$. n is the total number of nodes in a network. $t > 0$ is continuous time. For simplicity, a node takes two states: $X_i^{(w)}(t) = 1$ if node i is in disruption. $X_i^{(w)}(t) = 0$ if node i is in normal operation. w specifies three scenarios: $w = f$ for a failure induced by exogenous weather, $w = f'$ for a secondary failure, and $w = o$ for an outage. An outage or a secondary failure is induced by a failure occurred at a network neighbor. A network neighbor here is a node at the upstream of a distribution network with a tree topology.

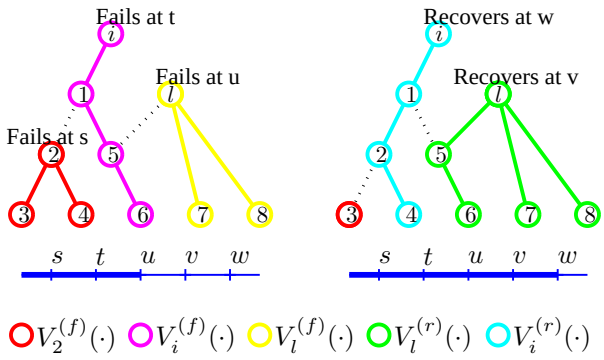

Figure 3.1: Example of neighborhoods.

Disruption $A_i^{(w)}(t)$ is a state transition from normal to disruption $\{X_i^{(w)}(t-\Delta t) = 0, X_i^{(w)}(t) = 1\}$, which occurs in $(t - \Delta t, t]$ at node i, $t > 0$, $w = \{f, f', o\}$. $\Delta t > 0$ is sufficiently small so that there is only one failure, and one set of secondary failures or outages occurred in $(t - \Delta t, t]$.

Failure neighborhood $V_i^{(f)}(t)$ is a new notion of dynamic topology, consisting of the downstream nodes that are in normal operation preceding failure i at $t - \Delta t$. That is, for any $j \in V_i^{(f)}(t)$, either outage $A_j^{(o)}(t)$ or secondary failure $A_j^{(f')}(t)$ occur with failure i. Hence, a failure neighborhood characterizes correlated failures and outages.

3.2.2 Recovery and Neighborhoods

Recovery $B_i^{(w)}(t)$ is the state transition from disruption to normal $\{X_j^{(w)}(t - \Delta t) = 1, X_j^{(w)}(t) = 0\}$, which occurs in $(t - \Delta t, t]$ at node i, $t > 0$, $w = \{f, f', o\}$. When $w = f$ (or $w = f'$), failure i is repaired. When $w = o$, an upstream neighbor of node i is repaired.

Recovery neighborhood $V_i^{(r)}(t)$ is another new notion of dynamic topology, consisting of the downstream neighbors of node i that are in outage at $(t-\Delta t, t)$ prior to the restoration. $\Delta t > 0$ is sufficiently small so that there is one restoration and one set $V_i^{(r)}(t)$ of recoveries in $(t - \Delta t, t]$.

3.2.3 Example

Figure 3.1 shows an example of disruption and recovery as well as the neighborhoods. First, node 2 fails at time s, inducing secondary failure 3 and outage 4, i.e., $V_2^{(f)}(s) = \{3, 4\}$. Then node i fails at $t > s$, inducing outages to nodes in failure neighborhood $V_i^{(f)}(t) = \{1, 5, 6\}$. Then node l fails at $u > t$, inducing outages to $V_l^{(f)}(u) = \{7, 8\}$. Note that node 5 is a downstream neighbor of both nodes i and l but only belongs to failure neighborhood $V_i^{(f)}(t)$ of node i by definition. Hence failure neighborhoods are non-overlapping for failures occurred at different locations and time.

Failure l is repaired at $v > u$, restoring failure l and outages in recovery neighborhood $V_l^{(r)}(v) = \{5, 6, 7, 8\}$. Finally, failure i is repaired at $w > v$, restoring failure i and outages in $V_i^{(r)}(v) = \{1, 2, 4\}$. Secondary failure 3 remains to be restored. This example illustrates failure- and recovery-neighborhoods that are dynamically changing due to evolving failures and reconfiguration in restoration.

Other patterns are possible for failure and recovery. For example, all outages $\{1, 2, 3, 4, 5, 6\}$ can be reconfigured to connect to node k that is in normal operation, thus recover at time v together. Failures i and l recover at later time y and z respectively, with empty recovery neighborhoods $V_i^{(r)}(y) = V_l^{(r)}(z) = \phi$. This scenario occurs when it is more time consuming to repair a failure than restore power to outages.

3.3 Non-Stationary Spatial Temporal Processes

A dynamic network environment emerges from the above problem setting: External severe weather causes network nodes to fail. The failed nodes induce secondary failures and outages at their network neighbors. Failures/outages then recover together with their neighbors. Such disruption and recovery are modeled as non-stationary spatial temporal random processes, with dynamic neighborhoods at the component-level, and aggregations of components in a service region.

3.3.1 Disruption Process

Our modeling starts from the component-level. n nodes in a tree topology form a spatial temporal process, consisting of a network of random state transitions as binary variables $\{I[A_i^{(w)}(t)], I[B_i^{(w)}(t)]\}$, for $t > 0, 1 \leq i \leq n, w = \{f, f', o\}$. $I(A)$ is an indicator function. $I(A) = 1$ if the event A occurs; otherwise, $I(A) = 0$. Let $\Delta N_i^{(d)}(t)$ be the number of nodes that are disrupted from electricity service in $(t - \Delta t, t]$. For a sufficiently small $\Delta t > 0$, it is natural to assume that only one weather-induced failure occurs at node i, and one set of related secondary failures and outages in $(t - \Delta t, t]$. Then

$$\Delta N_i^{(d)}(t) = I[A_i^{(f)}(t)] + v_i^{(f)}(t) I[A_i^{(f)}(t)], \tag{3.1}$$

where $v_i^{(f)}(t) I[A_i^{(f)}(t)]$ is a set of secondary failures and outages in neighborhood $V_i^{(f)}(t)$. $v_i^{(f)}(t) = \|V_i^{(f)}(t)\|$ is the size of the failure neighborhood at node i and time t. $v_i^{(f)}(t)$ characterizes correlated disruptions. The larger $v_i^{(f)}(t)$ is, the more correlated disruptions for the node at time t.

Definition 1 ***Failure, outage and disruption rate***. *Failure rate of node i at time t is the expected number of state transitions from normal to (weather-induced) failures per unit time at node i, which is*

$$\lambda_i^{(f)}(t) = \lim_{\Delta t \to 0} \frac{E\left\{I[A_i^{(f)}(t)]\right\}}{\Delta t}. \tag{3.2}$$

Here $E\{\cdot\}$ represents expectation. Outage rate that is induced by failure i at time t is the expected number of state transitions from normal to outage per unit time at failure neighborhood $V_i^{(f)}(t)$. For simplicity of notation, the outage rate here includes secondary failures also, where

$$\lambda_i^{(o)}(t) = \lim_{\Delta t \to 0} \frac{E\left\{v_i^{(f)}(t) I[A_i^{(f)}(t)]\right\}}{\Delta t}. \tag{3.3}$$

Disruption rate at node i is $\lambda_i^{(d)}(t) = \lim_{\Delta t \to 0} \frac{1}{\Delta t} E\{\Delta N_i^{(d)}(t)\}$,

$$\lambda_i^{(d)}(t) = \lambda_i^{(f)}(t) + \lambda_i^{(o)}(t). \tag{3.4}$$

A disruption rate shows the impact of severe weather and a network structure. A failure neighborhood shows explicitly impacts of topology and heterogeneous types of components. When $E\{v_i(t)I[A_i^{(f)}(t)]\} \approx E\{v_i(t)\}E\{I[A_i^{(f)}(t)]\}$,

$$\lambda_i^{(o)}(t) \approx \lambda_i^{(f)}(t)E\{v_i(t)\}, \tag{3.5}$$

$$\lambda_i^{(d)}(t) \approx \lambda_i^{(f)}(t)(1 + E\{v_i(t)\}). \tag{3.6}$$

These simple expressions show that the outage rate is approximately the failure rate multiplied by the expected neighborhood size. The resulting disruption rate is thus proportional to the failure rate and the total expected number of disruptions at node i and its neighbors.

3.3.2 Recovery Process

The number of nodes that are recovered in $(t - \Delta t, t]$ can be obtained similarly,

$$\Delta N_i^{(r)}(t) = I[B_i^{(f)}(t)] + v_i^{(r)}(t)I[B_i^{(f)}(t)], \tag{3.7}$$

where $I[B_i^{(f)}(t)]$ is the state of recovery for failure i. $v_i^{(r)}(t) = \|V_i^{(r)}(t)\|$ is the size of a recovery neighborhood $V_i^{(r)}(t)$. Recovery process is characterized by the recovery rate defined as follows.

Definition 2 ***Recovery rate***. *The recovery rate for node i and its neighbors in $V_i^{(r)}(t)$ at time t is*

$$\lambda_i^{(r)}(t) = \lim_{\Delta t \to 0} \frac{E\left\{I[B_i^{(f)}(t)](1 + v_i^{(r)}(t))\right\}}{\Delta t}. \tag{3.8}$$

The recovery rate and neighborhoods are dynamic, showing a changing topology in restoration. The time-varying rates and neighborhoods show the non-stationarity of disruption- and recovery-processes.

3.3.3 Joint Failure and Recovery Processes

Disruption and recovery are related through disruption durations. Let $D_i^{(w)}(\tau)$ be the disruption duration at node i and time τ, $w = f, o$. For node i, the total number of disruptions that occurred at $(\tau - \Delta\tau, \tau]$ and not restored at time t, $0 < \tau < t$, include failure

$I[A_i^{(f)}(\tau)]I[D_i^{(f)}(\tau) > t-\tau]$, and failure- induced outages $\sum_{j\in V_i^{(f)}(t)} I[A_j^{(o)}(\tau), A_i^{(f)}(\tau)]I[D_j^{(o)}(\tau) > t-\tau]$, i.e.,

$$N_i(t;\tau) = I[A_i^{(f)}(\tau)]I[D_i^{(f)}(\tau) > t-\tau] + \sum_{j\in V_i^{(f)}(t)} I[A_j^{(o)}(\tau), A_i^{(f)}(\tau)]I[D_j^{(o)}(\tau) > t-\tau]. \quad (3.9)$$

The rate for the number of disruptions yet to be restored at node i and time t is obtained as follows.

Theorem Assume a failure duration is independent of the failure- or the outage occurrence time in $(\tau-\Delta\tau, \tau]$ at node i [59]. Then, rate $\lambda_i(t)$ for the number of disruptions yet to be restored is

$$\lambda_i(t) = \lim_{\Delta t\to 0} \frac{E\{\Delta N_i(t;\tau)\}}{\Delta t} = \lambda_i^{(f)} g_i^{(f)}(t-\tau) + E_{V_i^{(f)}(\tau)} \sum_{j\in V_i^{(f)}(\tau)} h_j, \quad (3.10)$$

where $g_i^{(f)}(t-\tau)$ is the probability density function of failure duration for node i given the failure occurrence time. h_j is the conditional expectation, i.e., the rate of change for outages not yet restored at time t given failure neighborhood $V_i^{(f)}(\tau)$,

$$h_j = E\left\{I[A_j^{(o)}(\tau), A_i^{(f)}(\tau)]\right\} g_i^{(o)}(t-\tau), \quad (3.11)$$

$g_j^{(o)}(t-\tau)$ is the probability density function for outage j occurred at τ lasted for duration of $t-\tau$, given $j \in V_i^{(f)}(\tau)$. $E_{V_i^{(f)}(\tau)}\{\cdot\}$ is the expectation over $V_i^{(f)}(\tau)$. Then the rate of change for disruptions yet to be restored at node i is $\lambda_i(t) = \lim_{\Delta t\to 0} \frac{E\{N_i(t;\tau)\}}{\Delta t}$, where

$$\lambda_i(t) = \lambda_i^{(d)}(t) - \lambda_i^{(r)}(t). \quad (3.12)$$

The proofs draw approaches from [59]. Intuitively, the theorem shows that failure- and recovery-processes jointly determine the speed of restoration in terms of the number of disruptions yet to be restored at any given time.

3.3.4 Aggregation at Subnetwork-Level

Now let $N^{(w)}(t)$ be the number of disruptions in a subnetwork in a service region,

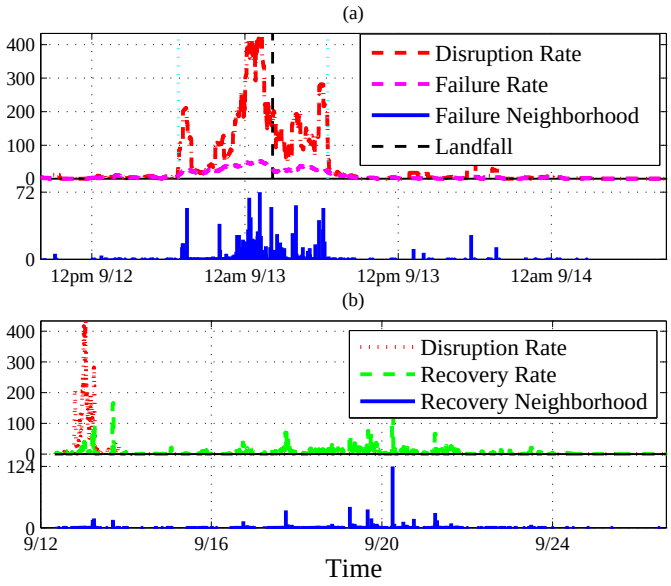

Figure 3.2: Empirical rate functions of the network: (a) Failure rate, disruption rate, and size of failure neighborhood; (b) Recovery rate and size of recovery neighborhood.

$$E\{N^{(w)}(t)\} = \int_0^t \lambda^{(w)}_{i(\tau)}(\tau)d\tau, \tag{3.13}$$

where $w = \{f, f', o\}$. $i(\tau)$ indicates the location of a disruption i at time τ. $d\tau$ is assumed to be small so that at most one failure and one neighborhood of secondary failures/outages occur in $(\tau - d\tau, \tau)$. The expected number of disruptions $E\{N^{(d)}(t)\}$ occurred up to time t is the sum of expected failures and outages (with secondary failures),

$$E\{N^{(d)}(t)\} = E\{N^{(f)}(t)\} + E\{N^{(o)}(t)\}. \tag{3.14}$$

Let $E\{N^{(r)}(t)\}$ be the expected number of nodes which recover in $[0, t]$ in a subnetwork, then

$$E\{N^{(r)}(t)\} = \int_0^t \lambda^{(r)}_{i(\tau)}(\tau)d\tau. \tag{3.15}$$

3.4 Hurricane Ike and Large-Scale Real Data

The non-stationary spatial temporal model is now applied to studying the impact of a major hurricane. Real data from an operational network is used to obtain empirical disruption and

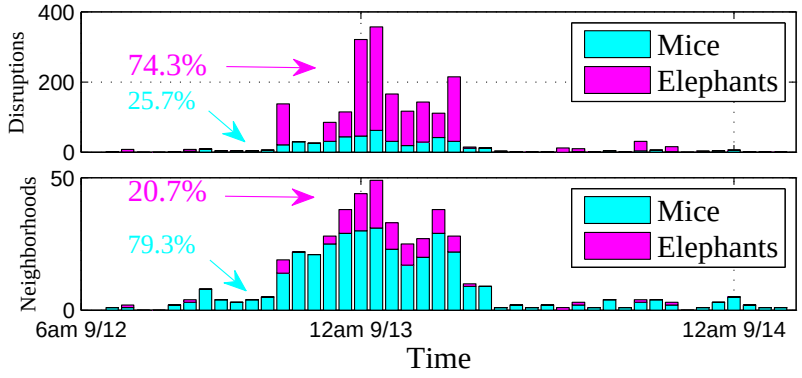

Figure 3.3: Histogram of the disruptions and failure neighborhoods over time. Size of elephants neighborhoods is more than 2.

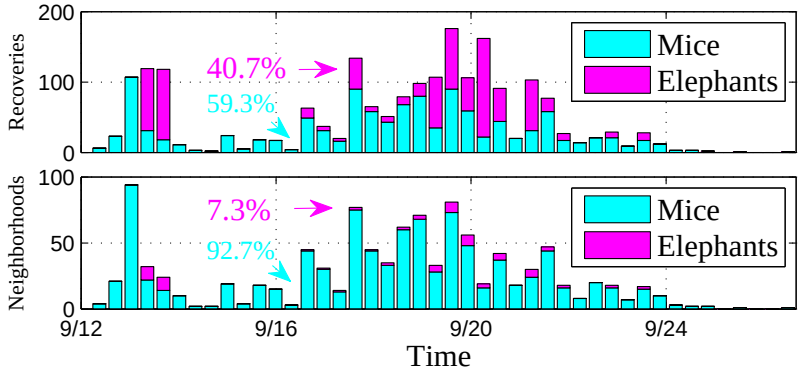

Figure 3.4: Histogram of the recoveries and recovery neighborhoods over time. Size of elephants neighborhoods is more than 2.

recovery rates and to understand impacts of network structures.

3.4.1 Real Data and Processing

Hurricane Ike is one of the strongest hurricanes that occurred in 2008. Ike resulted in more than two million customers without electricity in Louisiana and Texas [102]. A major utility provider collected data on component failures and outages. Our data set consists of 2004 samples (failures or outages) that occurred from 7 a.m. September 12th to 4 a.m. September 14th, during which Hurricane Ike made the landfall. Each sample consists of occurrence time, duration and location (latitude and longitude) of a disruption for a component in a distribution network. The accuracy for time t is one minute.

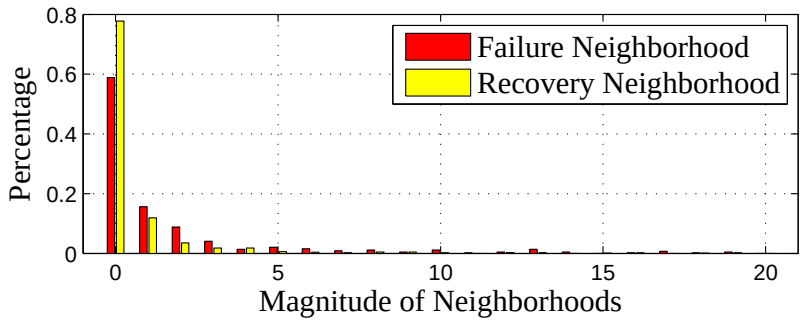

Figure 3.5: Histogram of the sizes of neighborhoods, where size 0 indicates isolated failures, outages or recoveries.

A failure neighborhood includes samples whose failure/ outage occurrences fall within a minute. There are 204 failure neighborhoods of sizes $1 \sim 72$. The remaining 260 failures occurred individually with minutes apart. Similarly, samples with recovery occurrences within a minute are in a recovery neighborhood. There are 241 recovery neighborhoods and 824 individual recoveries.

3.4.2 Empirical Non-Stationary Processes

We now study the empirical non-stationary processes, the impact of topological network structures, and the resilience using the real data.

3.4.2.1 Empirical Disruption Process

We estimate empirical failure rate $\hat{\lambda}^{(f)}(t)$ and disruption rate $\hat{\lambda}^{(d)}(t)$ by aggregating over the components. The disruption rate takes into account of failure neighborhoods. The failure rate is calculated by aggregating disruptions occurred in a minute as one "failure". A simple moving average is used [104], where $\hat{\lambda}^{(w)}(t) = \frac{1}{2\tau}\left(\hat{N}^{(w)}(t+\tau) - \hat{N}^{(w)}(t-\tau)\right)$, with $\tau = 1$ hour, $w = \{d, f\}$. Figure 3.2(a) shows the disruption and failure rates respectively.

The rates and the failure neighborhoods are time-varying, showing the non-stationarity of the disruption process. The failure rate increased to the peak value of 50 new failures per hour around the landfall. The disruption rate exhibited a similar behavior but had a larger peak value of 450 new disruptions per hour around the landfall.

The much larger disruption rate reflects the impact of dynamic network structure: There

were a large number of correlated disruptions during the hurricane. This is further shown in Figure 3.2(a) where large failure neighborhoods occurred mainly during the intense hurricane period, with as many as 72 disruptions in one neighborhood. Hence, the network components and topology were impacted by the hurricane differently during its evolution.

3.4.2.2 Empirical Recovery Process

Recovery rate $\hat{\lambda}^{(r)}(t)$ and the size of recovery neighborhood $v^{(r)}_{i(t)}(t)$ are estimated similarly and shown in Figure 3.2(b). Two bursts of recoveries emerge. The first is infant recovery that occurred along with major failures within six hours after the landfall. The second is aging recovery that occurred about 7.7 hours after. The recovery rate and the size of the recovery-neighborhoods vary with time, showing the non-stationarity of the recovery process.

3.4.3 Neighborhoods: Impact of Network Structures

Dynamic failure neighborhoods are indicative of the impacts of topological network structures and the hurricane. The large failure neighborhoods around the landfall shown in Figure 3.2(a) indicate that the hurricane induced a large number of correlated disruptions. In contrast, failures that occurred individually happened mainly before and after the hurricane. This suggests that correlated failures/outages occurred at the small time scale of subminutes is a pertinent characteristic of the hurricane-induced disruptions.

Using the analogy of elephant and mice flows in computer communication [107], we refer large neighborhoods as elephants, and small neighborhoods as mice. An 80/20 rule emerges for the disruption process: Elephants failure neighborhoods of size more than 2 contribute to 74.3% of total disruptions as shown in Figure 3.3. However, the elephants failure neighborhoods amount to only 20.7% of the total failure neighborhoods. This implies that the majority of disruptions are correlated and induced by elephant failures.

Unlike the disruptions, recovery neighborhoods follow the 60/90 rule: The mice recovery neighborhoods of size 2 or less take up 92.7% of all recovery neighborhoods, amounting

to 59.3% of recoveries, as shown in Figure 3.4. This suggests that around 60% recoveries were uncorrelated, and thus required individual restorations.

Figure 3.5 compares the distributions of the sizes of the failure- and recovery-neighborhoods. 260 (about 13.0%) failures occurred individually whose neighborhood sizes are zero. In contrast, there are 824 (about 41.1%) individual recoveries. Summarizing all observation, failure and recovery processes exhibit significantly different characteristics: The majority of the failures and outages occurred in correlation as elephants, however, recoveries occurred in small patches as mice.

3.5 Conclusion

This work develops a spatial-temporal non-stationary random process to model large-scale disruptions of power distribution induced by severe weather. The model combines non-stationary failure- and recovery-random processes with network structures. Dynamic failure- and recovery-neighborhoods are defined to characterize a topological network structure. The neighborhoods characterize correlated failures and recoveries within networks. Dynamic disruption- and recovery-rates are used as simple quantities for failure- and recovery processes at both component- and subnetwork-level. A resilience metric resulting from the model then characterizes the evolution of failure and recovery. Real data from an operational network during Hurricane Ike is used to study the resilience and the impact of dynamic neighborhoods. An 80/20 rule emerges for failures, showing that hurricane-induced power-disruptions are mostly correlated due to network structures. In contrast, recoveries occur mainly in small patches, and thus required individual restorations. These findings reveal disparities between large-scale failures and recoveries processes, suggesting more in-depth studies at the component level for identifying vulnerabilities and improving resilience.

CHAPTER 4

DATA ANALYSIS OF DISTRIBUTION SYSTEMS ACROSS MULTIPLE SERVICE REGIONS

In this chapter, we expand our study to including the impact of power infrastructure and utility services. We analyse data from four major service regions representing Upstate New York during Super Storm Sandy and daily operations. Using non-stationary spatiotemporal random processes that relate infrastructural failures to recoveries and cost, our data analysis shows that local power failures have a disproportionally large non-local impact on people (i.e., the top 20% of failures interrupted 84% of services to customers). A large number (89%) of small failures, represented by the bottom 34% of customers and commonplace devices, resulted in 56% of the total cost of 28 million customer interruption hours. Our study shows that extreme weather does not cause but rather exacerbates existing vulnerabilities, which are obscured in daily operations.

The rest of the chapter is organized as follows. Section 4.1 provides background knowledge and describe the problem. Section 4.2 develops a problem formulation of dependent non-stationary random processes that include the impact to customers (services and cost). Section 4.3 describes the real data of power distribution failures of four system operators from Hurricane Sandy. Section 4.4 presents the data analysis for the impact of power failures on the system infrastructures. Section 4.5 presents the data analysis for the impact (or cost) of power failures on the utility services to the customers. Section 4.6 discusses our findings and concludes the chapter.

4.1 Problem Statement

Severe weather disruptions, such as hurricanes and winter storms, have become an important initiating cause of large-scale failures to the electric power grid. During Super Storm

Sandy in 2012, power failures occurred across distribution system operators (DSOs) service regions in 21 states, affecting more than 8.5 million customers [21]. Power distribution (i.e., the final stage of energy infrastructure) is particularly vulnerable, representing $\sim 90\%$ of failures [6, 28]. Each disruption has left millions of people without electricity for days, motivating the need to characterize resilience and ultimately re-design energy infrastructure [4, 6, 29].

Resilience is defined as the ability of the power grid to resist failures induced by external hazards, to reduce their impacts on people as much as possible, and to rapidly restore services to utility customers after disruptions [4, 6, 18, 108]. Although the frequency and severity of extreme weather events vary, each event provides a unique opportunity to examine the otherwise hidden vulnerability (i.e., lack of resilience) of power grids. However, the lack of comprehensive and sufficiently detailed failure and recovery data as well as an attendant mathematical model has impeded such analyses. In addition to data granularity, previous studies have been hampered by a lack of geographical scale spanning multiple service territories.

The necessity of obtaining both high-resolution and large-scale failure data poses a scientific challenge to studying resilience [9, 109]. Data on failure and recovery have traditionally been collected mainly for reporting purposes [21]. Such data are stored within individual service territories, each managed by a DSO, and are not generally shared beyond service regions. For example, U.S. federal and state governments only require aggregated information such as the total customer service interruption duration from investor-owned DSOs during major storms [6]. These data are often aggregated into hourly or daily statistics over townships, too crude to study the resilience of the infrastructure and services. As a result, there are only a small number of studies that utilize failure data from even one service region [16, 30, 36–38].

A recent study examines power failures at a national scale across the United States for daily operations, where the data are aggregated annually and over service territories

[95]. At a regional scale, existing studies examine resilience in terms of economic impacts through what-if scenarios (e.g., potential blackout due to failures of power transmission in Los Angeles [110]). However, a resilience study that combines detailed failure data with a large scale across multiple service territories does not hitherto exist.

In addition to real data, a resilience study requires the analytical modeling of failure, recovery and costs with respect to time, geolocation, system location, customers, and their interdependencies. Models capturing the economic impacts of these events are also needed [110].

We study resilience characteristics by examining detailed data from both Super Storm Sandy and daily operations across four major service regions representing Upstate New York, an area of 50,590 square miles. We develop a model that integrates failure, recovery and impact variables from the bottom up [48, 49]. The resulting model is multi-scale in nature, starting from individual components, incorporating structures of power distribution and support to customers, then aggregating to DSO service regions (Methods). Failures, recoveries, and their customer impacts form non-stationary random processes that are dependent on time, geolocation, and system location (Methods). Therefore, resilience is a network property derived from the physical infrastructure to services and customers. We characterize these interdependent processes with network-wide metrics, such as disruption rates, and time-varying failure/recovery probability distributions. These metrics serve as guidelines for identifying vulnerabilities and quantifying time-varying cost using large-scale real data (Methods). In particular, we demonstrate that extreme weather does not cause, but rather exacerbates, certain existing infrastructural vulnerabilities; traditional restoration approaches prioritizing disruptions that affect the highest number of customers are inadequate for minimizing total customer outage times.

4.2 Joint Disruption-Recovery-Cost Processes

4.2.1 Variables and Spatiotemporal Scales

We develop an analytical model for a larger number of interdependent variables at multiple spatiotemporal scales. The variables are provided as follows:

- Failures induced by exogenous severe weather, outages caused by failures within a distribution system (i.e., components that lose power due to a failure upstream but are not damaged). A disruption refers to either a failure or an outage.
- Recoveries.
- Cost to customers.
- Characteristics of a device: Type, geo-location and system location.

Two temporal scales are considered. One is the time scale for failures to occur and recover, in minutes, hours to days. The other is for outages to occur (and recover) within a distribution system, in subseconds [18]. Spatial scales start with components, extend to customers in a given area such as a township, then aggregate to a service region.

4.2.2 Dependent Non-Stationary Processes

Modeling starts from a basic level of a node (i.e., a power component or a protective device). A node failure corresponds to either a damaged power component or an activated protective device. Activated protective devices are included as failures since they interrupt electricity supply to end users. Let $X_i(t)$ be the status of node i at time t. $X_i(t) = 1$ corresponds to failure and $X_i(t) = 0$ is normal. The occurrence of failure i is represented by an indicator function $I[F_i^{(f)}(t)]$, where $F_i^{(f)}(t) = \{X_i(t - \Delta t) = 0, X_i(t) = 1\}$ is an event that node i fails in time duration $(t - \Delta t, t]$ for sufficiently small $\Delta t > 0$. $I[]$ is an indicator function, where $I[A] = 1$ if event A occurs; and $I[A] = 0$, otherwise.

For power distribution with a radial topology, a failure occurs locally without cascading [18]. However, a failure can cause outages where a node loses power without being

damaged. For example, a failure at the upstream of a radial topology usually results in outages at components downstream [18, 111]. The occurrence of an outage (j) is represented by an indicator function $I[F_j^{(o)}(t)]$, where $F_j^{(o)}(t) = \{X_j(t-\Delta t) = 0, X_j(t) = 1 | X_i(t-\Delta t) = 0, X_i(t) = 1\}$. We define $N_i(t)$ as the neighborhood of failure i that consists of the induced outages [18]. Then $j \in N_i(t)$. The outages and the failure are assumed to occur at the same time, i.e., $I[F_j^{(o)}(t)|F_i^{(i)}(t)] = 1$ for $j \in N_i(t)$, as outages proceed a failure in subseconds [18]. A system disruption $F_i^{(d)}(t)$ is either a failure ($d = f$) or an outage ($d = o$). The occurrence of a system disruption is denated as $I_i^{(d)}(t) = I[F_i^{(d)}(t)]$ in Methods. In this work, we assume that a disruption is already detected [13, 112]. This simplifies modeling; meanwhile, enables us to use the real data collected from power distribution.

Recovery occurs when failures and outages are restored. The speed of recovery is characterized by how long disruptions last. Let $D_k(v)$ be the duration of a disruption that occurs at node k and time v. Indicator function $I[D_k(v) > t - v]$ represents a recovery event, where a system disruption occurs at v is not yet recovered at t, $0 < v < t$.

Reconfiguration is not included explicitly in modeling failures and outages. However, disruption durations reflect the effect of reconfiguration that usually reduces the service interruption time for customers.

Failures occur randomly in time and locations. For example, given a severe weather event such as Super Storm Sandy, fallen debris can randomly induce failures (e.g., by bringing down wires or resulting in nonfunctional substations). Likewise, recoveries involve random factors such as terrene conditions in the aftermath of a severe weather event. Recoveries also involve constraints such as restoration strategies, limited resources, and planning. Spatiotemporal random processes [49] can thus be used to model failures and recoveries:

1. Disruption process: $\{I[F_i^{(d)}(v)], i \in S(v), v > 0\}$,

2. Recovery process: $\{I[D_k(v) > t - v], k \in \overline{S(t)}, 0 < v < t\}$,

3. Joint disruption-recovery process: $\{I[F_i^{(d)}(v)], I[D_k(v) > t - v], i \in S(v), k \in \overline{S}(t), 0 < v < t\}$,

where $S(v)$ and $\overline{S}(t)$ consist of nodes in normal operations at time v and disruptions at time t respectively. Because disruptions are random and time-varying, so are $S(v)$ and $\overline{S}(t)$. A joint process results from the fact that disruptions and recoveries can occur concurrently in an area.

A system disruption i at power distribution directly interrupts electricity service to customers, and thus induces cost $C_i^{(d)}(t)$. Disruption rate $\lambda_i^{(d)}(t)$ is the first moment that characterizes both the disruption process and its cost. In particular, $\lambda_i^{(d)}(t)$ is the expected increment of cost $\Delta C_i^{(d)}(t)$ caused by system disruption i in $(t - \Delta t, t]$. Such a disruption rate can be obtained from the stochastic equation [49, 59]. Given $S(t)$ (i.e., a set of nodes in normal operation at $t - \Delta t$),

$$\lambda_i^{(d)}(t) = \lim_{\Delta t, \Delta A_i \to 0} \frac{E\left[\Delta C_i^{(d)}(t) | S(t)\right]}{\Delta t \Delta A_i}, \tag{4.1}$$

where ΔA_i is a small area around location i. $E[\cdot]$ is the conditional expectation over randomly occurring disruptions. For $\Delta t > 0$ to be sufficiently small, at most one disruption occurs in $(t - \Delta t, t]$.

As an example, assume the occurrence of disruption i incurs cost c_i to the affected customers. The cost to customers at time t from the failure and the outages are respectively,

$$\begin{aligned} C_i^{(f)}(t) &= c_i I\left[F_i^{(f)}(t)\right], \\ C_i^{(o)}(t) &= \sum_{j \in N_i(t)} c_j I\left[F_j^{(o)}(t) | F_i^{(f)}(t)\right] I\left[F_i^{(f)}(t)\right]. \end{aligned} \tag{4.2}$$

As a special case, c_i represents the number of affected customers. We then have the customer disruption rate that is the expected number of newly affected customers per unit time. The more customers affected by a system disruption, the higher the cost. Furthermore, when each disruption incurs unit cost $c_i = 1$, the customer disruption rate reduces to the system disruption rate, which is the average number of new failures and outages occurred per unit time. Hence disruption rate $\lambda_i^{(d)}(t)$ relates failures with power distribution

infrastructure and impacts to customers.

As prolonged service interruptions are detrimental to customers, the cost needs to incorporate disruption durations. We consider disruption i that occurs in $(v - \Delta v, v]$. Let $G_i(v, t)$ be the to customers evaluated at time t, which in general is a function $f()$ of duration $D_i(v)$, the cost of disruption occurrence $C_i^{(d)}(v)$,

$$G_i(v, t) = f_i(C_i^{(d)}(v), D_i(v), t). \tag{4.3}$$

The cost forms another spatiotemporal point process connecting system disruptions, recoveries and impacts on customers altogether:

$$\{G_i(v, t), i \in S(v), 0 < v < t\}, \tag{4.4}$$

where t is the time for the cost to be assessed and v is when disruption i occurs.

We now adopt an assumption: Given the occurrence time v and the network state $S(v)$, a disruption and its recovery are conditionally independent [59]. The conditional expectation of the cost given $i \in S(v)$ can be characterized by the system failure rate and the conditional expected cost,

$$\begin{aligned} &E\{I[F_i^{(f)}(v)]G_i(v, t)|S(v)\} \\ &\approx \lambda_i^{(d)}(v|S(v))\Delta v E[G_i(v, t)|S(v)]. \end{aligned} \tag{4.5}$$

Let $G_i(v, t)$ include costs from failure i and its induced outages. The total cost at a given area is then obtained by aggregating all system disruptions occurred up to time t,

$$E[C(t)] = \int_0^t E_{S(v)}\{\lambda_i^{(d)}(v|S(v))E[G_i(v, t)|S(v)]\}dv, \tag{4.6}$$

where $E[\cdot|S(v)]$ is the conditional expectation over randomly occurring disruptions to components previously in normal operation at the area. $\lambda_i^{(d)}(v)$ is the system disruption rate. Intuitively, $\lambda_i^{(d)}(v)dv$ is the average number of newly occurred system disruptions in $(v-dv, v]$. $E[G_i(v, t)|S(v)]$ characterizes the cost from both the occurrence and recovery of disruption i. $\lambda_i^{(s)}(v|S(v))E[G_i(v, t)|S(v)]dv$ is the resulting total cost to the interrupted customers at time

t, $0 < v < t$. The integration adds up all system disruptions and thus all costs occurring in $[0, t]$.

An example cost is the total customer interruption time due to system disruption i

$$G_i(v, t) = c_i \min\{D_i(v), t - v\}, \tag{4.7}$$

where c_i is the number of interrupted customers. When disruption i is already recovered at time t, $D_i(v) < t - v$, $G_i(v, t) = c_i D_i(v)$. Otherwise, $G_i(v, t) = c_i(t - v)$. When summing up over all disruptions, such cost is the aggregated customer interruption time, which is a commonly used and simple economic cost by Distribution System Operators (DSOs) [64]. Such a cost can be measured using the available data.

As failures, recoveries and costs are dependent in a network setting, the above formulation is stochastic in nature, i.e., derived from bottom-up, starting at the component level and then resulting in network-wide quantities. The rates and the expected cost vary spatially and temporally. Hence the disruption, recovery and cost processes are non-stationary spatially and temporally. Furthermore, $\lambda_i^{(d)}(v|S(v))$ and $E[G_i(v, t)|S(v)]$ are coupled with network state $S(v)$, resulting in non-linear relationships among disruptions and recoveries.

We consider the assumption as reasonable that a disruption and its downtime duration are conditionally independent given the occurrence time v and network state $S(v)$. For example, when recovery prioritizes on restoring a source such as a non-functioning substation, dependencies exist among downtime of disruptions that affect the highest number of customers. However, given the occurrence of one disruption, its downtime exhibits randomness (e.g., due to terrene conditions) which is conditionally independent of failure time. If such an assumption is not adopted, the cost can still be computed but will lose intuitive interpretation in terms of the disruption rate and the conditional expected cost.

4.2.3 Comparison with Prior Work

The cost in Equation 4.6 is motivated by and extends from non-stationary queuing network and our prior works [16, 18, 59]. These prior works assume first-come-first-serve policy for

restoration which does not apply to recovery strategies with priorities used by DSOs. The cost obtained in this work includes not only temporal but also spatial variables. Moreover, our formulation extends the previous works to include costs on customers. As customers are supported by power distribution infrastructure, the formulation must be bottom-up, i.e., starting from individual components, each of which supports various customers. Therefore, aggregated models such as those in the prior work [59] cannot be applied to this work by brute force. One other related work uses reactive point processes to model failures and their evolution [93]. There, parametric models are learned for failure rates; recovery and costs are not considered.

In a broader context, simulation models are developed for resilience under potential large-scale blackout [110]. The models emphasize on economic impacts of blackouts and benefit to resilience through using external resources. Failures and recoveries are not a focus, nor their linkage to cost at the detailed spatiotemporal scales. The types of failures are drawn from what-if scenarios at power transmission, which is different from the actual disruptions and recoveries occurring at power distirbution. Vulnerabilities are studied for the energy infrastructure under the rising temperature and climate change [5, 113]. These models include simulations on weather variables; use topological data from the power grids; thus have a different focus from this work [5].

To complement the prior works, the model derived here exhibits an analytical form on interdependent processes from fine to aggregated spatiotemporal scales. The model characterizes infrastructural failures, restoration by DSOs, and costs to customers in a networked setting. This enables the use of sufficiently detailed real data, resulting in realistic aspects of resilience that complements the existing what-if scenarios. Limited by the available data on cost, our model is applied so far to a simple cost measure commonly used by DSO in Equation 4.7. The current model does not include weather variables.

In summary, the following quantities are used to quantify the first moments of disruption, recovery and cost processes: System and customer disruption rates, probabilities of

disruption durations (or conditional probability distributions of downtime durations given the top percentage of disruptions), and expected cost. These quantities are used in data analysis described by the subsequent sections.

4.3 Data Description

Real data used in this work are both sufficiently detailed and at a large scale. Data are rarely available that provides detailed information at power distribution (e.g., the occurrence and restoration time as well as the geo-location on each failure and recovery). Data in this work are provided by four DSOs in Upstate New York. DSO 1 and DSO4 are medium-size distribution system operators (i.e., each serving $< 500,000$ customers) while DSO 2 and DSO3 are large system operators (i.e., each serving $> 500,000$ customers) [92]. The four DSOs have disjointed service territories, spanning more than $50,950$ square miles. The data set consists of 6,266 system disruptions that occurred during the four-day period ($10/28/2012 \sim 10/31/2012$) when Super Storm Sandy affected Upstate New York (Table 4.1). As many as 646,768 customers lost electricity service. The data sets also consist of 31,721 disruptions during daily operations in the same year.

The data contain detailed information regarding failures and recoveries at the final stage of the electric grid (Table 4.1). Each data sample consists of the following common information across the four service territories: (1) Time when the first customer reported loss of power, (2) time when power was restored, (3) the number of customers affected, (4) the type(s) of activated protective device(s), (5) geo-location and system location of an activated protective device. Activated protective devices include blown fuses at feeders and transformers, open substation breakers and reclosers. The accuracy of each sample is a minute in time, latitude and longitude in geo-locations. System locations of the activated protective devices are provided in terms of the hierarchy (i.e., primary distribution, secondary distribution and customer properties). From the data sets, the cost can be obtained as customer interruption time but not the actual economic loss used in [110].

Table 4.1: Data sets. Size: Number of disruptions and the number of affected customers. Occurrence time: time durations in which the disruptions occurred. Time accuracy of disruption and recovery: one minute. Location accuracy: latitude and Longitude for each disruption. The data sets are preprocessed to remove the disruptions from intentional or prearranged operations, and small storms for normal daily operations.

	Daily Operation		Super Storm Sandy	
	Disruptions (Occurrence time)	Affected Customers	Disruptions (Occurrence time)	Affected Customers
DSO 1	5643 (10/28/2011 ~ 10/28/2012)	302688	1334 (7:43am 10/28/2012 ~ 12:59 pm 10/31/2012)	109392
DSO 2	9992 (10/1/2011 ~ 10/28/2012)	764988	1184 (1:53 am 10/28/2012 ~ 12:51pm 10/31/2012)	113488
DSO 3	13063 (1/1/2012 ~ 10/28/2012)	961114	1866 (1:58 am 10/28/2012 ~ 12:57pm 10/31/2012)	249339
DSO 4	3023 (1/1/2012 ~ 10/28/2012)	225997	1882 (2:39 am 10/28/2012 ~ 12:56pm 10/31/2012)	174549
Total	31721	2254787	6266	646768

The data set from DSO4 has the following exceptions on protective devices. The information on system locations is only provided for activated protective devices at the primary distribution. Two thirds of the samples do not have the recovery time specified uniquely on the types of disrupted devices. Hence, when the cost is examined with respect to different types of devices (Table 4.3), data samples used are ony those disruptions that are uniquely identified by their device types. This results in a reduced data set of 5171 samples used for (Table 4.3).

Overall, it is challenging to obtain sufficiently accurate data during a severe weather event, where data accuracy can be compromised when the impact is severe. The data from Upstate New York are sufficiently accurate, and thus chosen for this study. Although the time of a disruption was taken from the customer calls, the occurrence time is expected to be reasonably accurate (i.e., in minutes) at Upstate New York. This is because there were often multiple calls from customers reporting loss of electricity, especially during a severe weather event.

4.3.1 Super Storm Sandy

Super Storm Sandy was one of the most damaging natural disasters that occurred in 2012. During Super Storm Sandy, power distribution was disrupted for more than 29 DSOs in eight most impacted northeastern states, affecting 8,511,251 customers at the peak of the storm [21]. As reported by National Hurricane Center [114], the storm started to impact the Northeastern coast of the United on October 28, 2012, and the center of the storm made

landfall at about 11:30 p.m. UTC in New Jersey. After the landfall, the storm turned toward the west and then northeast and gradually weakened. The center of the storm became ill defined and the hurricane was considered dissipated after 12 a.m. October 31 UTC [114].

We identify when the service territories were under the impact of Super Storm Sandy based on the following information: the observed best-track of the hurricane [115], the radius of the hurricane-force winds and the tropical-storm-force winds [116]. As the result, October 28 to October 31 2012 is considered as the dominant period of the hurricane for the four DSOs in Upstate New York.

4.3.2 GIS Database

ArcMap, an ArcGIS product, was used to process the data on geo-locations. In particular, spatial analyses were utilized to compare such factors as system locations and DSO service regions, in addition to converting coordinate systems to standard GPS coordinates for plotting. The coordinate system for data was mixed between the United States State Plane Coordinate System (SPCS) in survey feet and the Universal Transverse Mercator (UTM) grid system, using suitable zone codes for New York State. No precision was lost in the coordinate transformation. The resulting GPS coordinates are significant up to and including the sixth decimal place or 0.11 meters, which was more than suitable for our needs. A shape file for the service territory boundaries of the four DSOs was provided by the New York State Department of Public Service.

4.4 Infrastructural Vulnerability

Failures that occurred with respect to power distribution during a severe weather event are largely due to local causes (e.g., fallen debris, damaged poles and area flooding). Unlike transmission systems [51, 117, 118], such failures typically do not cascade in radial power distribution designs. This is problematic because the majority of power distribution for our four DSOs has an overhead radial topology and corresponding protective devices [108]. Failures induced by severe weather can result in outages to downstream devices, which

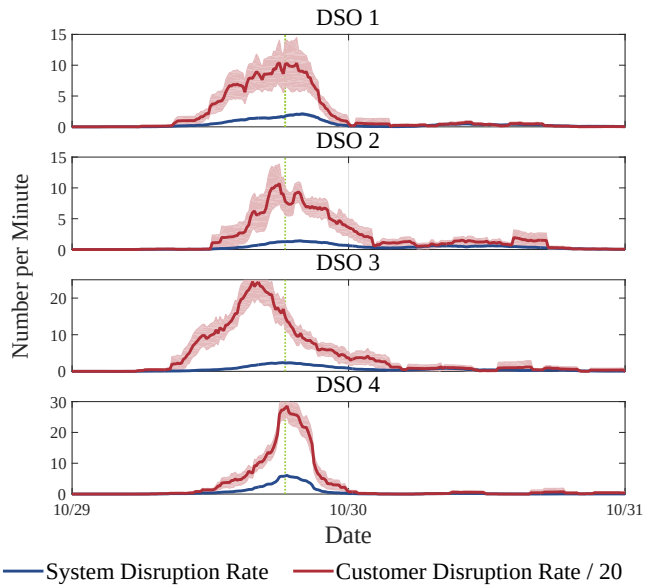

Figure 4.1: System and customer disruption rates of the four DSOs. The rates represent the number of new system (or customer) disruptions per minute. Shaded areas illustrate the error bounds at the 95% confidence interval.

lose power without being damaged (see Section SI1). Nevertheless, disruptions (i.e., either failures or outages) resulting from exogenous events are expected to remain largely local (at individual devices and geolocations [1, 108]). Here, a fundamental question arises: Is the impact of a local failure is also local, affecting only a small number of customers? Disruption rates, which correspond to the marginal temporal costs per unit time, provide an answer (Methods). In evaluating customers and system-level disruptions, we find that a common behavior emerges for the four DSOs shown in Figure 4.1. During Super Storm Sandy, customer disruption rates were 93 to 193 times larger than system disruption rates. These higher rates demonstrate the existence of infrastructural vulnerability, in which local failures have a distinctly non-local impact on customers (Figure 4.6(a)). In fact, the top 20% of system disruptions affected 79% $\sim$ 89% of customers for the four DSOs, and each such disruption interrupted services for more than 74 $\sim$ 107 customers.

4.4.1 Generalized Scaling Law

To quantify the prevalence of non-local impacts on customers, we analyze the dependence between infrastructural failures and affected customers. Because operational power distribution systems are based on engineering design and exhibit irregularities, the scaling behavior we observe (e.g., $20 \sim 80$) cannot be represented using a simple power law distribution [119]. Thus, we obtain a generalized scaling law drawn from the data: a mapping between probability $W(x)$ for a customer affected by a disruption that interrupts electricity service for more than x users and probability $P(x)$ of such a disruption. Taking DSO 1 as an example, the generalized scaling law demonstrates that the top $0.1\% \sim 76\%$ of system disruptions affected $2\% \sim 99.6\%$ of all customers at the 90% confidence interval (Supplementary Table A.3). A similar generalized scaling law applies to the other three DSOs, with small variations, as shown in Figure 4.2(a) (and Supplementary Table A.3).

4.4.2 Comparison to Daily Operations

Do exogenous events, such as Super Storm Sandy, create the infrastructural vulnerability or instead exacerbate an underlying lack of resilience? We apply the methodology outlined above to daily operations to show that vulnerability is inherent to the power distribution infrastructure. Using data on failures in daily operations from the year prior to the hurricane, a similar non-local impact on customers holds (Figure 4.2(b), Supplementary Figure A.2 and Supplementary Table A.3). The mapping between the two probabilities differs by less than $2\% \sim 9\%$ for daily operations and Super Storm Sandy at the 95% confidence level. Thus, customers interrupted by disruptions in daily operations and the storm follow a similar scaling law. Compared to Super Storm Sandy, each disruption in daily operations affected 29, 19, 48, and 21 fewer customers for the four respective DSOs. The similarity between the scaling laws for the storm and daily operations demonstrates that Super Storm Sandy did not create but only exacerbated the non-local impacts on customers.

4.4.3 Cause of Infrastructure Vulnerability

Although the overhead power distribution infrastructure is a complex combination of topology, protection schemes, and supporting mechanism for customers, the four service regions have a common radial and hierarchical structure. The infrastructure and disruptions can be represented by three commonly used system locations [1]: primary distribution, secondary distribution, and customer property. A disruption at the top level can disconnect customers away from a power source in the existing overheard power distribution [18] due to a lack of reconfiguration and distributed generation. Demonstrated by the data (Figure 4.3(a)), among the top 20% of disruptions from Super Storm Sandy, approximately 77% occurred at the primary distribution; each such disruption affected $\sim$ 524 customers on average. The remaining 23% of disruptions occurred at the secondary distribution, each of which affected $\sim$ 218 customers on average.

The impact of the hierarchical design on the number of affected customers is further characterized by the five major types of activated protective devices at the corresponding system locations and through the generalized scaling law (Figure 4.2(b), Figure 4.3(b), Supplementary Figure A.2). For example, non-functional substations, open reclosers, and blown fuses at primary distribution almost exclusively represent the top 20% of disruptions that occurred during both Super Storm Sandy and daily operations; the same type of devices had a non-local impact on customers regardless of weather. Thus, the hierarchical structure is an important underlying cause of the infrastructural vulnerability for overhead power distribution with a radial topology.

4.4.4 Infrastructural Vulnerability Exacerbated by Super Storm Sandy

The degree to which Super Storm Sandy exacerbated the infrastructural vulnerability is characterized by the non-stationary probability distribution $P_1(t)$ for at least one disruption occurring in a service region at time t measured in a minute. Using empirical data from both Super Storm Sandy and daily operations (Supplementary Equation A.3), we find that $P_1(t)$ was less than 0.02 per minute in daily operations but increased to 1.0 at the peak impact

of the storm. The increase in the probability was particularly pronounced for the top (e.g., 20%) disruptions, in which $P_1(t)$ was less than 0.003 in daily operations but increased to the maximum values of 0.6 $\sim$ 1.0 during the storm for the four DSOs (Figure 4.3, Figure A.3 and Supplementary Table A.4). Further relating to the hierarchy, the probability of a disruption at the primary distribution shows a disproportionally large increase of 28 times for the top 20%, compared with 15 times at the two remaining levels (Figure 3(a) and Supplementary Figure A.4(a)). Thus, our study demonstrates that the infrastructural vulnerability was only present at low levels during daily operations until magnified by severe weather events such as Super Storm Sandy.

4.5 Impact to Service and Cost

Multiple failures (i.e., 6,266 system disruptions occurred during Super Storm Sandy) challenge the state of the art in recovery [108]. Demonstrated by the data from our DSOs (Figure 4.4), in daily operations, 90% of the interrupted customers recovered within 6 hours, and all services were restored in one day (Figure 4.4). However, recoveries from Super Storm Sandy lasted 8, 4, 10, and 15 days for the four DSOs.

4.5.1 Recovery

We quantify recovery through the interdependence between failure and recovery processes. The probability density functions of downtime duration given the top percentage of disruptions exhibit a common characteristic in Figure 4.5 for the four service regions during Super Storm Sandy. Disruptions that affected the highest number of customers were usually restored at an early stage of recovery (i.e., the first 24%, 8%, 15%, and 34% of the total restoration time) with peak probability density (0.006, 0.04, 0.003, and 0.002 per minute, respectively). These high-customer disruptions with early recovery constitute so-called Category 1 (”large and early”), amounting to 9% of the total system disruptions; each affected more than 89 customers (Section SI5). Such a characteristic reflects a common practice of repairs: power sources, such as substations, are restored first, followed by

other components downstream. Such a pattern of recovery persists through daily operations except that all disruptions are restored rapidly in minutes or hours (Supplementary Figure A.7). The remaining disruptions are in so-called Category 2, which mainly consists of "small" system disruptions, each of which either affects the bottom 34% of customers or is represented by a common place device, such as a fuse (89%). Category 2 disruptions dominate the late stage of recovery at the four service regions almost exclusively (Supplementary Figure A.6). Category 2 also consists of a small number of disruptions (2%) that affected a large number of customers but recovered late (Table 4.2 and Section SI5).

4.5.2 Cost

The total service cost quantifies the impact of prolonged disruptions on customers, which, as a special case of Equation 4.6, is measured as the total customer interruption time by the data set. Aggregating over only disruptions occurred during the first four days when Super Storm Sandy impacted Upstate New York, the four service territories together experienced approximately 28 million customer hours of interruptions. The "small" disruptions in Category 2 together contribute to approximately 56% of the total cost but only amount to 34% affected customers (Table 4.2). Thus, while "large" disruptions (9% of the total) that affected the highest number of customers were restored early, the large number of small disruptions together (89% of the total) contribute to the major cost (Table 4.2). This illustrates that the aggregation of Category 2 disruptions from low-customer and small-device disruptions results in a disproportionately larger portion of the total cost. Hence, the total service cost in Figure 4.6 (b) exhibits a different behavior than the generalized scaling law for disruptions in Figure 4.6 (a). This suggests that recovery, which is compounded by restoration strategies, available resources, the infrastructural vulnerability and the cost of enhancement, requires consideration of the overall cost of restoration in addition to individual disruptions that affect the highest number of customers.

We further examine the service cost in terms of disrupted devices and the power distribution hierarchy. Data samples with clearly labeled device types are used for this purpose

(Methods). The total cost for the reduced data sets is 20 million customer interruption hours (Table 4.3). Approximately 32% of the total cost results from disruptions by "large devices" (i.e., open substation/circuit breakers and reclosers, as well as non-functioning transformers at the primary distribution). These interrupted devices resulted in 47% of the affected customers. Approximately 69% of the "large devices" are in Category 1 (i.e., recovered "early"). In contrast, 94% blown fuses and other interrupted devices at the lower levels of the system hierarchy are Category 2 "small" disruptions. These interrupted devices amounted to 53% interrupted customers but 68% of the 20 million customer disruption hours (Table 4.3).

This implies that aggregation of the small devices represented by blown fuses and other components at lower level of the system hierarchy, although each affected a moderate number of customers, resulted in a larger portion of the total customer downtime. This again suggests that the early recovery of the components that affected the highest number of customers is insufficient for reducing the total cost to end-users.

Data from daily operations is also studied for disrupted devices as a comparison (Table 4.3). Disruptions in normal daily operations are clearly identified with the types of interrupted devices by the four DSOs. Open substation breakers and reclosers as well as non-functioning transformers at primary distribution amounted to 47% of the interrupted customers and 29% of customer interruption hours. Therefore, a similar disparity of the costs is observed in daily operations between major devices at the primary distribution and the others at the lower levels of the system hierarchy (Table 4.3). Hence, a similar trend of recovery on prioritizing disruptions that affected the highest number of customers is observed for daily operations.

4.6 Discussion and Conclusion

Using large-scale data collected by DSOs in Upstate New York, we obtain critical insights revealing that severe weather events, such as Super Storm Sandy, do not fundamentally

cause infrastructural vulnerabilities. Vulnerabilities are inherently a complement of infrastructure resilience and exist regardless of exogenous factors. Although such infrastructural vulnerabilities may manifest themselves locally, together, they have a profoundly non-local impact on customers. We characterize this asymmetrical relationship between disruptions and affected customers using the generalized scaling law estimated empirically from the data. The similarities of the scaling law for different service territories, and for Super Storm Sandy and daily operations, suggest that the infrastructural vulnerability exists independently of the exogenous events themselves and their effects. Whereas the number of DSOs analyzed is small, their combined service regions span nearly the entirety of Upstate New York. A large-scale analysis of data from multiple DSOs is necessary to understand the prevalence of such vulnerabilities and as a control against exogenous events [83]. As industry increasingly realizes the importance of data collection and study beyond experiences [83], the availability of more detailed data [12], especially regarding restoration and the root causes of failures, may allow for further analysis in recovery dynamics and yield optimal cooperative strategies.

When the recovery process was compounded by multiple factors (e.g., infrastructure vulnerability, cost of enhancement, impacts from severe weather, and available resources), the restoration was apt to prioritize the recovery of disruptions that affected the highest number of customers during both the storm and daily operations. Although such system disruptions incur major costs, the aggregation of smaller disruptions proved to be a significant factor that must be considered in recovery. Unfortunately, recovery is also compelled by constraints introduced by the current power distribution infrastructure: major components, such as substations, must be repaired first due to a lack of distributed generation. Moreover, whereas some failures are easily repairable (resetting breakers or replacing fuses), others may be arduous to restore due to damaged power components or external circumstances, such as flooding [89]. Therefore, multiple factors should be considered jointly when designing enhancement options and recovery strategies for resilience. DSOs must

weigh the impact of infrastructural vulnerability against the economic and societal costs of such improvements [110], in addition to factors not considered in this section, such as life cycle cost [60].

Resilience has a profound impact at all scales, from DSOs to states and nations. Ideally, the inclusion of additional weather data would enable a more comprehensive analysis of power distribution under the effect of extreme meteorological events and, more broadly, climate change [5, 113, 120]. It is challenging for multiple organizations to participate in a large-scale study with detailed organizational data due to a variety of issues, ranging from proprietary information and confidentiality among DSOs to governmental regulations. Using data from a portion of the geographic area affected by Super Storm Sandy, this work demonstrates the feasibility and potential for multiple DSOs and policy makers to collaborate with a common goal of resilience and to make meaningful advances.

As the power industry traditionally learns from severe weather through experience [83, 111], this work demonstrates how the knowledge of resilience can be learned from large-scale data. We have created a theoretical framework that provides a system perspective, starting with detailed information, on infrastructural vulnerabilities, service, and cost to customers by employing spatiotemporal non-stationary random processes. Such a model connects interdependent networks from the infrastructure and DSOs to customers. Moreover, we demonstrate the potential and feasibility of large-scale data analysis guided by modeling at the final stage of the energy grid. Advancing data collection and analysis will benefit DSOs, customers, and policy makers alike, moving all of us toward a resilient energy infrastructure. We hope that our study stimulates more organizations to actively participate in resilience studies.

Table 4.2: Cost. Cost is estimated from the data as the number of affected customers and customer interruption hours for the two categories during Super Storm Sandy. Category 1: system disruptions that affected relatively large numbers of customers and recovered early. Category 2 (Small): disruptions that either affected a relatively small number of customers or on commonplace devices. Category 2 (Large/late): disruptions that affected a large number of customers but recovered late.

	Disruptions			Customers			Customer Interruption Hours		
	Category 1 (Large/Early)	Category 2 (Small)	Category 2 (Large/Late)	Category 1 (Large/Early)	Category 2 (Small)	Category 2 (Large/Late)	Category 1 (Large/Early)	Category 2 (Small)	Category 2 (Large/Late)
DSO 1	102	1228	4	61461	44080	3851	645268	2060193	198880
DSO 2	109	1055	16	68848	30426	14040	113404	284584	90927
DSO 3	154	1635	77	93897	79108	76334	623126	5569573	5342695
DSO 4	186	1618	5	99350	63161	4960	4297389	7701248	812104
Total	551	5536	102	323556	216775	99185	5679187	15615598	6444606
Total		6189			639516			27739390	
Fraction	8.9%	89.4%	1.6%	50.6%	33.9%	15.5%	20.5%	56.3%	23.2%

Table 4.3: Estimated cost with respect to the two groups of most affected devices. The first type ("1") includes substation breakers, reclosers, and transformers located at primary distribution. The second ("2") includes blown fuses and the other affected devices at the secondary distribution and customer property. Partial data of DSO4 is used whose durations are uniquely identified by the device types.

Hurricane								
	Customers				Customer Interruption Hours			
Group of Devices	1		2		1		2	
Category	1	2	1	2	1	2	1	2
DSO 1	40562	8957	20899	38974	379818	500827	265451	1758246
	81.9%	18.1%	34.9%	65.1%	43.1%	56.9%	13.1%	86.9%
DSO 2	51415	17329	17433	27311	80714	122338	32689	252061
	74.8%	25.2%	39.0%	61.0%	39.8%	60.2%	11.5%	88.5%
DSO 3	49469	70379	29846	75122	278769	4791444	320530	5276011
	41.3%	58.7%	28.4%	71.6%	5.5%	94.5%	5.7%	94.3%
DSO 4	2981	1415	34731	33450	86744	147021	1511251	4006487
	67.8%	32.2%	50.9%	49.1%	37.1%	62.9%	27.4%	72.6%
Total	144427	98080	102909	174857	826045	5561630	2129921	11292805
Fraction	27.8%	18.8%	19.8%	33.6%	4.1%	28.1%	10.8%	57.0%
Total	242507		277766		6387675		13422726	
Fraction	46.6%		53.4%		32.2%		67.8%	
Total	520273				19810401			

Daily Operations								
	Customers				Customer Interruption Hours			
Group of Devices	1		2		1		2	
Category	1	2	1	2	1	2	1	2
DSO 1	58207	32870	83207	115353	55505	124957	94143	379492
	63.9%	36.1%	41.9%	58.1%	30.8%	69.2%	19.9%	80.1%
DSO 2	315091	94595	102923	244133	302428	358424	124660	735485
	76.9%	23.1%	29.7%	70.3%	45.8%	54.2%	14.5%	85.5%
DSO 3	147819	177919	67072	304153	153533	813071	64357	1511449
	45.4%	54.6%	18.1%	81.9%	15.9%	84.1%	4.1%	95.9%
DSO 4	20000	10847	10381	29671	23575	49820	12732	109376
	64.8%	35.2%	25.9%	74.1%	32.1%	67.9%	10.4%	89.6%
Total	541117	316231	263583	693310	535042	1346272	295892	2735802
Fraction	29.9%	17.4%	14.5%	38.2%	10.9%	27.4%	6.0%	55.7%
Total	857348		956893		1881314		3031694	
Fraction	47.3%		52.7%		38.3%		61.7%	
Total	1814241				4913008			

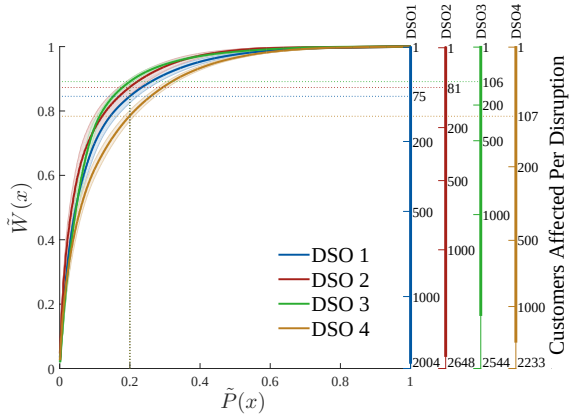

(a)

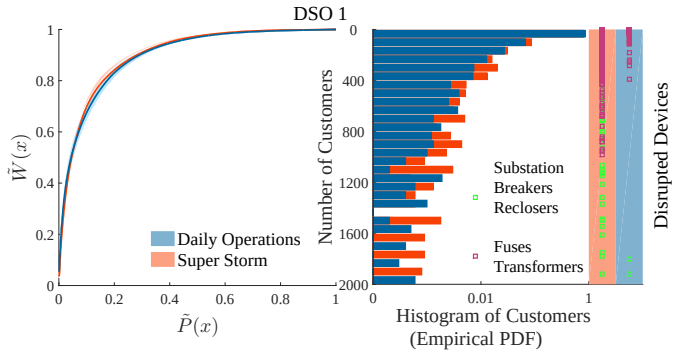

(b)

Figure 4.2: Generalized scaling law. (a) For the four DSOs during Super Storm Sandy: empirical probability $\tilde{W}(x)$ of the number of affected customers, where each of the disruptions affected more than x customers, and empirical probability $\tilde{P}(x)$ that a disruption affected more than x customers. Shaded areas illustrate the estimation error at the 95% confidence level. (b) For DSO 1 during Super Storm Sandy and daily operations as an illustration. Types of disrupted devices are shown on the right with respect to the number of interrupted customers. The histogram shows the percentage of customers from the storm and the daily operations. The generalized scaling laws for the other DSOs during daily operations are in Supplementary Figure A.2.

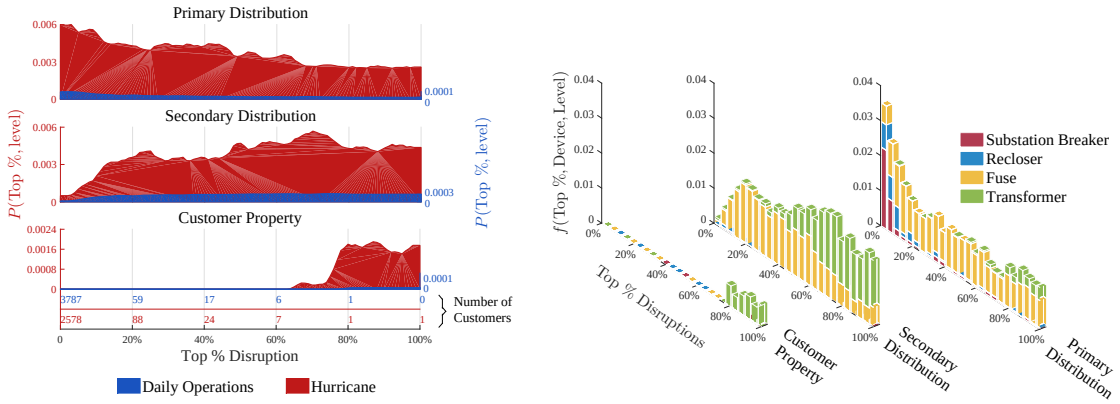

(a) (b)

Figure 4.3: Empirical probability of disruptions. (a) Empirical probability distribution $P(\text{Top }\%, \text{level})$ of the top percentage of disruptions at the three levels of the hierarchy from the storm and daily operations. The horizontal axis shows the percentage of disruptions from 0 (the very top) to 100% and level represents the primary and secondary distributions as well as customer properties. The vertical axis shows the empirical probability distribution per minute for every 1% of the disruptions. (b) Empirical probability distribution $f(\text{Top }\%, \text{level, device})$ of system disruptions specified further by the type of device at the three levels of the hierarchy for Super Storm Sandy. The five types are chosen from the most disrupted devices in the data set.

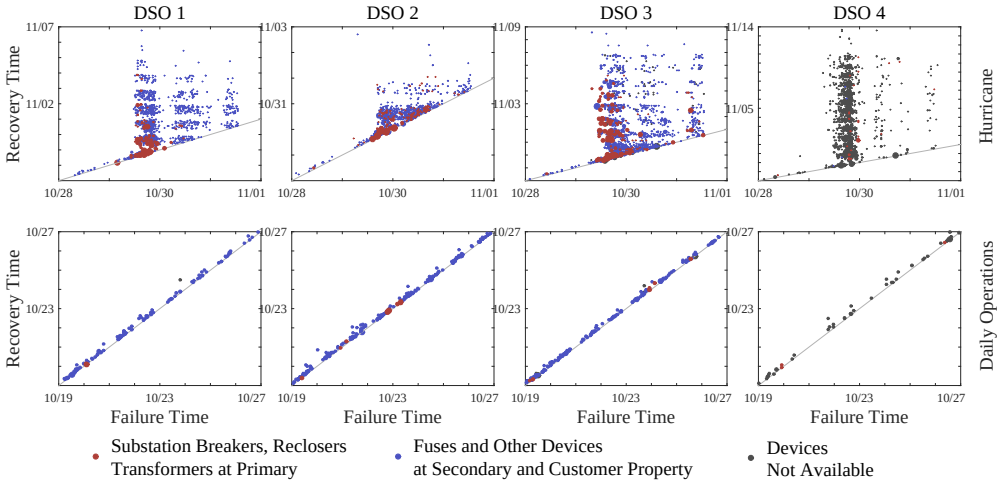

Figure 4.4: Scatter plots of downtime durations during the storm (top row) and daily operations (bottom row). Each data point corresponds to a disruption. The horizontal and vertical coordinates are the time of the disruption occurrence and recovery, respectively. The diagonal line represents the same disruption and recovery occurrence time. The distance of the disruptions above the diagonal line indicates the delay (i.e., downtime). The colors represent various types of disrupted devices.

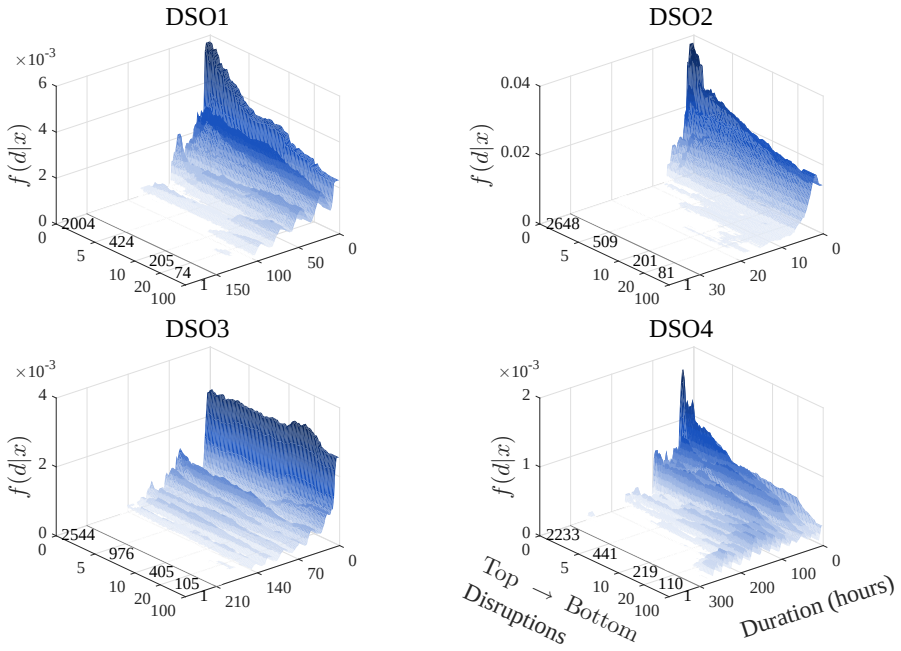

Figure 4.5: Probability density function of recovery. $f(d|z)$: probability density function of downtime duration d given the top z percentage of disruptions for the four DSOs during Super Storm Sandy. The number of customers is given for each corresponding percentage.

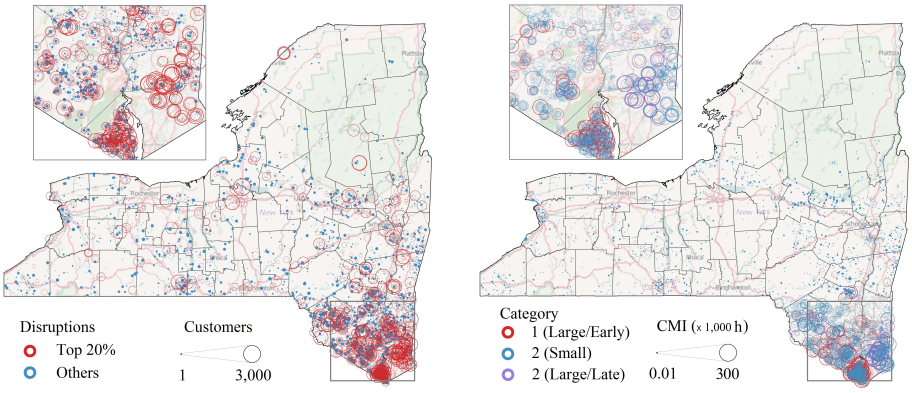

(a) (b)

Figure 4.6: Geographical distribution of the cost in Upstate New York during Super Storm Sandy: (a) number of disrupted customers; (b) customer interruption hours (CMI). Colors in (a) represent top 20% versus the remaining disruptions. Colors in (b) represent Category 1 and Category 2 disruptions. Each marker represents a system disruption. The size of a marker represents the number of interrupted customers for (a) and customer interruption hours for (b).

CHAPTER 5

DYNAMIC RESILIENCE OF POWER DISTRIBUTION SYSTEMS

In this chapter, we develop a resilience metric from bottom-up that incorporates such pertinent characteristics as non-stationary failure-recovery processes and impacts to customers. The metric builds from our prior work that derives a problem formulation and a spatiotemporal model [16, 18]. The modeling starts from failures and recoveries at individual components. Topological dependence of disruptions and recoveries in power distribution is characterized through a dynamic topology [18]. Component disruptions and recoveries are then aggregated to a larger spatial scale of a service region and temporal scale of minutes or beyond. Dependent failures and recoveries are thus characterized by non-stationary spatiotemporal random processes [16]. We further include impacts on customers in the model. As customers are connected with the infrastructure (i.e., power distribution systems), this requires a bottom-up formulation from random failures to recoveries and costs to customers. The resulting model is a coupled non-stationary random process on costs, allowing us to measure not only the resilience of the infrastructure but combined impacts with services on customers.

The rest of the chapter is organized as follows. Section 5.1 introduces the concept of resilience. Section 5.2 reviews the existing and ongoing works of resilience metrics and discusses the invalidity of the existing metrics. Section 5.3 derives a temporal resilience metric from the temporal failure-recovery processes that is formulated in Chapter 2. Section 5.4 derives a spatiotemporal resilience metric from the spatiotemporal dependent random processes in Chapter 3. Section 2.7 discusses and concludes the chapter.

5.1 Resilience Concept

Resilience is a system measure in response to exogenous disruptions. Here a system corresponds to large-scale power distribution, and exogenous disruptions are severe weather

events. Definitions and approaches on resilience are extensible beyond power distribution under severe weather [23]. Various definitions have been provided previously (for example, [4, 6, 29, 61], just to name a few). Despite the differences in terminologies, the definitions share a common concept that resilience is the capacity of a system to adapt to changes from environments and the climate [6]. In relating to severe weather disruptions of the infrastructure, resilience is defined through the two aspects:

- The ability to avoid failures under exogenous disruptions,
- The ability to restore services rapidly if failures occur.

Industry adopts similar definitions of resilience, with an emphasis on providing seamless services to customers. Rapid recovery from damages is the focus of power utilities in the U.S. [31, 62]. This corresponds to the second aspect of resilience. The first aspect is often related to as hardening the power grid [31]. Hence, resilience adopted by power utilities also involves two aspects.

Resilience is a dynamic measure for the system performance in major disruptions. Distributed backup resources and highly flexible new loads are designed and installed, which makes today's power distribution system more dynamic [63]. The dynamic infrastructure further results in the dynamic system performance that evolves with environment changes, and finally the dynamic system resilience [6].

5.2 Resilience Metrics

Existing resilience metrics can be grouped to static metrics or dynamic metrics, depending on whether time variable is involved.

5.2.1 Existing and Ongoing Metrics

Most of existing resilience metrics are static metrics, which characterize the average measures of system performance. Power utilities use widely the IEEE defined standard sustained-interruption indices, such as System Average Interruption Frequency Index (SAIFI) and

System Average Interruption Duration Index (SAIDI) [64]. SAIFI/SAIDI characterize the system reliability in daily operations excluding major storm events [64]. To evaluate the severe weather events, SAIFI was revised to Storm Average Interruption Frequency Index (STAIFI) [65], and SAIDI was revised to Storm Average Interruption Duration Index (STAIDI) [66].

$$\text{STAIFI} = \frac{\text{Total Number of Customers Interrupted}}{\text{Total Number of Customers Served}}, \tag{5.1}$$

$$\text{STAIDI} = \frac{\text{Total Customer Storm Interruption Minutes}}{\text{Total Number of Customers Served}}. \tag{5.2}$$

They both aggregate the number of interrupted customers and customer interruption durations over an entire major storm.

There are other static metrics, such as the Estimated Time of Restoration (ETR) [62] and fragility [45]. These static metrics are also average measures and have the similar problems.

Estimated Time of Restoration (ETR) is another metric used by industry [83]. ETR informs customers of the expected time needed for restoring services after failures. While appealing to users, ETR is difficult to estimate accurately because of the uncertainty and dynamics from non-stationary failure and recovery processes.

Fragility and its variations relate failures to weather variables [45, 65, 67, 121]. Such a relationship is necessary to view resilience through potential threats, and thus is promising to characterize a performance metric. A challenge is how to include dynamics and system-wide performance in such a resilience measure.

Dynamic metrics such as Quality and its variations (i.e., Robustness and Rapidity) characterize over time parts of a system or the number of customers in normal operations [23, 71, 122]. These metrics include dynamic evolution of resilience but are based on pre-assumed functions of time.

Questions arising include, what factors should a resilience metric include; and how to derive such a metric. In principle, a resilience measure should include pertinent factors

from weather to failures, recoveries, impacts on customers, DSOs and policy makers [123]. As resilience quantifies system-wide performance, a fundamental approach is to derive such a metric from bottom-up based on modeling, including weather variables as potential causes, then failures, recoveries, and impacts as consequences [18, 19].

Grounded by the spatiotemporal model, resilience metrics in recent work are derived from the bottom-up to incorporate parts of the factors: non-stationary failure-recovery processes and impacts to customers [18, 19]. However, weather and other exogenous variables are not included. A metric $R(t)$ is defined as

$$R(t) = 1 - \frac{1}{C_0} E\Big\{C(t; d)\Big\}, \tag{5.3}$$

where $E\Big\{C(t; d)\Big\}$ is the expected cost/impact in time t [18, 19]. $d > 0$ is a threshold on tolerable delays for recovery. C_0 is a normalization factor. $R(t) = 1$ indicates the best resilience and $R(t) = 0$ is non-resilience. $1 - R(t)$ is the percentage of cost or impact, evolving with occurrences of failures and recoveries.

The impact/cost has been derived using failure-recovery processes developed through non-stationary queuing models [18, 19]. Data from Hurricane Ike has been used to obtain the value of the metric for an operational power distribution grid [18, 19]. The failure-recovery-cost processes in Section 1.2.2 [11] can potentially be used to evaluate the impact/cost on customers. Thus resilience metrics depend critically on modeling and data.

5.2.2 Invalidity of Standard Metrics

Are new metrics needed for resilience in the first place? We now compute STAIFI and STAIDI values for major storm events as an example. The objective is to find whether STAIFI/STAIDI have large errors for major storms [22].

Now consider a data set from a service region during Super Storm Sandy in Upstate New York. Each data sample is on a failure signified by an activated protective device with the occurrence time, duration and number of customers affected. There are 1334 failures from October 28, 2012 to October 31, 2012 (see [11] for details). The STAIFI and STAIDI

values and their standard deviations are obtained using Equations (1) and (2) and shown in Fig. 5.1. The standard deviations are so large for both indices that they allow a negative quantity when the error bars are taken into consideration. Such large deviations suggest that STAIFI and STAIDI exhibit too much uncertainty to be valid for characterizing resilience. Therefore, extending, by brute force, the reliability standards to resilience metrics is not viable.

Having the large standard deviation is not a coincidence but results naturally from non-stationary failure-recovery processes. Non-stationary random processes can of course exhibit time-varying mean functions [11, 16, 59]. This is clearly shown by the time-varying version of STAIFI and STAIDI from Equations (1) and (2) that are computed using samples at one-hour intervals in Fig. 5.1. In contrast, the STAIFI and STAIDI are static sample averages by definition, thus insufficient for representing non-stationary failure and recovery processes.

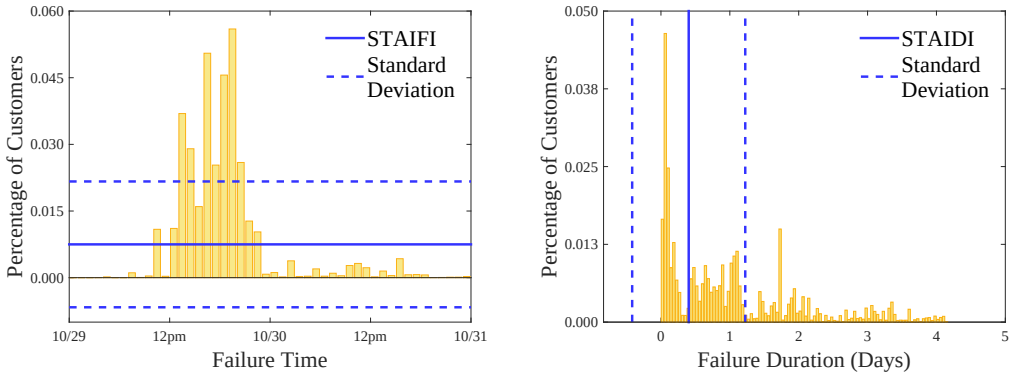

Figure 5.1: STAIFI and STAIDI values from a service region during Super Storm Sandy. The histogram shows the number of interrupted customers per hour. The error bars correspond to the standard deviation.

5.3 Temporal Resilience

In this section, we formulate the resilience based on the temporal process of failures and recoveries that is derived in Chapter 2, and apply such temporal metric to the real data.

5.3.1 Definition

As failure and recovery processes are dynamic, a resilience metric should be dynamic also. Furthermore, how resilience varies with time should result from the dynamic model of failure-recovery processes. Following such a principle, we define resilience from bottom-up, starting with one node. Probability $\Pr\{X_i(t) = 0\}$ that node i is in normal operations characterizes the ability to resist to failures at time t . Probability of infant recovery $\Pr\{D_i(t) < d_0\}$ characterizes the ability of the node to quickly recover. Combining these two abilities, we define resilience as follows.

Definition 3 *Resilience of a node*

Given threshold value $d_0 > 0$ on failure durations, resilience $r_i(t)$ for node i is the probability that the node is either functioning or exhibiting infant recovery, where

$$R_i(t) = \Pr\{X_i(t) = 0\} + \Pr\{D_i(t) < d_0, X_i(t) = 1\}. \tag{5.4}$$

Aggregating the resilience of nodes over an entire network, (system) resilience $R(t)$ is the expected percentage of nodes that are either functioning or recovering within d_0 upon failures.

Definition 4 *Resilience of a network*

Given threshold value d_0 on failure durations, resilience $r(t)$ of a network is

$$R(t) = \frac{1}{n} E\left\{\sum_i \mathbb{I}[X_i(t) = 0] + \mathbb{I}[D_i(t) < d_0, X_i(t) = 1]\right\}. \tag{5.5}$$

Hence, aggregating over spatial variables, network topology and automated reconfiguration, the resilience of a network is an average resilience of all network nodes:

$$R(t) = \frac{1}{n} \sum_i r_i(t). \tag{5.6}$$

$r(t)$ exhibits the following properties:

1. Resilience is a property of a distribution network as a whole to survive large-scale external disruptions.

2. Resilience is a function of time that reflects temporal evolutions of failures and recoveries in a network.

3. Resilience shows the ability of a distribution network to resist failures and recover rapidly.

4. Resilience depends on threshold d_0 on failure durations. The failures that can recover within d_0 are considered tolerable in terms of the resilience metric. When $d_0 = 0$, the resilience metric offers no tolerance to delays in recovery, and only characterize the ability of resisting to failures.

5.3.2 Parameters

The resilience metric can be characterized by the parameters of the model, i.e., non-stationary random processes in Chapter 2. In particular, the resilience metric (Equation 5.5) can be represented through a simple expressions owing to Transient Little's Law [19],

$$R(t) = 1 - \frac{1}{n}\int_0^{t-d_0} \lambda_f(v)\Pr\{D(v) > t - v\}dv. \tag{5.7}$$

The second term corresponds to the aging recoveries at time t. Let $\Pr\{D(v) > t - v\} = 1 - G(t - v|v)$ and $G(\cdot|v)$ is the conditional cumulative distribution function of duration $D(v)$. The resilience can also be viewed as one minus the expected percentage of nodes in aging recovery.

The above expression shows that given threshold d_0, two parameters $\lambda_f(t)$ and $G(d|t)$ together determine the system resilience. A smaller failure rate results in more functioning network nodes and thus a larger resilience. A higher percentage of infant recovery results in a fewer aging recoveries and thus a larger resilience. Our model is determined by these two time-varying parameters to the first moments (see Chapter 2). So is the resilience metric.

5.3.3 Threshold

Threshold d_0 is a pertinent parameter that measures the degree of resilience in terms of infant recovery. d_0 can be determined by service requirements. For example, $d_0 = 24$ hours

is used by Distribution System Operators (power utilities) when it is acceptable to restore a failure within 24 hours after severe weather strikes.

d_0 can characterize a special value of $E\{N(t)\}$ as follows. Consider a scenario where failures occur suddenly and intensely due to severe storm, e.g., from a hurricane. That is, $\lambda_f(t)$ characterizes impulse-like failures that increases sharply from a small value, λ_0, at time 0 (normal operation) to a large value, $\lambda_m(t)$, in short duration $0 \le t \le t_1$. The failure rate can then be written as $\lambda_f(t) = \lambda_m(t)(u(t) - u(t - t_1)) + \lambda_0$, where $u(t)$ is the unit step function and $\lambda_m(t) \gg \lambda_0$. Furthermore, consider a special case when infant recovery dominates, i.e., $G(d|t) \to 1$ for $d \ge d_0$. This implies that all failures recover within duration d_0. The expected number of nodes in failures at time t is

$$E\{N(t)\} = \begin{cases} \lambda_m(0)\,(1 - G(t|0))\min\{t, t_1\} + E\{N_0(t)\} + o\,(\min\{t, t_1\})\,, & 0 \le t < d_0, \\ E\{N_0(t)\} + o\,(\min\{t, t_1\} + 1)\,, & t \ge d_0, \end{cases} \tag{5.8}$$

where $E\{N_0(t)\} = \int_0^t \lambda_0[1 - G(t - v|v)]dv$. The terms $o(\cdot)$ include the remnants when $E\{N(t)\}$ is approximated using the first-moment $\lambda_f(t)$. This expression shows that infant recoveries occur within d_0 after failures erupt. Here d_0 is assumed to be larger than the duration of failure process t_1 for simplicity. In contrast, when aging recovery dominates, $G(d|t) \ll 1$ for $0 < d < d_0$. The expected number of nodes in failure at time t is

$$E\{N(t)\} = \begin{cases} \lambda_m(0)\min\{t, t_1\} + E\{N_0(t)\} + o\,(\min\{t, t_1\} + 1)\,, & 0 \le t < d_0, \\ \lambda_m(0)t_1[1 - G(t|0)] + E\{N_0(t)\} + o\,(\min\{t, t_1\})\,, & t \ge d_0, \end{cases} \tag{5.9}$$

where $d_0 > t_1$. This expression shows that aging recoveries do not start until delaying d_0 from the eruption of failures.

In general, a failure-recovery process can be regarded as a combination of these two special cases. At time $t = 0$, when a severe storm starts to impact a power grid, the failure process dominates, and $E\{N(t)\}$ increases rapidly. The recovery process starts after occurrences of failures, and gradually dominates. When parts of the failures recover within time duration d_0 (i.e., as infant recoveries), there can be a sharp decrease in $E\{N(t)\}$. The

remaining failures are restored with longer delays as aging recoveries. Therefore after the sharp decrease, $E\{N(t)\}$ may decrease at a slower rate. Following these scenarios, we expect to see a sharp decrease after a sharp increase in the temporal curve of $E\{N(t)\}$. The time delay between the two sharp changes can be chosen as d_0, where

$$d_0 = \underset{t}{\text{argmin}}\{\lambda_f(t) - \lambda_r(t)\} - \underset{t}{\text{argmax}}\{\lambda_f(t) - \lambda_r(t)\}. \tag{5.10}$$

5.3.4 Numerical Results

We now study time evolution of resilience using the same data that is described in Chapter 2. First, we obtain an optimal threshold d_0 for this power distribution network. The "optimal" threshold here refers to a best partition between the infant and aging recoveries. Such a partition is obtained empirically from data. Fig. 2(a) shows the comparison between $\lambda_f(t)$ and $\lambda_r(t)$. As we expected, $\hat{\lambda}_f(t) - \hat{\lambda}_r(t)$ first increased to its maximum value after the failures occurred, and then dropped to its minimum value. The duration between the maximum and the minimum is 15.50 hours. Thus $d_0 = 15.50$ hours is identified as the threshold. The mixture component that on the left of the threshold line corresponds to infant recovery. In total, 50.75% of the failures are categorized as infant recoveries.

The network resilience is then obtained through Equation 5.7 using the failure rate $\hat{\lambda}_f(t)$ and distribution of failure duration $\hat{g}(d|t)$. Fig. 2(b) shows the time evolution of network resilience $\hat{R}(t)$. The dynamic evolution of resilience provides the following observations.

- Prior to the hurricane, no failures occurred yet, and the resilience was close to 1.
- A large number of failures then occurred and reduced the resilience to a lower level. How fast the resilience decreased was measured by $\tilde{\lambda}_f(t) - \tilde{\lambda}_r(t + d_0)$. The decreasing speed reached the maximum after 16.45 hours since the first failure appeared. In the meantime, the failure rate also reached the maximum.
- At 3 am September 14th, about 42.7 hours after the first observed failure (24.8 hours after the landfall, and 26.25 hours after the failure rate reached the maximum value)

the resilience reached the minimum value. There, 46% (214 out of 463) of total failures were in aging recovery. The maximum reduction of resilience from that of the normal operation was $\frac{214}{n}$, where n was the total number of nodes in the network. At this time, the network was experiencing the most impact from the hurricane.

- After the minimum, the resilience increased when more failures were restored. The impact from the hurricane was fading gradually. It took about 10.7 days for the resilience to return to that of the normal operation from the minimum value.

The dynamic resilience metric $\hat{R}(t)$ resulting from the non-stationary model provides following insights and understanding. First, the static resilience developed in the previous works is overly-pessimistic for quantifying the resilience before and after the landfall of the hurricane, where either few failures occurred or most failures recovered. The static metrics are overly-optimistic around the landfall, where a large number of failures experienced aging recovery. Second, the dynamic resilience metric quantifies joint effects of failure and recovery processes, showing not only the failure rate but also the speed of recovery. Third, the dynamic metric reveals the worst-case resilience of the network during a hurricane. The dynamic resilience also identifies the time when the resilience reached the worst value, showing an important period during a life-cycle of failures and recoveries. For example, the network was the weakest in the duration (26.25 hours) between the failure rate reached its peak value and the resilience attained the minimum, when most failures already occurred but the restoration slowed down to aging recovery. When the network survived the weakest period, the resilience began to improve due to recovery and few additional failures.

5.4 Spatiotemporal Resilience

The non-stationary spatiotemporal model in Chapter 2 and Chapter 3 enable a spatiotemporal resilience metric for power distribution. Before the metric is defined, we first characterize fast versus slow recovery based on concepts from infant and aging mortality [99].

5.4.1 Definition

Definition 5 *Infant (fast) and aging (slow) recovery: Let $d_0 > 0$ be a threshold value. If a node remains in either failure or outage for less than d_0 duration, the node has infant recovery. Otherwise, the node has aging recovery.*

Using threshold d_0, we can define resilience. Intuitively, resilience measures network-wide performance from two aspects. One is for a power grid to withstand external disruptions as much as possible. The other is to rapidly restore electricity service from failures. Hence, aging recovery is a complement of these two characteristics [16]. Resilience is then characterized as one minus aging recovery.

Definition 6 ***Resilience**: Consider a sub-network in region Z with m number of disruptions. The resilience of the subnetwork is,*

$$R(t,Z) = 1 - \frac{1}{m}\int_{\tau=0}^{t}\Bigg(\sum_{w=f,o}\sum_{i(\tau)\in Z}\lambda_{i(\tau)}^{(w)}(\tau) \Pr\{D_{i(\tau)}^{(w)}(\tau) > t-\tau+d_0\}\Bigg)d\tau. \tag{5.11}$$

The second term corresponds to the expected percentage of aging recoveries at time t. The aging recoveries here correspond to disruptions at time t that would not recover for at least additional duration d_0. For example, when $w = f$, $\lambda_{i(\tau)}^{(f)}d\tau$ is the expected number of disruptions occurred in $(\tau - d\tau, \tau]$. $\Pr\{D_{i(\tau)}^{(w)}(\tau) > t - \tau + d_0\}$ is the probability for failures to last a duration longer than $t - \tau + d_0$. The product is the expected number of nodes that fail in $(\tau - d\tau, \tau]$ and do not recover at time $t + d_0$, which is simply the number of aging recoveries viewed at time t. The integral adds up all aging recoveries in duration $[0, t]$ and region Z. Hence, $R(t, Z)$ is the expected percentage of nodes in region Z at time t which are either in normal operation or recover within additional duration d_0. The resilience thus reflects temporal evolution of a network in response to severe weather.

5.4.2 Numerical Results

We now obtain the empirical resilience in terms of aging recovery using real data that is described in Chapter 3.

5.4.2.1 Vulnerable Time

In general, threshold d_0 can be determined through failure and recovery rates (see Chapter 2 and [16] for details). Here in Figure 3.2(b), the empirical recovery rate clearly shows that infant recovery occurred along with the majority of the failures, and is for the failures that lasted less than 12 hours. After the infant recovery, there is a delay of 7.7 hours before aging recovery occurred. Therefore, the threshold is $d_0 = 12$ hours.

The resilience is calculated using $d_0 = 12$ in Equation 5.11. As shown in Figure 5.3, the resilience decreased from the normal operations along with the failure occurrences, and reached a maximum reduction of 80.7% of total disruptions. The time at the minimum resilience is 32 hours since the initial failure occurrence. This was the most vulnerable time when the infant recovery already ended and the aging recovery was yet to begin. The minimum resilience indicates that 80.7% of total disruptions needed at least another $d_0 = 12$ hours to recover. This is consistent to the resilience curve that it took up to 14 days for all disruptions to recover.

What if threshold d_0 is chosen differently? If $d_0 = 0$ is chosen, the infant recovery would be incorrectly considered as a part of non-resilience. The resulting resilience is thus overly pessimistic with a maximum reduction of 83.7% rather than 80.7% in Figure 5.3. On the other hand, if $d_0 = 24$ is chosen, the threshold falsely excludes parts of aging recovery, resulting in overly optimistic resilience. Hence, identifying an optimal threshold is important and shall be considered in the future work.

5.4.2.2 Vulnerable Areas

The resilience metric can also be used to identify vulnerable areas in a service region. Figure 5.4(a1) and (b1) show the percentage reduction of the resilience at two time epoches: 4 hours before the landfall and the time of the minimum resilience. The regions with more than 15% and 6% reduction of resilience appear as vulnerable areas for the two time epoches. Figure 5.4(a2) and (b2) show the number of elephant failure neighborhoods at the two times respectively. The vulnerable areas coincide with the regions that have a large

number of elephant failure neighborhoods. This is consistent with the finding in Chapter 3 that elephant failure neighborhoods contribute to the majority of the disruptions and thus a significant deduction of the resilience. Mice failure neighborhoods, however, are not coupled with the vulnerable areas. These findings pose interesting directions for more detailed study at the component level.

5.5 Conclusion

Despite the progress made to date, there are yet to be performance measures that incorporate all three intrinsic characteristics at the system level: Spatiotemporal non-stationary failure-recovery; weather variables; service providers, customers and the community overall. Static metrics such as STAIFI and STAIDI characterize average behaviors of failures and recoveries but not the spatiotemporal evolutions during a severe weather event. The dynamic metrics recently developed include failure-recovery processes and impacts on customers but not weather.

The following research questions relating to resilience metrics arise. First, what resilience metrics can encompass cohesively the three pertinent characteristics: Exogenous weather variables, spatiotemporal non-stationary failures in the infrastructure, and recoveries of services for customers? Second, what approaches can lead to such resilience metrics at the system-level, combining weather with failure-recovery-impact processes? Third, what (additional) data are needed to evaluate resilience of the infrastructure and services?

Answers to those questions are expected to result from both development of system-wide metrics and modeling that incorporates the variables from bottom-up. Extensive data analytics are also needed to obtain values of newly developed metrics and to compare them with the standards.

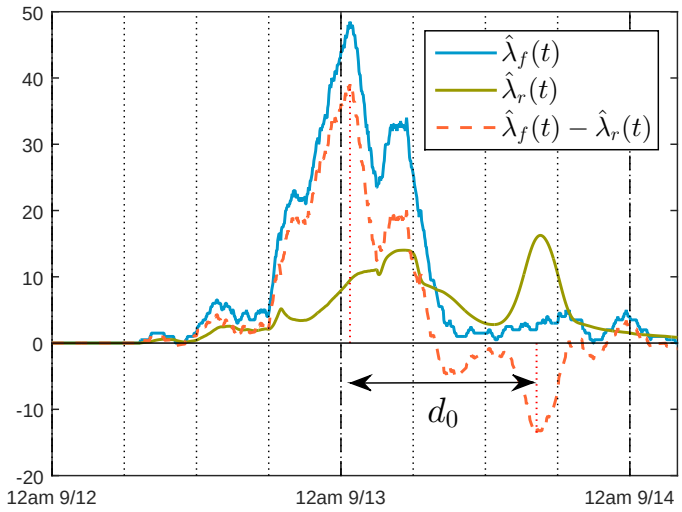

(a)

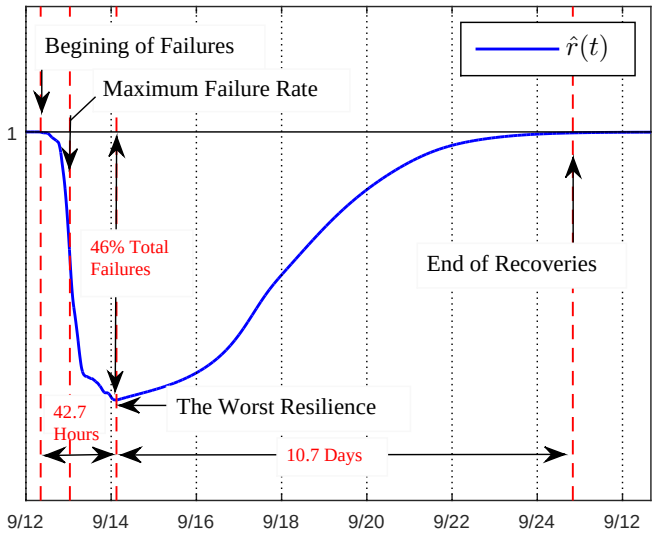

(b)

Figure 5.2: (a) Threshold d_0. (b) Dynamic evolution of resilience of the distribution network.

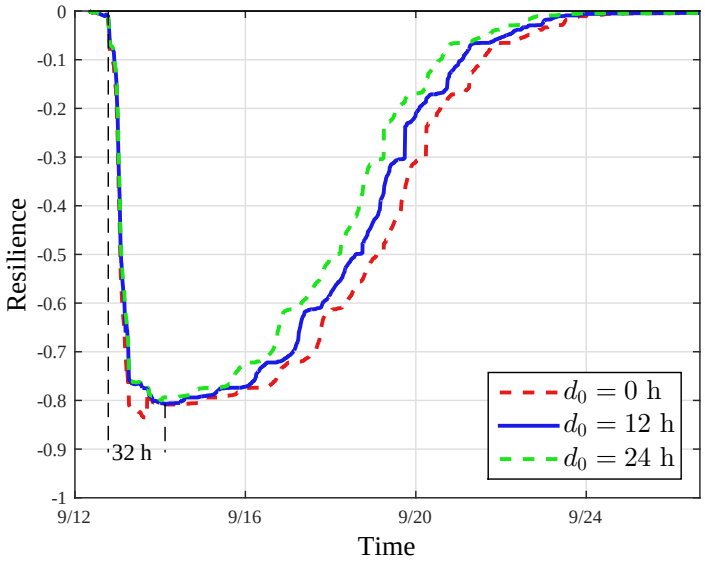

Figure 5.3: Resilience of the entire power distribution.

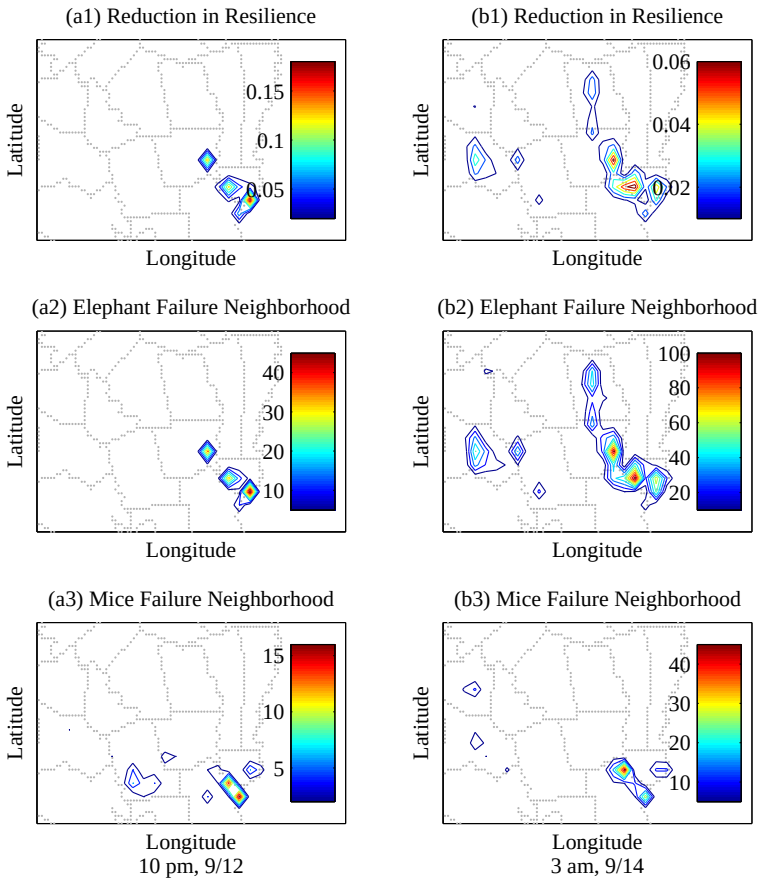

Figure 5.4: Two snapshots of the resilience over the geographical area of the power distributions: (a) Reduction in percentage (of total number of disruptions) for resilience; (b) Number of neighborhoods for elephants failures; (c) Number of neighborhoods for mice failures.

CHAPTER 6

CONCLUSION

In this dissertation, we have studied the fundamental problem of large-scale failures and recoveries of power distribution systems under severe weather impact. We also investigated the resilience of the power distribution systems from the dynamic non-stationary modeling and the large-scale data analytics.

Quantifying resilience of the energy infrastructure and services under severe weather is pertinent but understudied, as shown by the prior works. An immediate need is to understand how resilient the energy infrastructure and services really are. Such understanding enables fundamental enhancement of resilience beyond responding to severe weather. In this context, unique characteristics emerge involving weather, failure and recovery processes in the infrastructure and services, as well as impacts on community. These characteristics are inter-related and impact resilience together. Therefore, modeling, data analytics and resilience metrics need to be studied cohesively and at a large scale.

Models, when developed for separate aspects of the problem, are found incapable of characterizing these unique properties jointly. Formulating the problem from bottom-up through spatiotemporal random processes has the potential to characterize the interactions of failure-recovery-impact processes. While the modeling framework extends to customers as parts of community, roles of service providers and policy makers have been insufficiently studied. Relationships between weather variables and failures have been studied in a separated context. Models are yet to be developed to incorporate all pertinent factors.

Data analytics, although at an early stage, have started to show promise in learning knowledge about resilience. Data collected by DSOs, when sufficiently detailed, have shown potential in identifying generic vulnerabilities of the infrastructure and services. Large-scale and detailed data are particularly needed from multiple service territories. This provides an opportunity for collaboration among DSOs, policy makers, and researchers.

After all, resilience is for the benefit of the entire community. As big data is prospering in many fields of engineering, the resilience problem presents a new application area.

Modeling lays a foundation for deriving resilience metrics. Widely-used IEEE standards are mostly developed for reliability in daily operations. Those metrics, when directly extended to severe weather disruptions, are found to exhibit too much uncertainty to be reliable. Resilience metrics developed from bottom-up can incorporate non-stationary spatiotemporal failure-recovery-impact processes across multiple spatiotemporal scales. However, such metrics do not yet include weather variables. The metrics with weather variables are developed in a separate context. An open issue is how to derive resilience metrics, combining weather with the infrastructure and services.

Full of open issues and challenges, the problem of resilience provides a fertile ground for technical study. Modeling, data analytics and metrics are still very much open for development. Models and metrics are yet to include cohesively a wide range of exogenous variables. More details from the infrastructure such as power flows may be needed in the study of resilience.

In a broader context, while the methods discussed here focus on the power distribution infrastructure and services under severe weather, the approaches for quantifying resilience can be generalized to other dependent networks in a natural environment.

APPENDIX A

SUPPLEMENTARY MATERIAL FOR CHAPTER 4

A.1 Disruption Rate

Disruption rate $\tilde{\lambda}^{(d)}(t)$ is estimated from real data for both system disruptions and affected customers. The algorithm is based on moving average [104],

$$\tilde{\lambda}^{(d)}(t_i) = \frac{1}{\tau}[N^{(d)}(t_i) - N^{(d)}(t_i - \tau)], \tag{A.1}$$

where $N^{(d)}(t_i)$ is the number of system disruptions or affected customers that occur prior to time t_i. $\tau > 0$ is chosen as an interval of minutes. The procedure for estimating the rates is provided below for completeness.

Algorithm 1 *Estimating empirical disruption rate: Group all disruptions into m non-overlapping time intervals* $\{t_0, t_1, \ldots, t_m\}$.

1. *Construct an empirical probability distribution using bootstrapping from data set* $\{(c_i, v_i); 1 \leq i \leq n\}$*, where* c_i *is the number of customers affected by system disruption* i *and* v_i *is the disruption duration. For simplicity, we choose a uniform distribution for bootstrapping, where each sample is randomly drawn with probability* $\frac{1}{n}$*. Note that bootstrapping requires independent samples, which is a reasonable assumption at a time interval of a minute or longer.*

2. *At each bootstrap iteration k, draw a set of random samples of size n with replacement. Group n samples into m non-overlapping time intervals* $\{t_0, t_1, \ldots, t_m\}$*. At each time interval* t_j*, estimate rate* $\tilde{\lambda}_k^{(d)}(t_j)$ *through Eq. A.1.*

3. *Repeat Step 2 K times and obtain a set of estimators* $\{\tilde{\lambda}_1^{(d)}(t_j), \ldots, \tilde{\lambda}_K^{(d)}(t_j)\}$ *for* $1 \leq j \leq m$.

4. *The estimated rate at time t_j is the sample mean, and the estimation error is the sample variance.*

$$\begin{cases} \tilde{\lambda}^{(d)}(t_j) = \frac{1}{K}\sum_{k=1}^{K} \tilde{\lambda}_k^{(d)}(t_j), \\ \epsilon(t_j) = \frac{1}{K-1}\sum_{k=1}^{K} \left(\tilde{\lambda}_k^{(d)}(t_j) - \tilde{\lambda}^{(d)}(t_j)\right)^2. \end{cases}$$

5. *Obtain a confidence interval at time t_j: $\delta(t_j) = \Phi^{-1}_{1-0.5\alpha}\sqrt{\epsilon(t_j)}$ at $(1-\alpha)$ confidence level, where Φ_α is the inverse of the cumulative distribution function of the standard normal random variable. For example, $\Phi^{-1}_{0.975} = 1.96$ for 95% confidence interval when $\alpha = 0.05$.*

6. *Compute the normalized mean square error (NMSE)*

$$e = \frac{\sum_{j=1}^{m} \delta(t_j)^2}{m} \left(\frac{\sum_{j=1}^{m} \tilde{\lambda}^{(d)}(t_j)^2}{m}\right)^{-1}.$$

The following parameters are used: $\tau = 30$ min, $m = 5,100$ for the storm period; $\tau = 6$ hours, $m = 1464$ in daily operations, the number of bootstrap iterations $K = 100$. The number of samples (n) is given for each data set in Section SI1. Error bounds are computed at the 95% ($\alpha = 0.05$) confidence level. The estimated rates are shown in Fig. 4.1. Tables A.1 and A.2 provide the average and maximum values of the estimated rates for system disruptions and affected customers during the storm and daily operations. The accuracy of the estimated rates is measured by NMSE values that are less than 10% for all four DSOs. Both system and customer disruption rates had a significant increase during the hurricane. The four DSOs experienced 1.5 to six new disruptions per minute on the average, and 224 to 561 new disrupted customers per minute during the hurricane. This demonstrates that a system disruption affected a large number of customers.

Note that bootstrapping assumes independent samples. Given network state $S(v)$, disruptions can be considered as conditionally independent. Because the conditional independence is not the same as independence, the bootstraping method used here is an approximation.

A.2 Generalized Scaling-Law

To characterize the degree of impact in terms of affected customers by a local disruption, we define a generalized scaling law as a mapping between the two probability distributions: $W(x) : P(x)$. $P(x)$ is a probability distribution for a disruption to affect more than x customers. $W(x)$ is the probability for a customer to be affected by a disruption that impacts more than x users. Such a mapping is motivated by and extends the $80 - 20$ scaling rule [124], where $W(x) \sim 0.8$ when $P(x) \sim 0.2$. The $80 - 20$ rule does not scale up or down to power distribution systems that are by engineering design. Hence the generalized scaling law obtains an empirical mapping from data for $0 \leq W(x), P(x) \leq 1$ and a range of x. Intuitively, if every disruption would affect the same number of customers, the mapping from $P(x)$ to $W(x)$ would be linear. Hence a nonlinear mapping is expected to signify non-local and non-linear impacts from disruptions.

We define empirical probability distributions $\tilde{P}(x)$ and $\tilde{W}(x)$ as follows, where x is the number of customers affected by one disruption.

Definition 1 *Given data set $\{x_1, x_2, \ldots, x_n\}$, where x_i is the number of customers affected by the i-th system disruption. For $x > 0$,*

$$\begin{aligned} \tilde{P}(x) &= \frac{\sum_{i=1}^{n} I[x_i > x]}{n}, \\ \tilde{W}(x) &= \frac{\sum_{i=1}^{n} x_i I[x_i > x]}{\sum_{i=1}^{n} x_i}. \end{aligned} \tag{A.2}$$

$\tilde{P}(x)$ and $\tilde{W}(x)$ are estimated using bootstrapping methods; the procedure is given below for completeness.

Algorithm 2 *Estimating $\tilde{P}(x)$ and $\tilde{W}(x)$:*

1. *Construct an empirical probability distribution for bootstraping from data set $\{x_1, x_2, \ldots, x_n\}$. For simplicity, we choose a uniform distribution, where each sample is randomly drawn with probability $\frac{1}{n}$.*

2. *At each iteration k, draw a set of random samples of size n with replacement. Compute* $\tilde{P}_k(x)$ *and* $\tilde{W}_k(x)$ *for given x through Eq. A.2.*

3. *Repeat Step 2 K times to obtain a set of estimators* $\{\tilde{P}_1(x), \ldots, \tilde{P}_K(x)\}$*, where* $\tilde{P}(x)$ *is the sample mean of* $\{\tilde{P}_k(x), k = 1, ..., K\}$*. The estimation error* $\epsilon(\tilde{P}(x))$ *is the sample variance. Obtain confidence interval* $\delta(\tilde{P}(x)) = \Phi^{-1}_{1-0.5\alpha}\sqrt{\epsilon(\tilde{P}(x))}$ *at level* $(1-\alpha)$*.*

4. *Obtain* $\tilde{W}(x)$ *and the error bound* $\delta(\tilde{W}(x))$ *similarly to Step 3.*

The following parameters are chosen in our implementation: $\alpha = 0.05$ for the 95% confidence interval; $n = 1334, 1184, 1866, 1882$ for the data sets from the four DSOs; $K = 100$ as the number of iterations for bootstrapping. Fig. A.1 shows the empirical generalized scaling law $\tilde{W}(x) : \tilde{P}(x)$, for the four DSOs during the storm and daily operations. Table A.3 shows the NMSE that is less than 5%. Shown by Table A.3, $\tilde{P}(x) = 20\%$ disruptions affected $\tilde{W}(x) = 84\%, 88\%, 89\%, 79\%$ customers during the hurricane, where each of the 20% disruptions affected 74, 79, 105 and 107 customers respectively for the four DSOs. More detailed information is provided in Fig. 4.2 through the histogram of the number of affected customers. Hence a system disruption can affect a large number of customers. In daily operations, a similar mapping exists between $\tilde{W}(x)$ and $\tilde{P}(x)$. However, each top-20% disruption affected a smaller number of customers as shown through the histograms in Fig. 4.2(b) and A.2 for the four DSOs respectively.

The generalized scaling law holds for certain number of affected customers. Consider DSO 1 as an example. There are only a few samples of the disruptions that affected more than 2,004 customers. This results in more than 10% estimation error for $\tilde{W}(x)$ (Fig. A.1). Hence, the disruptions that affected from 1 to 2,004 customers are identified to be the valid range where the generalized scaling-law holds with the confidence 90%. Nevertheless, the disruptions that affected more customers than those in this range are still informative although not statistically sufficient (i.e., they may correspond to significant but rare failures and should be examined individually).

In summary, a generalized scaling law is obtained using bootstrapping from the data. In a probabilistic view, the generalized scaling law provides a mapping between probability distribution $W(x)$ of interrupted customers and probability $P(x)$ of disruptions, given that each system-disruption affected more than x customers. A valid range of customers that supports the mapping is obtained for each DSO during Super Storm Sandy and daily operations. A valid range is also obtained with the confidence 90% for the empirical scaling law to hold.

A.3 Probability of Disruptions

To quantify how Super Storm Sandy exacerbated the vulnerability, we define and estimate probability $P_1(t)$ for at least one disruption occurring at time t (per minute). The empirical probability $\tilde{P}_1(t)$ can be estimated as the frequency of the occurrences of disruptions. This can be done in a straightforward fashion for normal daily operations. During the hurricane, such a probability varied with time. Hence, the probability is estimated using the moving average similar to that for disruption rates except that the probability does not exceed one:

$$\tilde{P}_1(t) = \min\{1, \frac{1}{\tau}[N^{(d)}(t_i) - N^{(d)}(t_i - \tau)]\}. \tag{A.3}$$

Empirical probability $\tilde{P}_1(t)$ is estimated from real data using Algorithm 1. The probabilities of the four DSOs in daily operations and during the storm are shown in Fig. A.3 and Table A.4.

The probabilities for a disruption occurring at the hierarchy (primary-, secondary-distribution and customer properties) are estimated similarly and shown in Fig. A.4 and Table A.5.

A.4 Impact to Service and Cost

To understand the behavior of recovery, Figure A.6 shows scatter plots of system disruptions. Each system disruption is associated with two variables, the number of customers affected and the downtime duration.

A.4.1 Recovery

To characterize interdependencies between failure- and recovery-processes, we focus on the conditional probability density function $f(d|z)$ of downtime durarion d given top $z\%$ of disruptions for $0 \leq z \leq 1$. Empirical $f(d|z)$ is estimated as a histogram. In particular, $f(d|z)$ is obtained through counting the corresponding downtime durations given the ranking of the disruptions in the interval $[z - dz, z + dz]$. We select $dz = 0.015$ to ensure sufficient samples (i.e., 30 or more) for estimation.

The empirical mappings are illustrated through three-dimensional plots in Fig. 4.5 for Super Storm Sandy and Fig. A.7 for daily operations. These plots reveal a general trend: disruptions that affected the highest number of customers tend to be restored first. This appears to result from an underlying recovery strategy that is used for both extreme weather and daily operations, where power sources such as distribution substations are restored first, followed by other components downstream.

A.4.2 Category of Disruptions

To further understand the impact of such trend of recovery on customers, we classify system disruptions into two categories. Category 1 (C_1) includes system disruptions, each of which affected a relatively large number of customers and had a moderate downtime duration. Category 2 (C_2) includes the rest of the system disruptions, each of which either affected a moderate number of customers or affected a large number of customers but recovered late. Once classification is obtained, we can calculate the cost for the categories accordingly. The cost can shed light on the effectiveness of recovery strategies.

Consider a pair of random variables (X, Y), where X is the duration and Y is the number of affected customers of a system disruption. Consider two categories of system disruptions C_1 and C_2 as defined above. A small percentage of samples on (X, Y) evidently belong to C_1 (or C_2) based on prior knowledge (e.g., the disruptions that are known from the data to have affect a large number of costumers and recovered early). These samples are labeled samples with known category associations [41, 125]. Let $D_l = \{(x_i, y_i, \alpha_{ki})\}_{i=1}^{l}$ be a set

of labeled samples, where (x_i, y_i) is a sample on (X, Y) and corresponds to disruption i. $\alpha_{k,i}$ is a label for disruption i, where $\alpha_{k,i} = 1$ if the (x_i, y_i) is known to belong to C_k, and $\alpha_{k,i} = 0$ otherwise, $k = 1, 2$. In contrast, there are system disruptions that are unknown for the categories they belong. Let $D_u = \{(x_i, y_i)\}_{i=l+1}^{l+u}$ be a set of unlabeled samples, where disruption i is yet to be classified to one of the categories. Let $\gamma_{k,i}$ be an assigned label for such disruption i. Let $P_k(x, y)$ be the posterior probability that a system disruption which affected x customers and lasted y duration belongs to Category k ($k = 1, 2$). As there are only two categories, $P_2(x, y) = 1 - P_1(x, y)$. In this context, it suffices to classify labeled and unlabeled samples into the two categories [41].

We consider logistic regressions for classification of the two classes [126, 127],

$$\log \frac{P_1(x, y)}{P_2(x, y)} = \beta^T v, \tag{A.4}$$

where $v^T = (1, x, y, xy, x^2, y^2)$, and $\beta^T = (\beta_0, \beta_1, \ldots, \beta_5)$ is a set of unknown parameters. The resulting posterior probability is

$$P_1(x, y) = \frac{1}{1 + e^{-\beta^T v}}. \tag{A.5}$$

As shown above, we choose the quadratic polynomial $\beta^T v$ for the logistic function [125]. The quadratic polynomial is linear in β, enabling linear regression for learning the parameters from data. The quadratic polynomial is nonlinear in variables (x, y), resulting in nonlinear decision boundaries between the two classes. Note that the choice of a polynomial for the logistic function is appropriate as the variable space (x, y) is of low dimensions [125].

Two additional constraints posed by our problem must be included in the logistic regression. The number of customers for a disruption is lower bounded by a chosen value a for being large; the disruption duration is upper bounded by b for being short, i.e., $y > a, 0 < x < b$ if the corresponding system disruption belongs to C_1.

Finding decision boundaries between C_1 and C_2 can now be casted as logistic regression under constraints. Strictly speaking, logistic regression also need to minimize $\|\beta\|$ that is

L_1 norm of the parameters. As our problem is of low dimensions, this term is not included. Instead, we use partial data for validation. The algorithm finds parameters β by maximizing the log likelihood function $\log L(\beta|D_l, D_u)$ given labeled and unlabeled samples under constraints:

$$\max \log L(\beta|D_l, D_u) = \sum_{k=1}^{2} \Big\{ \sum_{i=1}^{l} \alpha_{k,i} \log P_k(x_i, y_i) + \sum_{i=l+1}^{u+l} \gamma_{k,i} \log P_k(x_i, y_i) \Big\}, \tag{A.6}$$

$$\text{subject to } y_i > a, 0 < x_i < b, \text{if } (x_i, y_i) \in C_1.$$

The first sum is for the labeled samples. The second sum is for the unlabeled samples, where $\gamma_{k,i}$ is an estimated label for the i-th system disruption in Category $k = 1, 2$. The algorithm implements a semi-supervised Logistic Classification Expectation-Maximization (CEM) Algorithm [126] with extensions in this work to the quadratic logistic function and the constraints. The algorithm is described below for completeness that follows the general format given in [126].

Algorithm 3 *Semi-supervised Logistic CEM Algorithm.*

- *Initialization: Obtain initial $\beta^{(0)}$ using labeled samples D_l.*
- *At the j-th iteration $1 \leq j$:*
  - *Expectation-step: Estimate posterior probability $P_k^{(j)}(x, y)$ for unlabeled sample (x_i, y_i) to be in Class C_k ($k = 1, 2$) for $i = l + 1, ..., l + u$ at the j-th iteration.*
  - *Classification-step: For $l+1 \leq i \leq l+u$, assign unlabeled sample (x_i, y_i) to Class C_k if $P_k^{(j)}(x_i, y_i) = \max[P_1^{(j)}(x_i, y_i), P_2^{(j)}(x_i, y_i)]$, and the constraints are satisfied: $y_i > a, 0 < x_i < b$ when the i-th system disruption is classified to C_1. Compute an updated label for $(x_i, y_i) \in D_u$:*

$$\begin{cases} \gamma_{1,i}^{(j+1)} = I[P_1^{(j)}(x_i, y_i) \geq 0.5 \bigwedge y_i > a, 0 < x_i < b], \\ \gamma_{2,i}^{(j+1)} = I[P_2^{(j)}(x_i, y_i) \geq 0.5]. \end{cases} \tag{A.7}$$

Let $D_l^{(j+1)}, D_u^{(j+1)}$ *be the samples with assigned labels at iteration* j*. Update the likelihood function* $\log L(\beta^{(j)}|D_l^{(j+1)}, D_u^{(j+1)})$.

– *Maximization-step: Find new* $\beta^{(j+1)}$ *that maximize likelihood function* $\log L(\beta^{(j)}|D_l^{(j+1)}, D_u^{(j+1)})$*. As in [126], Newton Method is used to update* $\beta^{(j+1)}$*:*

$$\beta^{(j+1)} = \beta^{(j)} - [\mathbf{H} \log L]^{-1} \nabla \log L, \tag{A.8}$$

where $\mathbf{H}$ *is the Hessian Matrix, and* ∇ *is the gradient.*

- *If* $||\beta^{(j+1)} - \beta^{(j)}|| < \delta$*, stop the iterations. Otherwise, go back to Expectation-step.* $\delta > 0$ *is a chosen small constant.*

Experimental setup To obtain labelled samples, we select a small number of system disruptions which exhibit obvious characteristics of Category 1 or Category 2. For example, disruptions affected more than 1,000 customers (i.e., top 1%, 2%, 4%, 1% disruptions for the four DSOs) and recovered within 2.5, 1.2, 2, 30 hours (i.e., the first 10% recoveries) were labeled as Categority 1. The disruptions that affected less than 10 customers (i.e., bottom 44%, 49%, 44%, 36% disruptions for the four DSOs) or recovered after 93, 19, 131, 241 hours (i.e., the last 10% recoveries) were labeled as Category 2. As a result, there are 52%, 56%, 52%, 42% samples that are labeled in the four data sets.

Different service territories were impacted differently by the hurricane; so was recovery. Thus the algorithm is applied to the data sets from the four DSOs individually. The parameters must be chosen differently also. a in the constraint is selected so that Category 1 includes at most top 20% disruptions. Based on our findings from the generalized scaling law (Fig. 2(a)), the following values can be chosen as $a = 74, 79, 105, 107$ customers (see Table A.3). To select value for b, we note that Category 1 disruptions should be among the first 50% recoveries. This results in $b = 37, 4, 31, 141$ hours for the four data sets respectively. Furthermore, $\delta = 1e - 4$ is chosen for the convergence of the algorithm.

Each of the four data sets is randomly partitioned into a training set with 80% samples and a testing set with the remaining 20% samples. The training sets obtain the decision

boundaries as shown in Fig.A.6 for the four DSOs. The test sets are then used to assess the performance of classification. The accuracy of classification using the testing set is 94.4%, 97.6%, 98.4% and 93.3% for the four DSOs while that based on the training set is 100%.

Category 1 samples from the four data sets together consists of 9% of the total disruptions at Upstate New York. Those disruptions affected more than 98, 83, 117, 135 customers and recovered within 36, 4, 30, 122 hours for the four DSOs. This shows that the decision boundaries are confined by but differ from the constraints. The remaining samples are assigned to Category 2.

Category 2 includes a small fraction of disruptions that differ from the majority (i.e., 0.3%, 1.4%, 0.4%, 0.3% for the four DSOs). The fraction corresponds to disruptions that affected a large number of customers but recovered late. Such disruptions are first identified as those falling in the upper right quadrant defined by the decisions boundaries: At downtime duration b, the corresponding numbers of customers at the quadratic decision boundary are identified as 496, 336, 194, 498 for the four DSOs respectively. Among the disruptions in this quadrant, we filter out those that correspond to "small devices" (i.e., fuses and other components at the secondary distribution and customer property) for DSOs 1, 2 and 3. The remaining disruptions are identified as "large/late" in Category 2 (i.e., those that affected a large number of customers and recovered late). The rest in Category 2 are the majority, referring to as "small" disruptions that either affected a moderate number of customers or were commonplace devices. For DSO4 data set, we use only those disruptions identified with information on device types for filtering out "large/late" samples. On average, each small disruption in Category 2 affected 36, 29, 48, 37 customers for the four DSOs.

Table A.1: Estimated system-disruption rate at the 95% confidence interval.

	Daily Operation		Hurricane		NMSE
	Average	Maximum	Average	Maximum	
DSO 1	0.0086 ± 0.0094	0.0340 ± 0.0192	0.2611 ± 0.0701	2.0675 ± 0.1791	0.0169
DSO 2	0.0143 ± 0.0120	0.0726 ± 0.0269	0.2321 ± 0.0713	1.4536 ± 0.1552	0.0238
DSO 3	0.0166 ± 0.0132	0.1170 ± 0.0359	0.3655 ± 0.0880	2.3550 ± 0.1933	0.0154
DSO 4	0.0035 ± 0.0059	0.0301 ± 0.0182	0.3527 ± 0.0847	6.0349 ± 0.2149	0.0034

Table A.2: Estimated customer disruption rate at the 95% confidence interval.

	Daily Operation		Hurricane		NMSE
	Average	Max	Average	Max	
DSO 1	0.287 ± 0.561	2.810 ± 5.525	21.592 ± 17.445	223.534 ± 62.921	0.087
DSO 2	1.294 ± 2.155	15.878 ± 12.676	22.397 ± 12.635	225.372 ± 69.940	0.174
DSO 3	0.957 ± 0.730	7.189 ± 4.387	48.588 ± 28.830	455.085 ± 104.264	0.077
DSO 4	0.263 ± 0.572	4.728 ± 7.818	32.607 ± 13.157	561.383 ± 80.579	0.032

Table A.3: Estimated complementary cumulative distribution function (CCDF). CCDF is for affected customers $\tilde{W}(x)$ and for disruptions $\tilde{P}(x)$, where x is the number of customers affected by one disruption. Estimation errors are at the 95% confidence interval.

	$\tilde{W}(x)$	$\tilde{P}(x) \sim 20\%$	x (UB, LB)	NMSE($\tilde{P}(x)$)	NMSE($\tilde{W}(x)$)
Hurricane					
DSO 1	84.2% ± 2.5%	19.9% ± 1.9%	74(83, 66)	0.0279	0.0325
DSO 2	87.7% ± 2.7%	20.1% ± 2.4%	79(91, 68)	0.0447	0.0476
DSO 3	89.3% ± 1.5%	19.9% ± 1.9%	105(122, 89)	0.0189	0.0126
DSO 4	78.7% ± 2.9%	20.0% ± 1.8%	107(124, 99)	0.0213	0.0382
Daily Operation					
DSO 1	85.9% ± 1.2%	20.1% ± 1.0%	48(52, 45)	0.0113	0.0203
DSO 2	88.5% ± 0.8%	20.1% ± 0.7%	57(60, 54)	0.0068	0.0099
DSO 3	87.0% ± 0.8%	19.9% ± 0.8%	71(75, 67)	0.0065	0.0105
DSO 4	87.7% ± 1.9%	20.1% ± 1.8%	57(68, 51)	0.029	0.0413

Table A.4: Estimated probability $\tilde{P}_1(t)$ of at least one disruption occurring for the four DSOs. Estimation errors are at the 95% confidence interval.

	Daily Operation Average	Maximum	Hurricane Average	Maximum	NMSE
All					
DSO 1	0.0071 ± 0.0085	0.0322 ± 0.0172	0.2246 ± 0.1317	1.0000 ± 0.0000	0.049
DSO 2	0.0150 ± 0.0123	0.0453 ± 0.0237	0.2412 ± 0.1302	1.0000 ± 0.0000	0.067
DSO 3	0.0119 ± 0.0113	0.0386 ± 0.0189	0.2910 ± 0.1362	1.0000 ± 0.0000	0.0497
DSO 4	0.0027 ± 0.0052	0.0144 ± 0.0128	0.1687 ± 0.0875	1.0000 ± 0.0000	0.0378
Top-20					
DSO 1	0.0004 ± 0.0000	0.0049 ± 0.0068	0.0779 ± 0.0773	0.7558 ± 0.2154	0.1419
DSO 2	0.0028 ± 0.0051	0.0166 ± 0.0138	0.0652 ± 0.0631	0.6113 ± 0.1848	0.2113
DSO 3	0.0015 ± 0.0058	0.0088 ± 0.0094	0.0974 ± 0.0859	0.8287 ± 0.2171	0.1458
DSO 4	0.0007 ± 0.0000	0.0077 ± 0.0103	0.0840 ± 0.0805	1.0000 ± 0.0000	0.0549

Table A.5: Estimated probability $\tilde{P}_1(t)$ for a disruption occurring at the three system-locations. The estimation errors are at the 95% confidence interval.

Network location	Daily Operation MAX	Average	Hurricane MAX	Average	NMSE
Primary Distribution	0.2183 ± 0.0503	0.0144 ± 0.0126	1.0000 ± 0.0000	0.4068 ± 0.0890	0.0145
Secondary Distribution	0.2593 ± 0.0637	0.0286 ± 0.0185	1.0000 ± 0.0000	0.4046 ± 0.1165	0.0198
Customer Property	0.0132 ± 0.0090	0.0008 ± 0.0028	0.1601 ± 0.0441	0.0437 ± 0.0339	0.2

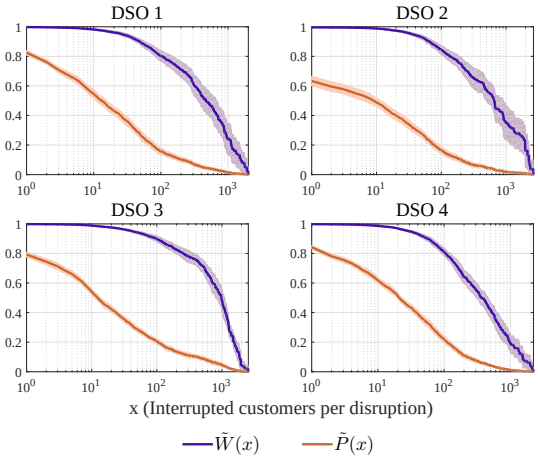

(a)

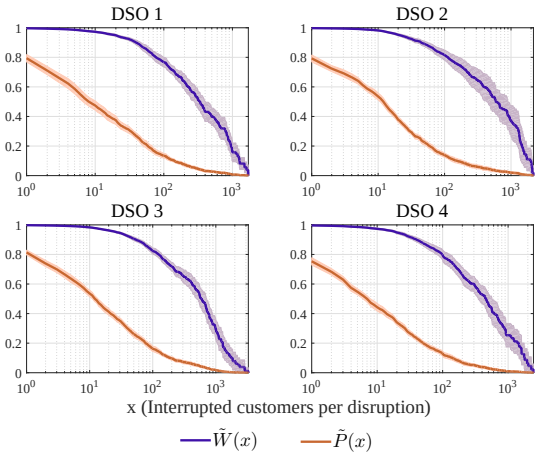

(b)

Figure A.1: Estimated probabilities. $\tilde{W}(x)$ is the probability for a customer to be affected by a disruption that impacts x customets; and $\tilde{P}(x)$ is the probability of such a disruption: (a) during Super Storm Sandy; (b) in daily operations. $\tilde{W}(x)$ and $\tilde{P}(x)$ are estimated through Algorithm 2. The shaded areas show the estimation error with the 95% confidence interval. The difference between $W(x)$ and $P(x)$ illustrates the non-local impact of a system disruption.

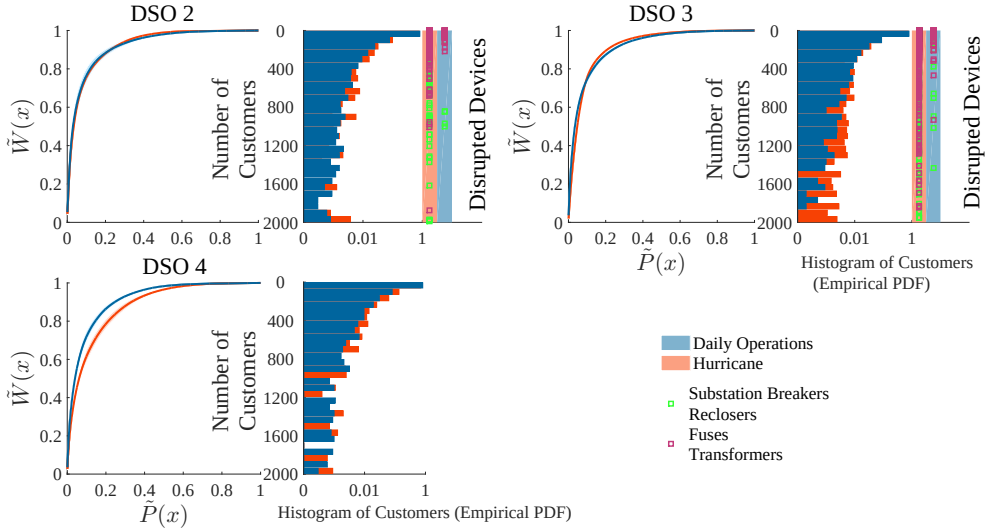

Figure A.2: Generalized scaling law for DSO2, 3 and 4 during Super Storm Sandy and daily operations. Types of disrupted devices are shown to the right of the number of affected customers. The histogram shows the empirical probability mass function for the number of customers from Super Storm Sandy and daily operations. The generalized scaling laws for DSO1 is shown in Fig. 2(b).

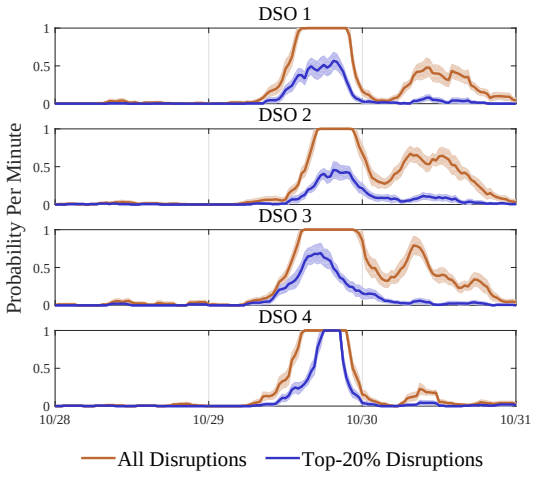

Figure A.3: Empirical probability $P_1(t)$ for a disruption occurring per minute during Super Storm Sandy. The shaded areas show the error bars estimated with the 95% confidence interval.

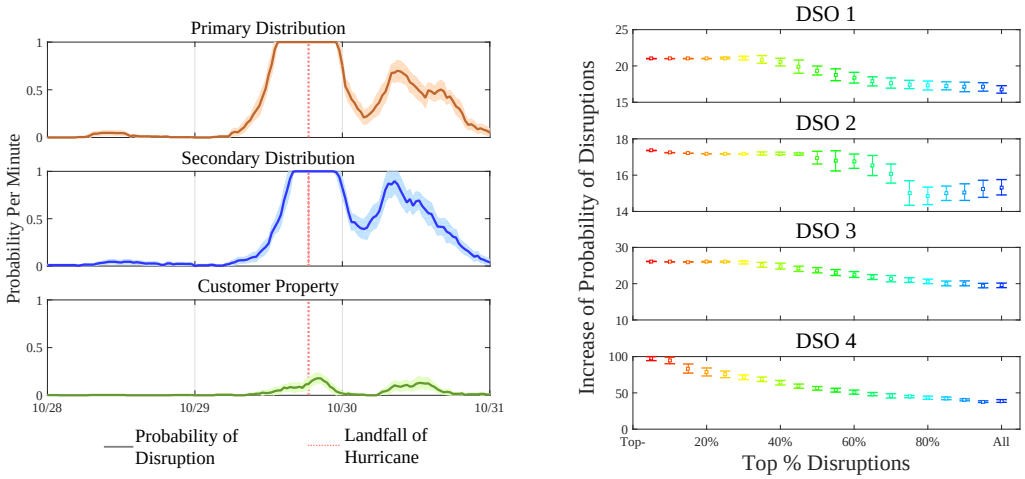

Figure A.4: (a) Empirical probability $\tilde{P}_1(t)$ that a disruption occurs per minute for the three network locations. The shaded area shows the estimation error at the 95% confidence interval. (b) Ratio between the probabilities during the storm and that in daily operations estimations. The error bounds are within the 95% confidence interval.

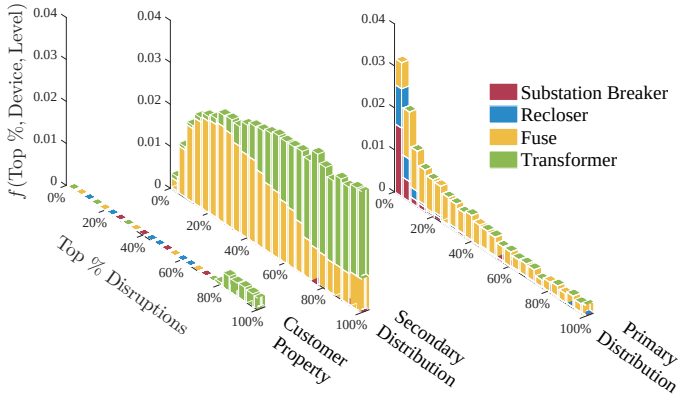

Figure A.5: Histogram of system disruptions at the three levels of the hierarchy during daily operations. The color spectrum represents the percentages of disruptions that affected a varying number of customers. The five major types of devices are plotted that correspond to most disruptions. Horizontal axis shows the percentage of disruptions for each type of device. Vertical axis shows the percentage of customers affected by each type of device.

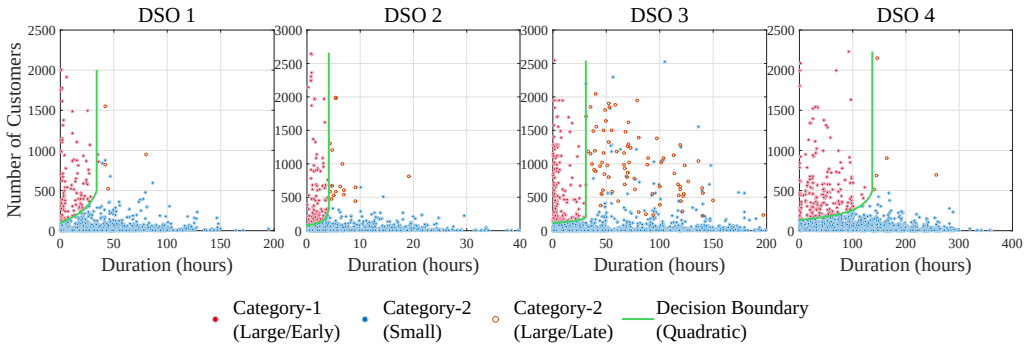

Figure A.6: Scatter plots of system disruptions for the four DSOs from the storm. Each data point corresponds to a disruption. The horizontal and vertical coordinates are down-time duration in hours and the number of affected customers for each disruption. Colors represent different categories of disruptions. Category 1 (large/early) includes disruptions that affected large numbers of customers and recovered early. Category 2 (small) includes the disruptions that either affected relatively small numbers of customers or were small devices (i.e., fuses and components at lower level of the system hierarchy). Category 2 (large/late) includes a small number of disruptions that affected relatively large numbers of customers and recovered late.

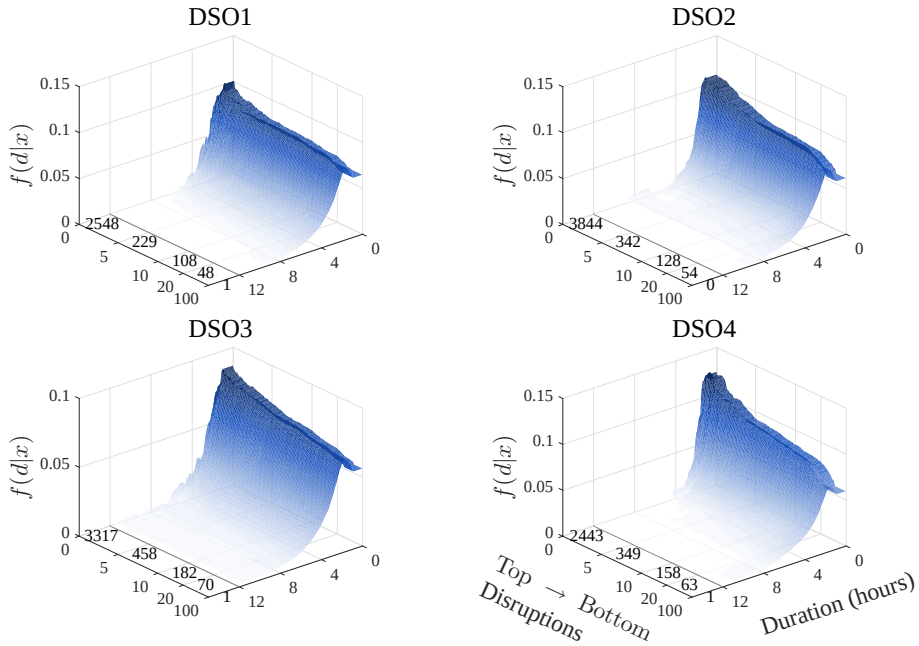

Figure A.7: Probability distribution function $f(d|z)$ of failure duration d given top $z\%$ disruptions for the four DSOs during daily operations. The number of affected customers is given for each corresponding percentage of disruptions.

REFERENCES

[1] W. H. Kersting, *Distribution System Modeling and Analysis*, 3rd ed. CRC Press, January 2012.

[2] D. B. Campbell, *Electric Power Distribution Systems Operations*, Naval Facilities Engineering Command, Alexandria, Virginia, April 1990.

[3] P. Hoffman and W. Bryan, "Comparing the Impacts of the 2005 and 2008 Hurricanes on U.S. Energy Infrastructure," Office of Electricity Delivery and Energy Reliability of U.S. Department of Energy, OE/ISER Report, February 2009.

[4] M. R. Bloomberg, "A Stronger, More Resilient New York," City of New York, PlaNYC Report, June 2013.

[5] J. A. Sathaye, L. L. Dalea, P. H. Larsena, G. A. Fittsa, K. Koyc, S. M. Lewisd, and A. F. Lucena, "Estimating Impacts of Warming Temperatures on California's Electricity System," *Global Environmental Change*, vol. 23, no. 2, pp. 499–511, 2013.

[6] Executive Office of the President, "Economic Benefits of Increasing Electric Grid Resilience to Weather Outages," President's Council of Economic Advisers and the U.S. Department of Energy's Office of Electricity Delivery and Energy Reliability, Washington, DC, Technical Report, August 2013.

[7] U.S. Department of Energyy, "U.S. Energy Sector Vulnerabilities to Climate Change and Extreme Weather," Tech. Rep. DOE-PI-0013, July 2013.

[8] H. Rudnick, "Natural Disasters Their Impact on Electricity Supply," *IEEE Power and Energy Magazine*, vol. 9, no. 2, pp. 22–26, March/April 2011, 2011.

[9] Committee on Increasing National Resilience to Hazards and Disasters, Committee on Science, Engineering, and Public Policy, *Disaster Resilience: A National Imperative*. National Academies Press, 2012.

[10] Office of Governor Martin O'Malley, "Weathering The Storm: Report of the Grid Resiliency Task Force," Tech. Rep., September 2012.

[11] C. Ji, Y. Wei, H. Mei, J. Calzada, M. Carey, S. Church, T. Hayes, B. Nugent, G. Stella, M. Wallace, J. White, and R. Wilcox, "Resilience of Power Grid: Large-Scale Data Analysis across Multiple Service Regions," *Nature Energy*, vol. 1, no. 5, p. 16052, 2016.

[12] A. G. Phadke and J. S. Thorp, *Synchronized Phasor Measurements and Their Applications*. Springer Science & Business Media, 2008.

[13] Y. Zhao, J. Chen, A. Goldsmith, and V. Poor, "Identification of Outages in Power Systems with Uncertain States and Optimal Sensor Locations," *IEEE Journal Selected Topics in Signal Processing*, vol. 8, no. 6, pp. 1140–1153, 2014.

[14] B. P. Wiseman, Y. Chen, L. Xie, and P. R. Kumar, "PMU-Based Reduced-Order Modeling of Power System Dynamics via Selective Modal Analysis," in *2016 IEEE/PES Transmission and Distribution Conference and Exposition*, May 2016, pp. 1–5.

[15] Workshop on Resilient Smart Grid Customers, Brookhaven National Laboratory, Long Island, New York, April 3 - 4 2014. [Online]. Available: http://bnl.gov/rcsg2014/

[16] Y. Wei, C. Ji, F. Galvan, S. Couvillon, G. Orellana, and J. Momoh, "Learning Geotemporal Nonstationary Failure and Recovery of Power Distribution," *Neural Networks and Learning Systems, IEEE Transactions on*, vol. 25, no. 1, pp. 229–240, 2014.

[17] Z. Zhong, C. Xu, B. Billian, L. Zhang, S. Tsai, R. Conners, V. Centeno, A. Phadke, and Y. Liu, "Power System Frequency Monitoring Network (FNET) Implementation," *Power Systems, IEEE Transactions on*, vol. 20, no. 4, pp. 1914–1921, Nov 2005.

[18] Y. Wei, C. Ji, F. Galvan, S. Couvillon, and G. Orellana, "Dynamic Modeling and Resilience for Power Distribution," in *IEEE SmartGridComm 2013 Symposium - Cyber-Physical Wide-Area Monitoring,Protection & Control (Cyber-Physical WAMPAC)*, Vancouver, Canada, October 2013, pp. 85–90.

[19] Y. Wei, C. Ji, F. Galvan, S. Couvillon, G. Orellana, and J. Momoh, "Non-Stationary Random Process for Large-Scale Failure-Recovery and Resilience of Power Distribution," *Applied Mathematics*, vol. 7, no. 3, pp. 233–249, 2016.

[20] T. Gonen, *Electric Power Distribution System Engineering*. Mcgraw-Hill College, July 1985.

[21] W. N. Bryan, "Emergency Situation Reports: Hurricane Sandy," Office of Electricity Delivery and Energy Reliability of U.S. Department of Energy, Hurricane Sandy Situation Report 20, November 2012.

[22] C. Ji and Y. Wei, "Dynamic Resilience for Power Distribution System and Customers," in *2015 IEEE International Conference on Smart Grid Communications (SmartGridComm): Architectures, Control and Operation for Smart Grids and Microgrids (IEEE SmartGridComm'15 Symposium - Architecture and Control)*, Miami, USA, November 2015, pp. 833–838.

[23] M. Bruneau, S. E. Chang, R. T. Eguchi, G. C. Lee, T. D. O'Rourke, A. M. Reinhorn, M. Shinozuka, K. Tierney, W. A. Wallace, and D. von Winterfeldt, "A Framework to Quantitatively Assess and Enhance the Seismic Resilience of Communities," *Earthquake Spectra*, vol. 19, no. 4, pp. 733–752, November 2003.

[24] S. D. Guikema, S.-R. Han, and S. Quiring, "Estimating Power Outages during Hurricanes Using Semi-Parametric Statistical Methods," in *Structures Congress*, 2008, pp. 1–9.

[25] A. Bernstein, D. Bienstock, D. Hay, M. Uzunoglu, and G. Zussman, "Power Grid Vulnerability to Geographically Correlated Failures Analysis and Control Implications," Columbia University, Technical Report 2011-05-06, November 2011.

[26] Y. Liu and C. Singh, "A Methodology for Evaluation of Hurricane Impact on Composite Power System Reliability," *IEEE Transactions on Power Systems*, vol. 26, no. 1, pp. 145 – 152, February 2011.

[27] R. A. Davidson, H. Liu, I. K. Sarpong, P. Sparks, and D. V. Rosowsky, "Electric Power Distribution System Performance in Carolina Hurricanes," *Natural Hazards Review*, vol. 4, no. 1, pp. 36–45, 2003.

[28] R. E. Brown, *Electric Power Distribution Reliability*, 2nd ed. CRC Press, 2008.

[29] P. Hoffman, W. Bryan, A. Lippert, M. Farber-DeAnda, M. Cleaver, C. Lewandowski, and K. Young, "Hardening and Resiliency: U.S. Energy Industry Response to Recent Hurricane Seasons," Office of Electricity Delivery and Energy Reliability, U.S. Department of Energy, OE/ISER Final Report, August 2010.

[30] H. Liu, R. A. Davidson, D. V. Rosowsky, and J. R. Stedinger, "Negative Binomial Regression of Electric Power Outages in Hurricanes," *Journal of Infrastructure Systems*, vol. 11, no. 4, pp. 258–267, 2005.

[31] Edison Electric Institute, "Before and After the Storm: A Compilation of Recent Studies, Programs, and Policies Related to Storm Hardening and Resiliency," Washington, D.C., Tech. Rep., January 2013.

[32] M. Amin and J. Stringer, "The Electric Power Grid: Today and Tomorrow," *MRS Bulletin*, vol. 33, no. 4, pp. 399–407, Apr. 2008.

[33] Office of Electric, Gas, and Water, "2011 Electric Reliability Performance Report," Department of Public Service of State of New York, Technical Report, June 2012.

[34] S. Pigford, "Hearing How Utilities Are Finding And Isolating Faults Rapidly To Inform The Response During Reduced Communication And Network Visibility," in *Storm Outage Restoration Conference*, Atlanta, December 2013.

[35] L. Philipson and H. L. Willis, *Understanding Electric Utilities and De-regulation*, 1st ed. New York: Marcel Dekker, 1998.

[36] M. Angalakudati, J. Calzada, V. Farias, J. Gonynor, M. Monsch, A. Papush, G. Perakis, N. Raad, J. Schein, C. Warren, S. Whipple, and J. Williams, "Improving Emergency Storm Planning Using Machine Learning," in *T& D Conference and Exposition, 2014 IEEE PES*, April 2014, pp. 1–6.

[37] R. Nateghi, S. D. Guikema, and S. M. Quiring, "Comparison and Validation of Statistical Methods for Predicting Power Outage Durations in the Event of Hurricanes," *Risk Analysis*, vol. 31, no. 12, pp. 1897–1906, December 2011.

[38] C. Rudin, D. Waltz, R. Anderson, A. Boulanger, A. Salleb-Aouissi, M. Chow, H. Dutta, P. Gross, B. Huang, and S. Ierome, "Machine Learning for the New York City Power Grid," *IEEE Trans. Pattern Anal. Mach. Intell.*, vol. 34, no. 2, pp. 328–345, Feb. 2012.

[39] D. A. Reed, K. C. Kapur, and R. D. Christie, "Methodology for Assessing the Resilience of Networked Infrastructure," *Systems Journal, IEEE*, vol. 3, no. 2, pp. 174–180, 2009.

[40] D. A. Reed, M. Powell, and J. Westerman, "Energy Supply System Performance for Hurricane Katrina," *Journal of Energy Engineering*, vol. 136, no. 4, p. 95102, 2010.

[41] R. O. Duda, P. E. Hart, and D. G. Stork, *Pattern Classification*, 2nd ed. Wiley, November 2000.

[42] H. Liu, R. A. Davidson, and T. V. Apanasovich, "Spatial Generalized Linear Mixed Models of Electric Power Outages Due to Hurricanes and Ice Storms," *Reliability Engineering & System Safety*, vol. 93, no. 6, pp. 897 – 912, 2008.

[43] S.-R. Han, S. D. Guikema, S. M. Quiring, K.-H. Lee, D. Rosowsky, and R. A. Davidson, "Estimating the Spatial Distribution of Power Outages During Hurricanes in the Gulf Coast Region," *Reliability Engineering & System Safety*, vol. 94, no. 2, pp. 199 – 210, 2009.

[44] Y. J. Park, "Reliability Assessment of the Florida Electric Power Network System Against Hurricanes," PHD Thesis, University of Florida, 2012.

[45] J. Winkler, L. Duenas-Osorio, R. Stein, and D. Subramanian, "Performance Assessment of Topologically Diverse Power Systems Subjected to Hurricane Events," *Reliability Engineering & System Safety*, vol. 95, no. 4, pp. 323–336, 2010.

[46] B. J. Cerruti and S. G. Decker, "A Statistical Forecast Model of Weather-Related Damage to a Major Electric Utility," *Journal of Applied Meteorology and Climatology*, vol. 51, no. 2, pp. 191–204, February 2012.

[47] H. Liu, R. Davidson, and T. Apanasovich, "Statistical Forecasting of Electric Power Restoration Times in Hurricanes and Ice Storms," *Power Systems, IEEE Transactions on*, vol. 22, no. 4, pp. 2270–2279, 2007.

[48] R. G. Gallager, *Stochastic Processes: Theory for Applications*. Cambridge University Press, 2014.

[49] B. Hajek, *Random Processes for Engineers*, 1st ed. Cambridge University Press, March 2015.

[50] T. Kailath and V. Poor, "Detection of Stochastic Processes," *IEEE Transactions on Information Theory*, vol. 44, no. 6, pp. 2230–2231, Oct 1998.

[51] I. Dobson, B. A. Carreras, V. E. Lynch, and D. E. Newman, "Complex Systems Analysis of Series of Blackouts: Cascading Failure, Critical Points, and Self-Organization," *Chaos: An Interdisciplinary Journal of Nonlinear Science*, vol. 17, no. 2, p. 026103, 2007.

[52] D. Bienstock, *Electrical Transmission System Cascades and Vulnerability: An Operations Research Viewpoint*. Philadelphia, PA: Society for Industrial and Applied Mathematics, 2015.

[53] I. Dobson, B. A. Carreras, and D. E. Newman, "A Branching Process Approximation to Cascading Load-Dependent System Failure," in *37th Hawaii International Conference on System Sciences*, Hawaii, Jan 2004.

[54] Z. Wang, A. Scaglione, and R. J. Thomas, "A Markov-Transition Model for Cascading Failures in Power Grids," in *System Science (HICSS), 2012 45th Hawaii International Conference on*, 2012, pp. 2115–2124.

[55] I. A. Hiskens, "Power System Modeling for Inverse Problems," *Circuits and Systems I: Regular Papers, IEEE Transactions on*, vol. 51, no. 3, pp. 539–551, 2004.

[56] A. Bernstein, D. Bienstock, D. Hay, M. Uzunoglu, and G. Zussman, "Power Grid Vulnerability to Geographically Correlated Failures Analysis and Control Implications," in *IEEE INFOCOM 2014-IEEE Conference on Computer Communications*, May 2014, pp. 2634–2642.

[57] P. Hines, J. Apt, and S. Talukdar, "Large Blackouts in North America: Historical Trends and Policy Implications," *Energy Policy*, vol. 37, no. 12, pp. 5249–5259, December 2009.

[58] M. Ilic, L. Xie, and Q. Liu, *Engineering IT-Enabled Sustainable Electricity Services: The Tale of Two Low-Cost Green Azores Islands*, 2013th ed., ser. Power Electronics and Power Systems. Springer, June 2013, vol. 30.

[59] D. Bertsimas and G. Mourtzinou, "Transient Laws of Non-Stationary Queueing Systems and Their Applications," *Queueing Syst. Theory Appl.*, vol. 25, no. 1/4, pp. 115–155, Jan. 1997.

[60] E. Yamangil, R. Bent, and S. Backhaus, "Resilient Upgrade of Electrical Distribution Grids," in *Twenty-Ninth AAAI Conference on Artificial Intelligence*, 2015.

[61] A. R. Berkeley III and M. Wallace, "A Framework for Establishing Critical Infrastructure Resilience Goals," National Infrastructure Advisory Council, Final Report and Recommendations by the Council, October 19 2010.

[62] Consolidated Edison Co. of New York and Orange and Rockland Utilities, "Post Sandy Enhancement Plan," Tech. Rep., June 20 2013.

[63] J. Guckenheimer and J. M. Ottino, "Foundations for Complex Systems Research in the Physical Sciences and Engineering," National Science Foundation, NSF Workshop Report, September 2008.

[64] "IEEE Draft Guide for Electric Power Distribution Reliability Indices," *IEEE P1366/D6, November 2011*, pp. 1–40, 2011.

[65] D. A. Reed, "Electric Utility Distribution Analysis for Extreme Winds," *Journal of Wind Engineering and Industrial Aerodynamics*, vol. 96, no. 1, pp. 123 – 140, 2008.

[66] R. E. Brown, S. Gupta, R. D. Christie, S. S. Venkata, and R. Fletcher, "Distribution System Reliability Assessment: Momentary Interruptions and Storms," *Power Delivery, IEEE Transactions on*, vol. 12, no. 4, pp. 1569–1575, 1997.

[67] T. D. O'Rourke, S.-S. Jeon, R. T. Eguchi, and C. K. Huyck, "Advanced GIS for Loss Estimation and Rapid Post-Earthquake Assessment of Building Damage," in *MCEER Research Progress and Accomplishments*, 2001.

[68] J. Park, N. Nojima, and D. A. Reed, "Nisqually Earthquake Electric Utility Analysis," *Earthquake Spectra*, vol. 22, no. 2, pp. 491–509, May 2006.

[69] S. Bjarnadottir, Y. Li, and M. G. Stewart, "Hurricane Risk Assessment of Power Distribution Poles Considering Impacts of a Changing Climate," *Journal of Infrastructure Systems*, vol. 19, no. 1, pp. 12–24, March 2013.

[70] T. D. O'Rourke, "Critical Infrastructure, Interdependencies, and Resilience," *The Bridge*, vol. 37, no. 1, pp. 22–29, 2007.

[71] S. E. Chang and M. Shinozuka, "Measuring Improvements in the Disaster Resilience of Communities," *Earthquake Spectra*, vol. 20, no. 3, pp. 739–755, 2004.

[72] A. Kuh, T. Petsche, and R. L. Rivest, "Learning Time-Varying Concepts," in *Proceedings of the 1990 Conference on Advances in Neural Information Processing Systems 3*, ser. NIPS-3. San Francisco, CA, USA: Morgan Kaufmann Publishers Inc., 1990, pp. 183–189.

[73] G. Widmer and M. Kubat, "Learning in the Presence of Concept Drift and Hidden Contexts," *Machine Learning*, vol. 23, no. 1, pp. 69–101, 1996.

[74] J. Gama, P. Medas, G. Castillo, and P. P. Rodrigues, "Learning with Drift Detection," in *Advances in Artificial Intelligence - SBIA 2004, 17th Brazilian Symposium on Artificial Intelligence, Sao Luis, Maranhao, Brazil, September 29 - October 1, 2004, Proceedings*, ser. Lecture Notes in Computer Science, vol. 3171. Springer, 2004, pp. 286–295.

[75] R. Elwell and R. Polikar, "Incremental Learning of Concept Drift in Nonstationary Environments," *IEEE Transactions on Neural Networks*, vol. 22, no. 10, pp. 1517–1531, 2011.

[76] S. Geman, E. Bienenstock, and R. Doursat, "Neural Networks and the Bias/Variance Dilemma," *Neural Comput.*, vol. 4, no. 1, pp. 1–58, Jan. 1992.

[77] M. S. Bartlett, "The Statistical Analysis of Spatial Pattern," *Advances in Applied Probability*, vol. 6, no. 2, pp. 336–358, Jun 1974.

[78] O. Schabenberger and C. A. Gotway, *Statistical Methods for Spatial Data Analysis*. Chapman and Hall/CRC, December 2004.

[79] T. Overbye, P. Sauer, C. DeMarco, B. Lesieutre, and M. Venkatasubramanian, "Using PMU Data to Increase Situational Awareness," Power Systems Engineering Research Center, Final Project Report PSERC Publication 10-16, September 2010.

[80] A. von Meier, D. E. Culler, A. McEachern, and R. Arghandeh, "Micro-Synchrophasors for Distribution Systems," in *Innovative Smart Grid Technologies Conference (ISGT), 2014 IEEE PES*, Feb 2014, pp. 1–5.

[81] H. Tram, "Technical and Operation Considerations in Using Smart Metering for Outage Management," in *2008 IEEE/PES Transmission and Distribution Conference and Exposition*, April 2008, pp. 1–3.

[82] G. Madingou, M. Zarghami, and M. Vaziri, "Fault Detection and Isolation in a DC Microgrid Using a Central Processing Unit," in *Innovative Smart Grid Technologies Conference (ISGT), 2015 IEEE Power Energy Society*, Feb 2015, pp. 1–5.

[83] Consolidated Edison Co. of New York and Orange and Rockland Utilities, "Post Sandy Enhancement Plan," Tech. Rep., June 20 2013.

[84] National Center for Environmental Information, "Climate Monitoring," released September 8, 2016. [Online]. Available: http://www.ncdc.noaa.gov/climate-monitoring/

[85] E. Berger, "Meet Deep Thunder: IBM's Next Step in the Automation of Forecasting," 2016. [Online]. Available: http://arstechnica.com/science/2016/06/meet-deep-thunder-ibms-next-step-in-the-automation-of-forecasting/

[86] J. Foerster, "Hyper-Local Weather Data Provides Accuracy to Central Hudson Gas & Electric," *Power Engineering*, vol. 120, no. 4, April 2016.

[87] San Diego Gas & Electric. (2016) SDG&E Weather Awareness System. [Online]. Available: http://www.sdgeweather.com/

[88] Federal Emergency Management Agency (FEMA), "FEMA Flood Map Service Center," 2016. [Online]. Available: https://msc.fema.gov/portal

[89] N. Lin, K. Emanuel, M. Oppenheimer, and E. Vanmarcke, "Physically Based Assessment of Hurricane Surge Threat Under Climate Change," *Nature Clim. Change*, vol. 2, no. 6, pp. 462–267, 2012.

[90] F. Zhang, Y. Weng, J. A. Sippel, Z. Meng, and C. H. Bishop, "Cloud-resolving Hurricane Initialization and Prediction through Assimilation of Doppler Radar Observations with an Ensemble Kalman Filter: Humberto (2007)," *Monthly Weather Review*, vol. 137, pp. 2105–2125, July 2009.

[91] Connecticut Light & Power, "Outage Map." [Online]. Available: http://www.cl-p.com/outage/outagemap.aspx

[92] Office of Electric, Gas, and Water, "2012 Electric Reliability Performance Report," Department of Public Service of State of New York, Technical Report, June 2013.

[93] S. Ertekin, C. Rudin, and T. H. McCormick, "Reactive Point Processes: A New Approach to Predicting Power Failures in Underground Electrical Systems," *The Annals of Applied Statistics*, vol. 9, no. 1, pp. 122–144, 2015.

[94] R. D. Christie, "Statistical Classification of Major Event Days in Distribution System Reliability," *Power Delivery, IEEE Transactions on*, vol. 18, no. 4, pp. 1336–1341, Oct 2003.

[95] P. H. Larsen, K. H. LaCommare, J. H. Eto, and J. L. Sweeney, "Assessing Changes in the Reliability of the U.S. Electric Power System," Lawrence Berkeley National Laboratory, Report LBNL188741, August 2015.

[96] T. Perry, "Solar Sandy Project Brings Panels to the People," IEEE Spectrum, Technical Report, November 2012.

[97] "IEEE Standard for Use of the International System of Units (SI): the Modern Metric System," *IEEE/ASTM SI 10-1997*, pp. i–, 1997.

[98] D. W. Hosmer and S. Lemeshow, *Applied Survival Analysis: Regression Modeling of Time to Event Data*, 2nd ed. Wiley-Interscience New York, 2008.

[99] J. D. Kalbfleisch and R. L. Prentice, *The Statistical Analysis of Failure Time Data*, 2nd ed. New York: John Wiley and Sons, 2002.

[100] S. M. Ross, *Introduction to Probability Models*, 10th ed. Academic Press, 2010.

[101] E. S. Blake, C. W. Landsea, and E. J. Gibney, "The Deadliest, Costliest, and most Intense United States Tropical Cyclones from 1851 To 2010," National Hurricane Center, Miami, Florida, NOAA Technical Memorandum NWS NHC-6, August 2011.

[102] J. Colley and S. M. DeBlasio Sr, "Hurricane Ike Impact Report," U.S. Department of Homeland Security, Technical Report, December 2008.

[103] "A Digital Record of the Complete Best Track Data," National Hurricane Center, Tech. Rep., 2008. [Online]. Available: ftp://ftp.nhc.noaa.gov/atcf/archive/2008/bal092008.dat.gz

[104] H. L. V. Trees, K. L. Bell, and Z. Tian, *Detection Estimation and Modulation Theory*, 2nd ed. New York: Wiley, 2013.

[105] S. P. Chatzis and Y. Demiris, "Nonparametric Mixtures of Gaussian Processes With Power-Law Behavior." *IEEE Trans. Neural Netw. Learning Syst.*, vol. 23, no. 12, pp. 1862–1871, 2012.

[106] W. Fan, N. Bouguila, and D. Ziou, "Variational Learning for Finite Dirichlet Mixture Models and Applications." *IEEE Trans. Neural Netw. Learning Syst.*, vol. 23, no. 5, pp. 762–774, 2012.

[107] K. C. Lan and J. Heidemann, "A Measurement Study of Correlation of Internet Flow Characteristics," *Computer Networks*, vol. 50, no. 1, pp. 46–62, January 2006.

[108] Committee on Enhancing the Robustness and Resilience of Future Electrical Transmission and Distribution in the United States to Terrorist Attack; Board on Energy and Environmental Systems, Division on Engineering and Physical Sciences, National Research Council, *Terrorism and the Electric Power Delivery System*. National Academies Press, November 2012.

[109] S. Erjongmanee and C. Ji, "Large-Scale Network-Service Disruption: Dependencies and External Factors," *Network and Service Management, IEEE Transactions on*, vol. 8, no. 4, pp. 375–386, December 2011.

[110] R. Adam, G. Oladosu, and S.-Y. Liao, "Business Interruption Impacts of a Terrorist Attack on the Electric Power System of Los Angeles: Customer Resilience to a Total Blackout," *Risk Analysis*, vol. 27, no. 3, pp. 513–531, 2007.

[111] Mahnovski, Sergej and Delaney, Michael and Tsay, Candice, "Utilization of Underground and Overhead Power Lines in the City of New York," December 2013. [Online]. Available: http://www.nyc.gov/html/planyc2030/downloads/pdf/power_lines_study_2013.pdf

[112] K. Barnes, B. Johnson, and R. Nickelson, "Review Of Supervisory Control And Data Acquisition (SCADA) Systems," Idaho National Engineering and Environmental Laboratory, Bechtel BWXT Idaho, LLC, Tech. Rep. INEEL/EXT-04-01517, January 2004.

[113] C. Dorland, R. S. Tol, and J. P. Palutikof, "Vulnerability of the Netherlands and Northwest Europe to Storm Damage Under Climate Change," *Climatic Change*, vol. 43, no. 3, pp. 513–535, 1999.

[114] E. S. Blake, T. B. Kimberlain, R. J. Berg, J. P. Cangialosi, and J. L. Beven II, "Tropical Cyclone Report: Hurricane Sandy (AL182012) 22-29 October 2012," National Hurricane Center, Tech. Rep., February 2013.

[115] National Hurricane Center, National Oceanic and Atmospheric Administration, "Automated Tropical Cyclone Forecast (ATCF) Archive Best Track Database, Data file of storm number 18 of 2012," 2012. [Online]. Available: ftp://ftp.nhc.noaa.gov/atcf/archive/2012/

[116] ——, "Hurricane Sandy Advisory Number 29," 2012. [Online]. Available: http://www.nhc.noaa.gov/archive/2012/al18/al182012.public.029.shtml

[117] C. C. Liu, J. Jung, G. T. Heydt, V. Vittal, and A. G. Phadke, "The Strategic Power Infrastructure Defense (SPID) System: A Conceptual Design," *IEEE Control Systems*, vol. 20, no. 4, pp. 40–52, Aug 2000.

[118] J. Tollefson, "U.S. Electrical Grid on the Edge of Failure," *Nature News*, 2013.

[119] A. Clauset, C. R. Shalizi, and M. Newman, "Power-Law Distributions in Empirical Data," *SIAM Review*, vol. 51, no. 4, pp. 661–703, 2009.

[120] F. Estrada, W. Botzen, and R. Tol, "Economic Losses From US Hurricanes Consistent with an Influence from Climate Change," in *Nature Geoscience*, vol. 8, 2015, pp. 880–884.

[121] Q. Yan, T. Dokic, and M. Kezunovic, "Predicting Impact of Weather Caused Blackouts on Electricity Customers Based on Risk Assessment," in *IEEE Power and Energy Society General Meeting*, Boston, MA, July 2016.

[122] R. Arghandeh, A. von Meier, L. Mehrmanesh, and L. Mili, "On the Definition of Cyber-Physical Resilience in Power Systems," *Renewable and Sustainable Energy Reviews*, vol. 58, pp. 1060–1069, May 2016.

[123] J. P. Watson, R. Guttromson, C. Silva-Monroy, R. Jeffers, K. Jones, J. Ellison, C. Rath, J. Gearhart, D. Jones, T. Corbet, C. Hanley, and L. T. Walker, "Conceptual Framework for Developing Resilience Metrics for the Electricity, Oil, and Gas Sectors in the United States," Sandia National Laboratories, Sandia Report SAND2014-18019, September 2015.

[124] M. E. J. Newman, "Power Laws, Pareto Distributions and Zipf's Law," *Contemporary Physics*, vol. 46, pp. 323–351, December 2005.

[125] Y. S. Abu-Mostafa, M. Magdon-Ismail, and H.-T. Lin, *Learning From Data*. AML Book, 2012.

[126] M. Amini and P. Gallinari, "Semi-Supervised Logistic Regression," in *15th European Conference on Artificial Intelligence*. IOS Press, 2002, pp. 390–394.

[127] T. Hastie, J. H. Friedman, and R. Tibshirani, *The Elements of Statistical Learning*. Springer Series of Statistics, 2001.